Investigation of spectral characteristics of solitary diode lasers with integrated grating resonator

vorgelegt von
Master of Science
Phuong Thanh Nguyen
aus Sonla, Vietnam

von der Fakultät IV – Elektrotechnik und Informatik
der Technischen Universität Berlin
zur Erlangung des akademischen Grades
Doktor der Naturwissenschaften
- Dr. rer. nat. -

genehmigte Dissertation

Promotionsausschuss:

Vorsitzender:	Prof. Dr.-Ing. Dr. rer. nat. Holger Boche
Berichter:	Prof. Dr. rer. nat. Günther Tränkle
Berichter:	Prof. Dr.-Ing. Klaus Petermann
Berichter:	Prof. Achim Peters, PhD.

Tag der wissenschaftlichen Aussprache: ***10.09.2010***

Berlin 2010
D 83

Zusammenfassung

In der vorliegenden Arbeit wurden die Eigenschaften von Hochleistungs-DFB-Diodenlasern untersucht, die bei 780 nm emittieren. Der Schwerpunkt der Arbeit liegt auf der Realisierung von DFB-Lasern, die gleichzeitig eine hohe Ausgangsleistung und eine hohe spektrale Kurzzeitstabilität (geringe Kurzzeitlininebreite) besitzen. Im ersten Schritt wurden die Diodenlaser mit den am FBH implementierten Standard-Messverfahren optisch und elektro-optisch charakterisiert. Damit konnte die Performance individueller Chips ermittelt und optimale Bereiche der Laser-Betriebsparameter für weiterführende Untersuchungen bestimmt werden. Dann wurden mit *heterodyne* und *self-delayed-heterodyne* Methoden die Kurzzeitliniebreite der DFB-Laser analysiert, wobei deren Abhängigkeit von der Ausgangsleistung von wesentlichem Interesse ist. Einfache Modelle sagen eine umgekehrt-proportionale Abhängigkeit der Linienbreite von der Ausgangsleistung voraus. Die experimentellen Ergebnisse hingegen zeigen bei hohen Ausgangsleistungen ein *linewidth rebroadening* bzw. einen *linewidth floor*. Dies wird hauptsächlich dem Auftreten von räumlichen Lochbrennen zugeschrieben, *side mode partition noise* und *non-linear gain* Effekte spielen dabei eine untergeordnete Rolle.

- Die DFB laser zeigten einmodige Emission bis zu Leistungen von über 300 mW mit einem Seitenmodenunterdrückungsfaktor von mehr als 50 dB. Bei der Wellenlänge von 780 nm emittierten die besten Laser mit einer Kurzzeitlinienbreite von 40 Hz bei einer Ausgangsleistung von 190 mW.
- Eine Vergrößerung der Chiplänge (Verdopplung) führte zu einer deutlichen Reduktion der Linienbreite (um den Faktor 4). Diese Linienbreitenreduktion wurde zu sehr langen Kavitätslängen hin begrenzt durch das Auftreten von räumlichem Lochbrennen bei hohen Ausgangsleistungen. Eine Kavitätslänge von 3 mm erwies sich als optimal im Hinblick auf eine geringe Linienbreite bei gleichzeitig hoher maximaler Ausgangsleistung.
- Die experimentellen Ergebnisse zeigten, dass eine Erhöhung des Koppelkoeffizienten (κ) um den Faktor 2 einen wesentlich geringeren Einfluss hat, als die Erhöhung der Kavitätslänge um den gleichen Faktor.

- Eine Frontfacetten-Reflektivität von 5% bei einer Rückfacetten-Reflektivität von 95% lieferte die beste Performance im Hinblick auf stabilen *single-mode* Betrieb bei hoher Ausgangsleistung und geringer Linienbreite.
- Die experimentellen Ergebnisse weisen darauf hin, dass in TO3 oder SOT verbaute Laser eine bessere spektrale Performance bei hoher Ausgangsleistung besitzen als auf C-mount aufgebaute Laser.

Die Ergebnisse dieser Arbeit zeigen eine Strategie auf, nach der DFB-Laser im Hinblick af hohe Ausgangsleistung und hohe spektrale Kurzzeitstabilität optimiert werden können. Die beste Performance, sowohl im Hinblick auf zuverlässigen single-mode Betrieb bei hoher Ausgangsleistung sowie bezüglich einer geringen Linienbreite zeigen Lasersysteme mit einer Chiplänge von 3 mm, einem Koppelkoeffizienten von 2 cm^{-1} und einer Frontfacetten-Reflektivität von 5%. Diese Systeme lieferten eine Kurzzeitlinienbreite von 20 kHz bei einer Ausgangsleistung von 270 mW. Dies sind, nach bestem Wissen, die besten in der internationalen Literatur dokumentierten Leistungsdaten vergleichbarer Lasersysteme. Die in dieser Arbeit gewonnen Ergebnis lassen sich auf die Entwicklung von schmalbandigen GaAs-DFB Laser hoher Ausgangsleistung übertragen, die bei anderen Wellenlängen emittieren sollen.

Die folgenden Aspekte müssen in nachfolgenden Forschungsarbeiten untersucht werden, um ein vollständigeres Verständnis und eine genauere Kontrolle der spektralen Eigenschaften von schmalbandigen Hochleistungslaserdioden zu erreichen:

- Die Phase des DFB-Gitters an der Rückfacette wird zufällig beim Brechen der Halbleiterbauelemente festgelegt und hat einen signifikanten Einfluss auf die Kurzzeitlinienbreite der DFB-Laser. Dies hat zweierlei Konsequenzen. Zum einen ist Ausbeute von Lasern mit ähnlich, näherungsweise optimaler Gitterphase an der Rückfacette gering. Zum anderen sind Laser verschiedener Riegel nicht unbedingt vergleichbar, da der Einfluss zufälliger Unterschiede zwischen den Gitterphasen auf die Linienbreite den Einfluss eines zu untersuchenden Effektes überdecken könnte. Wichtige Herausforderungen sind daher die Entwicklung geeigneter Prozesstechnologien, die zu definierte Gitterphasen an den Rückfacetten führen, sowie die Entwicklung detaillierter Modelle, die den Einfluss der Gitterphase quantitativ adäquat beschreiben.
- Weitere experimentelle Untersuchungen müssen ergeben, ob sich der Aufbau der Laser in geschlossenen Gehäusen als vorteilhaft gegenüber dem Aufbau auf offenen Trägern erweist, wenn man die Linienbreite der Lasersysteme vergleicht.

Contents

Introduction

High power single frequency, single spatial mode lasers have important applications in communication, in the domain of non-linear frequency conversion, and in spectroscopy, specifically in laser cooling, precision spectroscopy, and optical metrology. A prominent example is the application of diode lasers for the implementation of microwave and optical atomic clocks. In the class of the single frequency lasers, ridge waveguide (RW) distributed feedback (DFB) diode lasers have become the optimal source of coherent radiation for many applications because of their compactness, the high energy conversion efficiency they provide, their reliability, and because of the large frequency modulation bandwidth that can be achieved. Especially, the solitary RW-DFB diode lasers emitting at 780 nm are of particular interest for some specific applications, e.g. rubidium spectroscopy [1], [2], Raman spectroscopy [3]-[5], Bose-Einstein condensation [6], and atom interferometry [7].

For Raman spectroscopy, a spectral width of 1 cm^{-1} or less is sufficient for most applications [8] so that single longitudinal mode DFB diode lasers can be applied. However, for other applications, for example for the spectroscopy of the D1 and D2 line of Rubidium, a spectral linewidth at the MHz scale or below is mandatory in order to resolve the natural lineshape of the corresponding transition (6 MHz) [9]. Further, high resolution spectroscopy requires good wavelength tuneability with high spectral resolution. Good tuneability can be achieved by implementing a Fabry-Perot laser diode together with a grating in an extended cavity configuration (ECDL) [10]-[12]. A spectral stabilization of (high power) laser diodes can be also realized by using volume holographic Bragg gratings (VHBGs) [13], [14]. A drawback of an extended cavity configuration is its high optomechanical complexity, which limits the mechanical stability. This is an important issue specifically for the design of portable devices and space applications of lasers

Our work is mainly motivated by the requirements that are posted by the following two applications:

- High resolution Rubidium spectroscopy near 780 nm as described in detail in Refs [1], [2].

- Projects QUANTUS (QUANTen Gase Unter Schwerelosigkeit) and LASUS (LASer Unter Schwerelosigkeit) [14]-[18]. These projects aim at an implementation of a compact, robust, and mobile experimental setup for the realization of a Bose-Einstein condensate and experiments related to it in a micro-gravity environment. The final step will be to operate the experimental setup in space. However, the existing laser technology is not yet ready for precision quantum optics experiments under micro-gravity conditions or in the space, because the laser systems are too large, too heavy, too power consumptive, and too complex, so that their suitability, reliability and robustness under space conditions are questionable. Therefore, miniaturization and improvement of reliability and robustness is urgent request. One of the goals of the above mentioned projects is to realize solitary DFB diode lasers emitting at 780 nm with an optical output power exceeding 50 mW and a spectral short term linewidth of less than 200 kHz.

At the Ferdinand-Braun Institut several technological steps are applied to realize high power DFB diode lasers for the above mentioned applications [19]. The epitaxial structure of the lasers is grown by low-pressure metal-organic vapour-phase epitaxy (MOVPE) in two steps. After the first step, the grating implementation process is inserted before the second step completes the wafer growing. The lateral structure of DFB diode lasers is implemented by standard processing steps applied for the realization of a RW laser structure. Fabrication is finished by the packaging process, which offers several package configurations, namely C-mount, TO3, and SOT. DFB diode lasers emitting near 785 nm region show a highly reliable operation, e.g. a life time of 8800 h at an optical power in excess of 150 mW [20]. The same level of reliability is expected for the DFB diode laser, that emits near 780 nm and are used throught the thesis work. The characterization of DFB diode lasers first starts with the fundamental characterisation of the electrical and electro-optical properties. Depending on the results of this characterization the short-term, intrinsic spectral linewidth is analyzed. The spectral linewidth is investigated by the means of a self-delayed heterodyne and a heterodyne technique. The first version of the heterodyne linewidth measurement setup at FBH is implemented as part of this thesis work. The laser structure, i.e. the cavity length, the grating coupling coefficient, and the front facet coating are varied and optimized for maximum output power and minimum intrinsic linewidth.

The thesis is organized as follows:

- First, a brief introduction on the fundamental concepts and properties of DFB diode lasers is given in chapter 1. The chapter focuses specifically on high power diode lasers. Further, the dependence of the intrinsic linewidth on the laser design

and operating parameters is dicussed, and the results of a simulation of the linewidth of high power 780 nm DFB diode lasers are presented.

- The experimental aspects of this thesis work are presented in chapter 2. The first section describes the technological approach applied for the realization of DFB diode lasers. After that, the measurement setup used for basic characterization is presented. The final section of this chapter focuses on the introduction of advanced characterization methods, namely on the self-delay heterodyne and heterodyne techniques, to characterize the spectral stability of narrow linewidth, high power DFB diode lasers.
- In chapter 3, experimental data gathered for this thesis work are presented, analyzed, and discussed. First, the results of the fundamental characterization, namely of the electro-optical and optical properties, are shown. Then, the extraction of DFB diode laser parameters from amplified spontaneous emission (ASE) spectra is explained. The characterisation of the spectral linewidth and the discussion of the corresponding results follow. Specifically the dependence of the linewidth on laser output power is analyzed. The linewidth-power product is then used in the following to analyze and discuss how the different laser parameters affect the laser linewidth. The main parameters considered are the cavity length, the coupling coefficient, and the front facet reflectivity. Based on these results, at the end of chapter 3, a strategy is proposed how to optimize the DFB laser parameters for the high power, narrow linewidth emission.

The last chapter concludes the discussion and presents an outlook to future work.

Chapter 1.

Fundamental of high power diode lasers with integrated grating resonator

1.1. Diode laser Basic principle

A *laser diode* is an optoelectronic device that operates under stimulated emission conditions. In order to generate the laser radiation, a gain medium together with optical confinement is necessary, which is known as the *active area* of the device. The active area bases on undoped layer of direct semiconductor material embedded between high-band-gap (p-doped region) and low-refractive-index (n- doped region) forming a *p-n* junction with a double-heterostructure (DH). In this *p-n* junction, carrier and optical confinements are achieved. Recently, in all of diode laser, the DH structure is substituted by a modern structure namely quantum-well (QW) structure. Another condition for laser operation of diode laser relies on an optical feedback by resonator mirrors in front and rear facet of diode laser that remain an enough gain for optical field inside active area. In this section, several basic elements of diode lasers will be introduced briefly.

1.1.1. Quantum well structures

In modern semiconductor diode lasers, due to development of epitaxial growth methods, the laser diode active area is fabricated based on QW structures. A quantum well is a potential well that confines particles, which were originally free to move in

three dimensions, to two dimensions, forcing them to occupy a planar region. The effects of quantum confinement take place when the QW thickness becomes comparable to, or smaller than, the de Broglie wavelength of the carriers (generally electrons and holes), e.g., in GaAs the Broglie wavelength ~ 50 nm [21]. In the QW, the energy band lead to energy levels called "energy subbands", i.e., the carriers can only have discrete energy values perpendicular to the potential well, and parallel to the well. They are free to move. The QW thickness varies from few nanometers to few tens nanometers. This QW layer is surrounded by material with a larger band gap. The injected carriers can now be captured in a very thin layer by the potential barriers of the larger band gap material. In this case, the density of electronic states versus energy $D(E)$ increases in steps which are located at the electronic energy levels of the quantum well as shown in Fig. 1.1. Therefore, the density of states close to the lowest-energy level in a quantum well is much higher than the density of states at the band edge in bulk material. The density of electronic carriers at a given energy is the product of the density of states $D(E)$ and the probability of being occupied by electrons $f_c(E,T)$ or holes $1 - f_v(E,T)$, which are exponentially decreasing functions and called Fermi functions (according to[21]). Thus, the carrier distribution for a quantum-well laser structure has a higher maximum value and a smaller energetic width comparing to a bulk-double heterostructure.

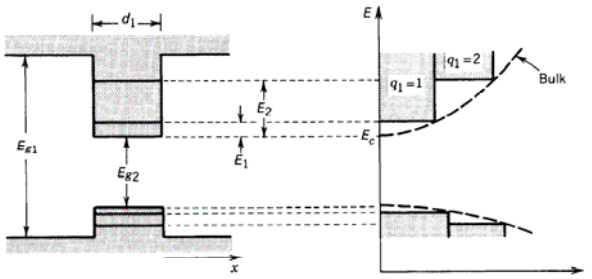

Figure 1.1. *Density of states for a quantum-well structure (solid) and for a bulk semiconductor (dashed). [21]*

In Fig. 1.2, the band gaps diagram is shown for a practical semiconductor laser structure operating at wavelength region of 780 nm. The quantum well layer consists of GaAsP material. The well embedded in AlGaAs barriers that made of alloy with larger band gap but nearly the same lattice constants as GaAs. Within the GaAsP quantum well some first subbands are shown in Fig. 1.2 and indicate the localization of the carriers. The laser operation is based on the optical transition between two closest subbands (E_{lh1} - E_{e1}) as shown in the Fig. 1.2.

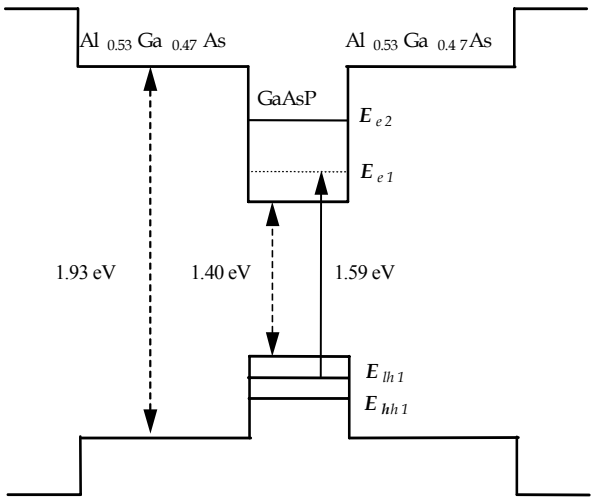

Figure 1.2. *Band gap distribution and relevant energy levels of GaAsPs-QW embedded in AlGaAs waveguide layers.*

Using a quantum well as the active region for diode lasers has several advantages over DH structures [22]:

- First, since the band gap is higher outside the QW, only the QW-region has to be pumped to generate inversion. The QW volume is very small. Therefore, the injection current is reduced by about three orders of magnitude in comparison to typical bulk-structure diode lasers.
- Second, the carriers are efficiently captured by the QW's barrier making it unnecessary to dope the regions close to junction. The efficiency of radiative recombination reaches more than 90% in modern standard devices, material of highest quality allows for efficiencies of nearly 100%. Further, the low doping results in diode laser structures with very low internal loss. Consequently, by using QW structure, the active region length can be increased while the high external efficiency, which represents for the conversion from electrical energy to optical energy, is maintained. The reduction of thermal and series resistance related to lengthening of the diode laser cavity allows for operation at higher output power.
- Third, the QW is a layer of typically about 10-nm thickness. Such thin layers do not require a fully matched lattice constant with GaAs-based material. Therefore, the material compositions of QW layer can be varied with less influence from strain effects. By replacing gallium partly (typically a few percent) with indium, the operating wavelength range can be extended from 870 nm up to 1100 nm. Similarly, the substitution of the arsenic atom by phosphorus atom will shift the laser emission wavelength down to 730 nm. The introduction of strain in a typical zincblende-type semiconductor like GaAs splits the degeneracy at the valence-band-edge maximum, and separates the heavy-hole and light-hole subbands. The change in the band structure leads to a reduction of the density of states at the edge of the valence band and also of the effective mass of electrons and holes. This reduces the threshold-current density of strained QWs in comparison to unstrained ones [23],[24]

Due to these advantages strained QW layers are nowadays used to form the active region of almost all diode laser structures [23].

1.1.2. Gain and threshold condition

In the semiconductor diode laser, the active region serves as a gain medium for optical field propagation. When passing through an absorption medium along the optical axis, e.g. along the z direction, the intensity J of an optical plane wave varies exponentially [25].

$$J(z) = J_0 \exp(-\alpha z) \qquad (1.1)$$

with J_0 being the initial intensity and α is the absorption coefficient. In active region of the diode laser, an amplification of the optical field is achieved. In this case, the exponential increase in intensity can be described by a negative value of α which is referred to as a net optical gain $g = -\alpha$. Fig. 1.3 shows a simulation curves with different excitation levels of optical gain calculated for QW structure.

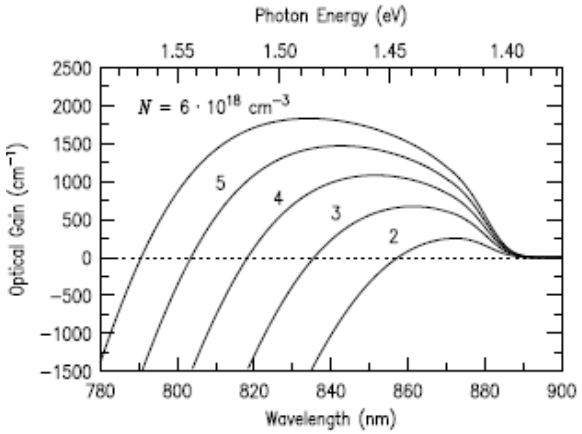

Figure 1.3. *Optical-gain spectrum of GaAs bulk material at carrier densities of N = 2-6 × 1018 cm−3. For photon energies below the band-gap energy of GaAs of Eg = 1.42 eV, the material is transparent. Optical gain occurs for energies near the band gap. The maximum of the optical-gain curve shifts towards shorter wavelengths for higher carrier densities N due to the band-filling effect. [25]*

For a QW structure, the first contribution to the net gain is material gain. This parameter is related to stimulated emission and absorption rates of active region itself and can be given by [22]:

$$g_{mat} = g_0 \,.\, ln\,(j/j_{tr}) \qquad (1.2)$$

where j is current density flowing through active region. The reference gain g_0 and transparency current density j_{tr} are parameters of the material that depend on composition, thickness and strain configuration of the QW and barrier material. However, this gain only shows the wavelength range where amplification by the QW is - in principle - possible. The more important value is modal gain g_{mod} that represents the degree of the overlap between optical field and QW. The modal gain g_{mod} is related to material gain g_{mat} via the confinement factor Γ [25].

$$g_{mod} = \Gamma g_{mat} \qquad (1.3)$$

where

$$\Gamma = \frac{\int_{-d/2}^{+d/2} J(x)dx}{\int_{-\infty}^{+\infty} J(x)dx} \qquad (1.4)$$

This formula applies generally for local optical field intensity J in a QW with thickness d. Confinement factors of a few percent are obtained with a typical QW thickness of about 10 nm.

For an optical field travelling through the active region the coefficient α usually consists of two parts, one representing the intrinsic modal absorption α_i (also termed

modal loss) and the other describing the modal gain $g_{\mathrm{mod}} = \Gamma g_{mat}$ which depends on the density of the injected carriers or current density [25].

$$\alpha = \alpha_i - \Gamma g_{mat} \qquad (1.5)$$

The intrinsic modal absorption is caused by scattering of the optical mode at rough interfaces, absorption at defects and by free-carrier absorption. Whereas the first two reasons can be neglected for semiconductor-diode lasers with good crystalline quality, free-carrier absorption cannot be avoided since part of the optical-mode pattern overlaps with the p- and n-doped cladding regions. When the modal gain Γg_{mat} is larger than the modal loss α_i, the propagating optical field is amplified.

In a diode laser device, the semiconductor optical waveguide is combined with a Fabry-Perot resonator having mirror reflectivity of R_1 and R_2. A fraction of the optical intensity leaves the cavity at these mirrors (cavity mirror loss) which defines the laser output beam. Therefore the intensity J_{rt} of the optical mode after a roundtrip in the cavity is given by [25]:

$$J_{rt} = J_0 R_1 R_2 \exp [2(\Gamma g_{mat} - \alpha_i)L] \qquad (1.6)$$

Lasing occurs when the gain provided to the optical mode compensates the intrinsic absorption and the mirror losses for a single roundtrip. The minimum gain g_{mat} where the device starts lasing operation is called the threshold gain g_{th}. At threshold gain the intensity J_{rt} after a single roundtrip through the cavity takes on its initial value J_0

$$J_{rt} = J_0 , \qquad (1.7)$$

Therefore, we got

$$1 = R_1 R_2 \exp [2(\Gamma g_{th} - \alpha_i)L], \qquad (1.8)$$

and

$$\Gamma g_{th} = \alpha_i + \frac{1}{2L}\ln\left(\frac{1}{R_1 R_2}\right) = \alpha_i + \alpha_m. \qquad (1.9)$$

At laser threshold, the modal gain Γg_{th} is the sum of the two terms, the intrinsic absorption α_i and the mirror losses α_m [25]. The mirror losses depend on the cavity length L and the mirror reflectivities R_1 and R_2.

1.1.3. Waveguide and Resonator

The laser operation of a diode laser requires an important condition, namely waveguiding of the optical wave in the active region. In a simplified picture, in the vertical direction, waveguiding is based on total internal reflection of the optical wave at the two interfaces according to Snell's law, see Fig. 1.4. The vertical structure, an

epitaxial layer structure, defines both an optical waveguide as well as a pn-junction by means of the quantum well. In Fig. 1.4, a three-layer dielectric slab waveguide consisting of a film embedded between two cladding layers is shown. Because a single QW is too thin to produce an efficient waveguide, several thin layers including multiple QWs and barriers may be grown to form this embedded film. The number of layers making up this film depends on the design of the individual diode laser. The refractive indices of these layers result in a refractive index n_f for whole film. The refractive indices of the cladding layers n_{c1} and n_{c2} are lower than the refractive index of the film n_f, the active layer has the highest refractive index and the lowest band gap, so that this structure provides waveguiding. This type of structure is designated separate confinement heterostructure. The waveguiding in vertical direction enhances the confinement factor Γ significantly which results in a reduction of threshold current density. Another benefit of the vertical waveguide structure is that it enforces single transverse mode emission in vertical direction. Typically, the waveguide thickness in vertical direction varies from few hundreds of nanometers to few micrometers.

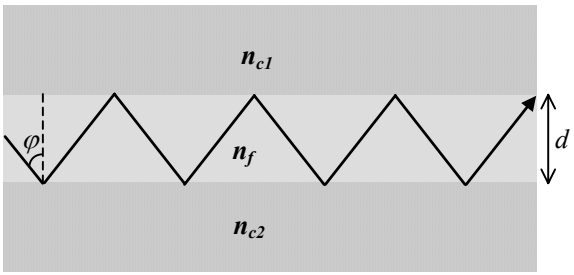

Figure 1.4. *Schematic of a three-layer waveguide: basic structure for diode lasers.*

In comparison to vertical waveguiding that is determined by the epitaxial layer system, the optimization of lateral waveguiding along the *pn*-junction is significantly more challenging. The lateral guiding of the optical wave can be achieved similarly to the vertical waveguiding described above. The active layer, in lateral direction, also is sandwiched between two lower refractive index slabs. This structure is hence called an index-guide or buried double heterostructure. The index-guide structure has a shortcoming in that it requires a sophisticated process of lateral laser structure fabrication [26]. Hence, in practice, the more popular design is a gain-guide structure that relies on defining a lateral current injection window. The width of the active region in lateral direction depends on the spreading of the injection current in that direction. The optical wave only is amplified within the pumped region. The gain guiding acts as an active waveguide in lateral direction during laser operation. The lateral confinement is described in Fig. 1.5, where the open distance between two insulator slabs will define the lateral window for the injection current. To

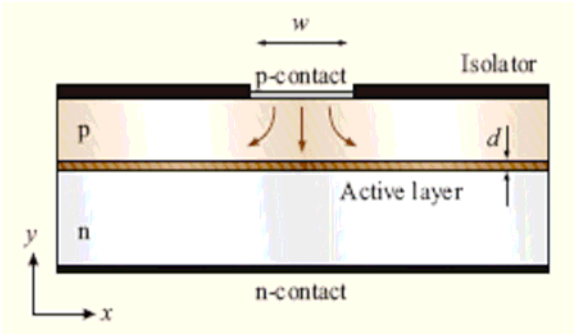

Figure 1.5. *The active waveguide during laser operation in lateral direction. [30].*

enforce single lateral mode laser operation, the lateral width of the injection current window should be of the order of a few micrometers [27]. For high power diode lasers that need to process a large injection current, a ridge-waveguide (RW) geometry is typically used instead to achieve single transverse mode operation.

The last condition to be mentioned for laser oscillation refers to the resonance condition that is defined by the laser resonator and has to be met by the optical modes of the laser. Almost all diode laser resonators can be considered a Fabry-Perot resonator. The Fabry-Perot resonator consists of two mirrors that are aligned parallel

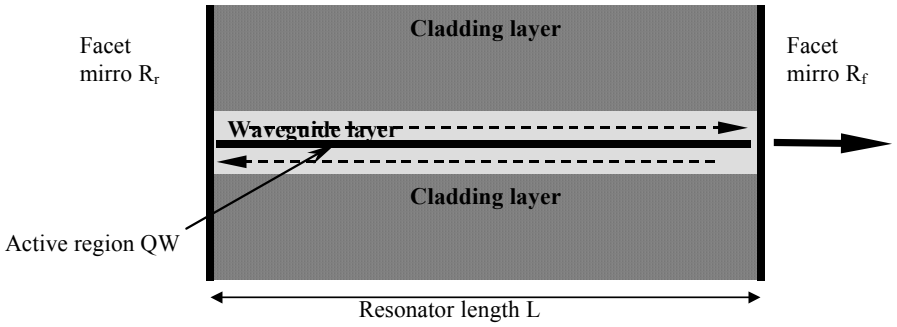

Figure 1.6. *The configuration of diode laser using Fabry-Perot resonator.*

each other. For a semiconductor laser parallel alignment is based on appropriately cleaving the facets of semiconductor crystal. The facets of diode laser are coated with high reflectivity at the rear side and with low reflectivity at the front side to from resonator mirrors to allow for efficient power scaling of the laser system. The configuration of a diode laser that is based upon a Fabry-Perot resonator is shown in Fig. 1.6. The optical wave travels back and forth, undergoing successive reflections at the facets. The optical resonator has multiple resonance frequencies called longitudinal modes. Each mode corresponds to a standing wave with nodes at the facets. Under this standing wave condition, the repeatedly reflected rays are in phase with each other, and positive interference between them preserves the state of coherence. The standing wave condition is satisfied when the resonator length L equals an integer multiple of half of the center wavelength λ_0:

$$L = m(\lambda_0 / 2n_{eff}) \qquad (1.10)$$

where m is an integer; n_{eff} is effective refractive index inside the waveguide. [25]

The separation of these longitudinal modes (mode spacing) is given by [25]:

$$\Delta\lambda \approx \lambda^2_0 / 2\, n_g L \qquad (1.11)$$

where

$$n_g \approx n_{eff} + \omega\frac{\partial n_{eff}}{\partial \omega} \approx n_{eff} - \lambda\frac{\partial n_{eff}}{\partial \lambda}, \qquad (1.12)$$

which is called group effective index known as $n_g = c/\upsilon_g$ with υ_g is group velocity of optical mode. Fabry-Perot diode lasers usually operate in multi longitudinal mode around the gain peak.

1.1.4. High power operation of diode lasers

For semiconductor lasers, above threshold, the dependence of output power on pumping current can be described by a linear relation [25],[27]:

$$P = \eta_i . \frac{\alpha_m}{\alpha_i + \alpha_m} . \frac{\hbar\omega}{q} . (I - I_{th}) = \eta_d . \frac{\hbar\omega}{q} . (I - I_{th}) \qquad (1.13)$$

The output power P linearly increases with drive current I above threshold. The differential efficiency η_d is defined as [25]

$$\eta_d = \frac{q}{\hbar\omega} . \frac{dP}{dI} = \frac{(dP)/(\hbar\omega)}{(dI)/q} \qquad (1.14)$$

η_d is the differential increase of photons per time $(dP)/(\hbar\omega)$ emitted from the diode laser per differential increase of injected electrons per time $(dI)/q$ above laser threshold. $(dP)/(dI)$ is called the slope efficiency. It is typically given in units of W/A and is derived from the linear part of the laser characteristic above threshold. The internal efficiency η_i is the fraction of carriers, which are above threshold injected additionally to the carriers already present at threshold and converted into photon. In the ideal layer, above threshold, every additionally injected electron-hole pair (carriers) is converted in photon by stimulated recombination. In Fig. 1.7, the output power

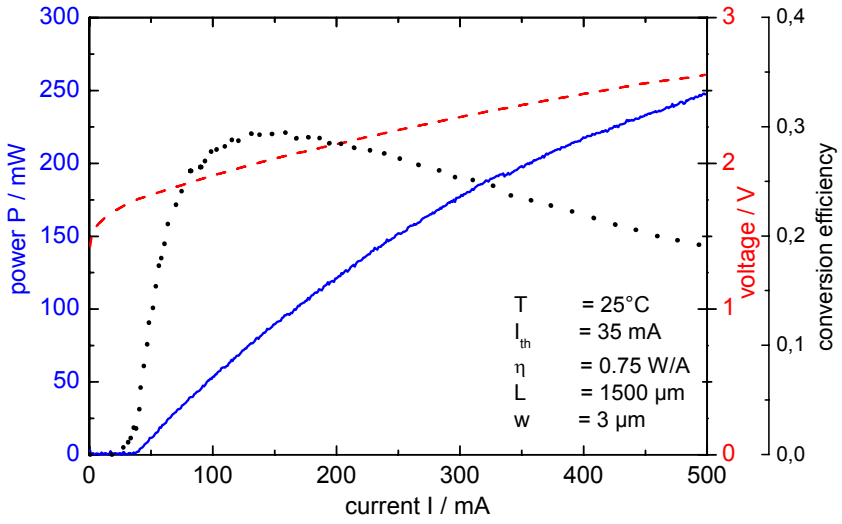

Figure 1. 7. *Typical current-power (solid), current-voltage (dashed) and wall plug efficiency (dotted) of a diode laser emitting at 780 nm.*

characteristics of a DFB diode laser and the current-voltage characteristics are shown as a continuous and dashed line, respectively. The electrical-to-optical conversion efficiency (dotted line) is about 30%.

The temperature dependence of the threshold current I_{th} and of the slope efficiency are given as follow:

$$I_{th}(T_{j2}) = I_{th}(T_{j1}).e^{\frac{T_{j2}-T_{j1}}{T_0}} \qquad (1.15)$$

$$\eta_d(T_{j2}) = \eta_d(T_{j1}).e^{-\frac{T_{j2}-T_{j1}}{T_1}} \qquad (1.16)$$

Here I_{th} and η_d are measured at the different junction temperature T_{j1} and T_{j2} [22]. The characteristic temperatures T_0 and T_1 are determined via measurements. They depend on the specific design of diode laser. The higher the values of T_0 and T_1 the better the temperature stability of the diode laser will be.

The distinction between low-power and high-power semiconductor lasers is not precisely defined. It may depend on the type of laser and wavelength. Generally speaking, 50 mW (or more) *cw* for single-mode, single-frequency lasers and 500 mW (or more) *cw* for broad-area multimode lasers and laser arrays are considered to be high power lasers. In practice, there are several key factors that limit the useful output power of a semiconductor laser: multimode operation, catastrophic optical damage, thermal rollover, and aging.

- Multimode operation, which is the onset of higher order spatial modes that manifest themselves in beam distortions in the lateral direction of the device. This phenomenon is called filamentation. It implies that there are hot regions inside the cavity where the refractive index is increased. This leads to parasitic optical waveguides, which destroy the lateral-mode profile. As a consequence, self-focusing points will be appear in the active region leading to “hot-spots” that degrade laser performance.
- Catastrophic optical damage (COD) refers to irreversible damage behaviour when the optical power drops dramatically at a certain injection current. The COD destroys the crystalline structure of diode laser mainly at the laser facets and is caused by heating due to high optical power density (therefore also called Catastrophic Optical Mirror Damage - COMD). One of the reasons for COD is strongly related to filamentation.
- The third power-limiting mechanism is thermal rollover. Its characteristic is a reduction of laser efficiency with increasing injection current. It is caused by increasing ohmic losses at high drive current levels. This increase results in increasing heat dissipation near the *pn* junction, which raises the temperature of

the active region and lowers its conversion efficiency. Eventually the optical output saturates and even decreases with increasing current. A principal reason for the reduction of optical output beyond saturation is the increased spillage of charge carriers out of the active region into the carrier confinement or cladding layers, where they cannot contribute to radiative recombination. As the temperature rise becomes dramatic, the laser gain decreases at fixed current density, eventually causing the optical output to diminish to near zero.

- The last limitation to the output power to be mentioned is aging of a semiconductor laser. All semiconductor lasers exhibit some degradation in optical output if operated at constant current and temperature for extended periods of time. Aging behaviour and the associated reliability of a given semiconductor laser are highly dependent upon its structure and operating conditions. Semiconductor laser reliability is usually limited by thermal dissipation, high current density, or COD. Thermal and current density induced degradation mechanisms are associated with the formation of point defects or dark-line defects, which can migrate into and along the active region, degrading the laser output over time. Often, the lifetime of a laser is specified as the number of hours at which the operating current increases by some percentage, for example 20%, to maintain a specified output power.

In practice, for high power operation, the Large Optical Cavity (LOC) concept with broadened waveguide layers is usually applied [28]. In this case the optical confinement is reduced which is likewise true for the facet load. Further the energy being transported in the cladding layers is very small. Therefore, the cladding layers can be highly doped and made relatively thin, both measures leading to small series and thermal resistances. The disadvantage of a lower modal gain is compensated by the very low loss of such waveguide structures. The low loss provides the means to make long resonator with a length in the range of 2 mm while maintaining high external efficiency. The vertical far-field divergence is determined by the thickness of waveduide layers and the difference of refractive indices between waveguide and cladding layer. Therefore, broadened waveguide layers have a narrow far-field.

1.2. Distributed feedback diode lasers

In the previous section, some basic concepts for high power diode lasers have been introduced. However, one important advantage of diode laser, namely the possibility to operate them in single frequency mode, was not considered. The focus of this section, therefore, will lay on fundamental points of distributed feedback (DFB) diode lasers

which are based on integrating an optical grating into the resonator. In DFB lasers the optical feedback, as the name implies, is not localized at the facets but is distributed throughout the cavity length [29]. This is achieved by the optical grating, that leads to a periodic variation of the longitudinal mode refractive index. Fig. 1.8 shows a typical structure of a DFB diode laser with a Bragg grating physically integrated outside the active region. Optical feedback occurs by means of *Bragg diffraction*, a phenomenon that couples the waves propagating in the forward and backward directions. Longitudinal mode selectivity of the DFB mechanism results from the *Bragg condition*: the coupling occurs only for wavelengths λ_B satisfying:

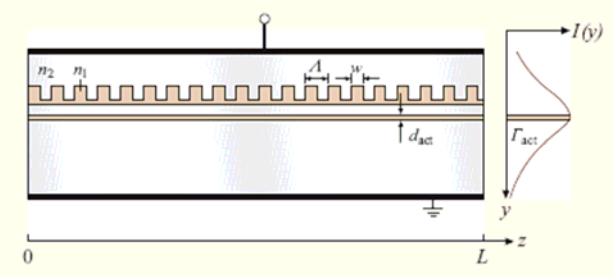

Figure 1.8. *Scheme of a DFB laser structure with an integrated rectangular Bragg grating including the corresponding transversal intensity distribution I(x). [30].*

$$\Lambda = \frac{m\lambda_B}{2n_{eff}} \qquad (1.17)$$

where Λ is the grating period, n_{eff} is the mode effective index, and the integer m represents the order of Bragg diffraction [30]. The coupling between the forward and backward waves is strongest for the first-order Bragg diffraction (m = 1). However, higher-order Bragg diffraction has also been realized [31]-[34]. For a DFB laser operating at λ_B = 0.78 μm, Λ is about 235 nm if we use m = 2 and n_{eff} = 3,3 in Eq. (1.17). Such gratings can be fabricated by using a holographic technique [35]. In this section, the mode coupling, the stopband concept and the spatial hole-burning effect in DFB diode lasers will be briefly discussed.

1.2.1. Mode coupling of DFB lasers

The analysis of coupling coefficient of a rectangular shaped corrugation κ can be described as following:

$$\kappa = \left(\frac{2\Delta n}{\lambda} + j\frac{\Delta\alpha}{2\pi}\right)\frac{\sin(m\pi D)}{m} = \kappa_i + j\kappa_g \qquad (1.18)$$

here κ_i includes all contributions from the refractive index perturbation whilst κ_g covers all contributions from the gain perturbation [36]. Δn denotes the size of the refractive index step and $\Delta\alpha$ designates the gain variation. The coupling coefficient is related to the order of Bragg diffraction (m), the shape, the depth and the grating period (Λ) of the corrugation. The duty cycle D of the Bragg grating given by the ratio

Λ_1/Λ (see Fig 1.18). To get maximal κ, for a first-order grating, $D = 0.5$, for a second-order grating, $D = 0.25$ (or 0.75).

Depending upon the nature of the coupling coefficient, DFB semiconductor lasers are classified into three different groups: purely index-coupled DFB diode lasers, mixed-coupled DFB diode lasers and purely gain- or loss-coupled DFB diode lasers. Fig. 1.9 shows simplified schematic diagrams of these DFB diode laser structures.

- Most practical DFB semiconductor lasers belong to purely index-coupled group, where coupling is solely generated by the refractive index perturbation. A single layer of corrugation is fabricated above (or below) the active layer, e.g. as shown in Fig. 1.9a. Since most carrier recombination is confined along the active layer, the amplitude gain of the DFB laser will not be affected. Therefore, with $\kappa_g = 0$, the coupling coefficient κ is purely real.

$$\kappa = \frac{2\Delta n}{\lambda}\frac{\sin(m\pi D)}{m} \qquad (1.19)$$

- If the corrugation layer is fabricated on the upper part of the active layer as shown in Fig. 1.9b the DFB semiconductor laser will show a mixed coupling characteristic [37]-[39]. Due to the variation of the refractive index along the corrugation layer, index coupling is induced. However, the occurrence of gain coupling needs further explanation. As illustrated in Fig. 1.9b, the active layer thickness becomes a periodic function along the longitudinal direction and so does the optical confinement factor. Such a periodic modulation of optical confinement factor modifies the amplitude gain along the longitudinal direction and so gain coupling is induced [40].

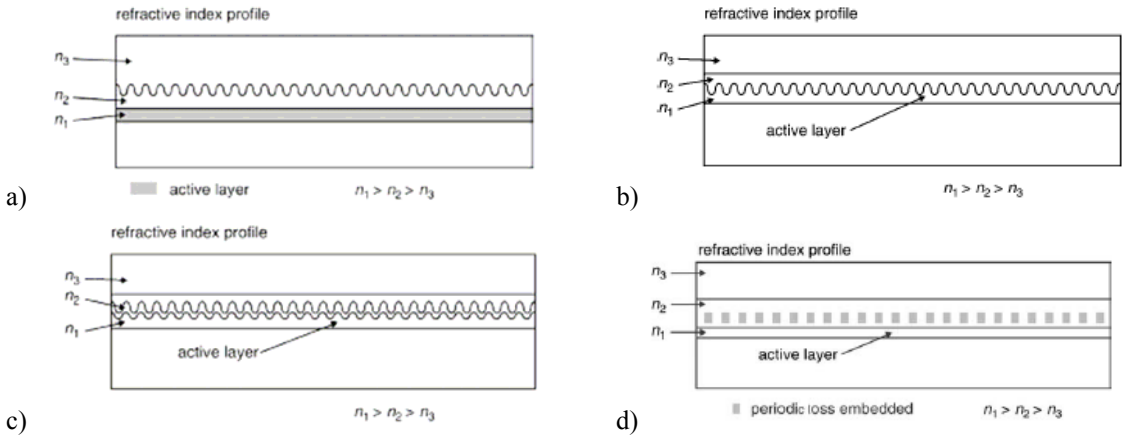

Figure 1.9. *Shematic view of cross section of DFB diode laser; a) purely index-couple DFB semiconductor laser; b) mixed-coupler DFB semiconductor laser; c) purely gain-coupled DFB semiconductor laser; d) purely loss-coupled DFB semiconductor laser. [36]*

- With only one single layer of grating, it is difficult to achieve a purely gain-coupled DFB device. However, by fabricating a second layer of grating on top

of the original one as shown earlier for the mixed-coupled DFB laser, the effect of index coupling can be cancelled out. As illustrated in Fig. 1.9c, the second corrugation demonstrates an inverse corrugation phase with respect to the first layer of grating. Due to the direct modulation of the active layer thickness, it was found that the actual gain coupling coefficient of this structure may fluctuate according to the strength of the injection current. For such a purely gain-coupled structure having $\kappa_i = 0$, the coupling coefficient becomes purely imaginary.

In addition to the possibility shown in Fig. 1.9c, a second method of realizing purely gain-coupled characteristics is to fabricate a periodic variation of loss as sketched in Fig. 1.9d. The optical confinement factor remains constant whilst the cavity loss becomes a periodic function of position z. With such a loss-coupling structure, the strength of gain coupling will not be affected by any change in injection current. On the other hand, owing to the additional loss, the loss-coupling structure results in a higher threshold current.

Comparatively, the design of purely index-coupled DFB semiconductor lasers has received significant attention in the past decade. There are several reasons why the developments of mixed- or gain-coupled DFB lasers were hindered. In a mixed-coupled DFB laser, a large number of non-radiative recombination centers were introduced during the fabrication of the corrugation layer. Since the corrugation layer has direct contact with the active layer, such an increase in non-radiative recombination centers implies an enormous increase in the threshold current. The performance of the laser also deteriorates rapidly as temperature increases. Additionally, the change of amplitude gain becomes complicated since the gain always depends on the injection current. Even though the loss-coupling structure which was proposed by Morthier et al. [41] may ease the problem, it is limited by a higher threshold current. When manufacturing the double grating structure, one must consider the alignment between the first and the second corrugations as this is crucial in the cancellation of the index coupling effect.

1.2.2. Stop-band of DFB diode lasers

First, the stop-band concept of purely index-coupled DFB diode lasers should be introduced to have an understanding about linewidth enhancement mechanism. For a conventional index-coupled DFB laser having zero facet reflection, based on coupled-wave theory for DFB lasers introduced by Kogelnik and Shank [42], the threshold eigenvalue equation in relation with coupling coefficient κ and cavity length L can be written as:

$$\kappa L \sinh(j\gamma L) = \pm \gamma L \qquad (1.20)$$

where γ is complex propagation constant contain gain g and defined by following expression:

$$\gamma = -j\sqrt{\kappa^2 + \left(\frac{g}{2} + j\Delta\right)^2} \qquad (1.21)$$

with $$\Delta \approx n(\omega - \omega_o)/c \qquad (1.22)$$

is considered as detuning parameter of frequency ω to Bragg frequency ω_o.

The detail analysis can be refer to [36], [42], [43]. Here, in Fig. 1.10, we show only the final result with the dependence of the normalized deviation ΔL of the oscillation wavelength from the Bragg wavelength and the normalized threshold gain gL on the normalized coupling coefficient κL. It shows that the threshold gain for a mode decreases with increasing ΔL, and that the deviation ΔL increases with increasing κL. Because of the significant mode dependence of the threshold gain [43], actual oscillation takes place in fundamental modes m = 1 and m = -1. Although these modes have different lasing wavelength the amplitudes of the gain is the same [36]. In fact, such two-mode oscillation has been experimentally observed.

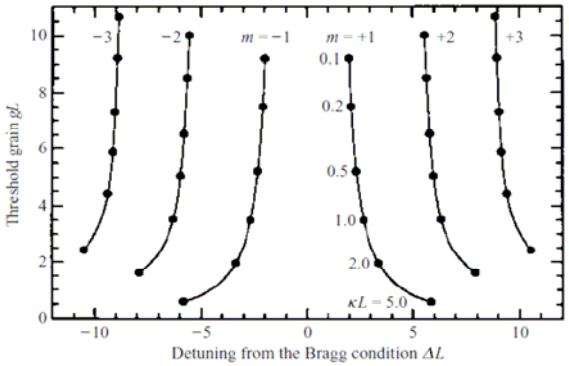

Figure 1.10. *Oscillation threshold gain and oscillation wavelength detuning of an index-coupled DFB laser. [36]*

The above result was obtained under the assumption of zero-reflection facets. For realistic lasers, the facet reflection cannot be neglected, unless the facets are antireflection coated. By reducing the reflectivity for the front facet and enhancing it for the rear facet, the output power can be enhanced, and single-mode oscillation may be achieved. For reflective facets, the oscillation condition is affected by the reflection phase determined by the position(s) of the facet(s) relative to the grating phase [43]. Since the facet is formed by cleaving, it is almost impossible to precisely control the facet position in

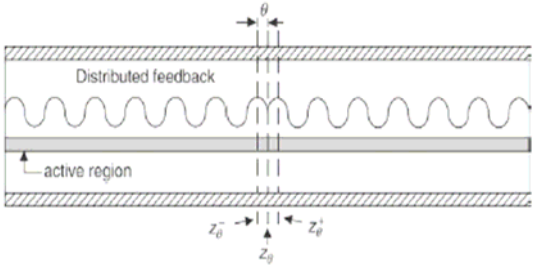

Figure 1.11. *λ/4 phase shift grating. [36]*

order to optimize the reflection phase which would require submicron cleaving accuracy. Accordingly, some fabricated lasers oscillate in two modes, and some of them oscillate in single mode. Due to the uncontrolled degree of freedom in cleaving the chip, there are significant sample-to-sample variations in the oscillation wavelength and the threshold current. This is the most serious shortcoming of index coupled DFB lasers.

To eliminate the problem of remaining two coincident oscillation modes outside the Bragg wavelength, the grating structure should be modified to satisfy the phase condition at the Bragg wavelength. From the boundary condition, to have oscillation at Bragg wavelength, a phase-shift between the right- and left-hand sections of the grating , i.e. a quarter of the optical wavelength in the waveguide (λ/4), must be fulfilled. By modifying the DFB structure as described in Fig. 1.11, we obtain Bragg wavelength at zero detuning ΔL as shown in Fig. 1.12.

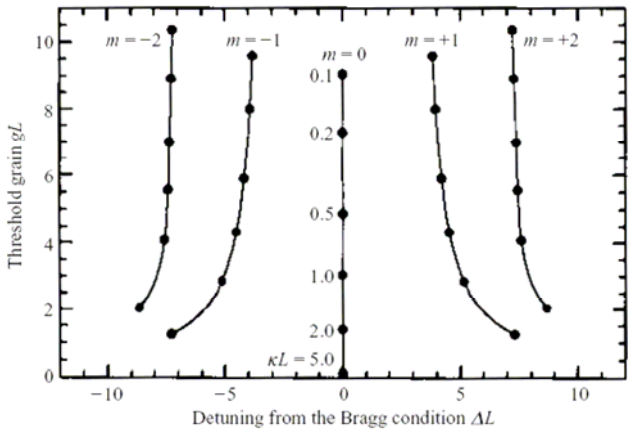

Figure 1.12. *Oscillation threshold gain and oscillation wavelength detuning of a λ/4 phase-shifted index-coupled DFB laser. [36]*

Based on the above discussion, the stop-band concept can be given as follows. For a purely index-coupled DFB laser diode, at the normalized detuning parameter $\Delta L = 0$ (corresponding to Bragg wavelength), the analysis of the complex propagation constant reveals an evanescent wave propagating in the spectral region between two lowest order modes $m = +1$ and $m = -1$ as shown in Fig. 1.10[43]. This is similar to the well-known phenomenon in the crystal structure, i.e. wave propagation in periodic real refractive index structures gives rise to a stop band or energy gap. The stop band here is defined by the gap between mode $m = +1$ and $m = -1$ in Fig. 1.10. The description in optical density distribution of DFB laser emission versus detuning ΔL is shown in the Fig. 1.13. Within this stop band, the wave exponentially decays and hence propagates only over a finite distance. Accordingly, any incident wave is reflected efficiently. Wave propagation only occurs outside the gap. Therefore, within a grating of finite length,

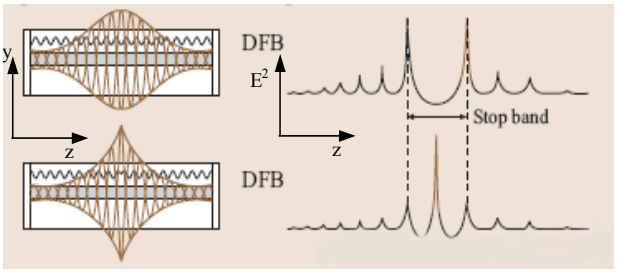

Figure 1.13. *Schematic structural cross sections (left) and the corresponding emission spectra (right) for a DFB laser with and without a λ/4 phase shift. [30]*

the decaying waves tend to only occur near places where the periodic grating is interrupted, such as at a boundary. Waves outside the stop band are travelling waves that show little interaction with the periodic structure of the DFB diode laser. The width of stop band is equal to 2κ and can be experimentally extracted by a measurement of Amplified Stimulated Emission (ASE) close proximity to the threshold of the DFB diode laser.

By introducing gain in the waveguide, the decay can be overcome. For gain-coupled gratings, no frequency stop band occurs. On the other hand, there is now a forbidden band of width 2κ in the wave vector. The calculation of gain-coupled DFB laser results is shown in Fig. 1.14. Another advantage of gain coupled structure DFB lasers is that they are less sensitive to the facet reflectivity phase [43].

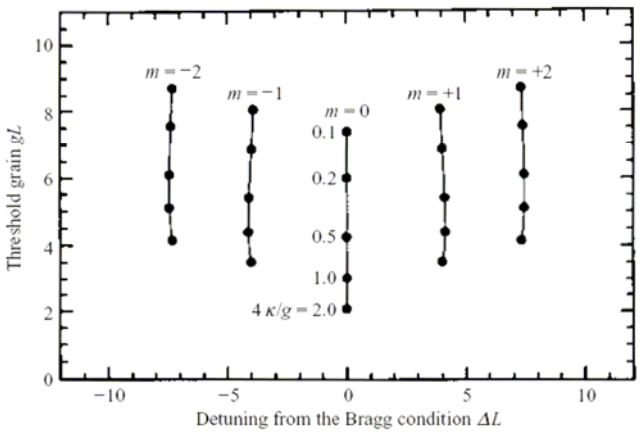

Figure 1.14. *Oscillation threshold gain and oscillation wavelength detuning of a gain-coupled DFB laser. [36]*

1.2.3. Spatial hole-burning effects in DFB diode lasers

Spatial-hole burning is a phrase which is used to describe the depletion of injected-charge carriers due to strong stimulated recombination in regions of high photon density. Because of the relation between refractive-index and charge-carrier density, the depletion of the charge carriers in regions of high photon density locally increases the real part of the refractive-index and reduces the gain or imaginary part of the refractive-index. This can lead to a self-focusing in lateral direction. Lateral carrier-hole burning can be detected by changes in near field and far field patterns as driving current is increased. Strong lateral spatial-hole burning in general invalidates the assumption that the confinement factor of the active region is spatially constant. However, with a sufficiently well designed index guiding structure, in RW laser, vertical spatial-hole burning effect can safely be neglected due to constant intensity in small QW thickness.

The longitudinal distribution of the light intensity in the cavity is connected to the mirror losses via the round-trip gain condition [30]. Thus, a decrease of the mirror losses for the longitudinal modes in a DFB grating is equivalent to increasing longitudinal optical confinement, which means that the photons are concentrated inside the cavity and only a small fraction of the light intensity leaves the resonator through

the end facets. The typical longitudinal photon distribution for a DFB laser with and without a $\lambda/4$ phase shift is shown in Fig. 1.13, revealing the pronounced maximum in the middle of the resonator even for moderate coupling coefficients. This strong in homogeneity of the photon density distribution in DFB lasers leads to an inhomogeneous carrier density distribution above threshold due to the recombination by stimulated emission. With increasing injection current, the carrier density is progressively depleted in regions with a high photon density. This phenomenon is called longitudinal spatial-hole burning (LSHB) and has several important consequences for the static and dynamic behavior of DFB lasers above threshold. First, the mode discrimination is influenced since a variation of the carrier density distribution changes the round-trip gain of the various modes differently, that have different photon density distributions. Thus, the side-mode suppression can degrade with increasing output power due to LSHB. Second, the mode wavelengths change, even above threshold, since the inhomogeneity of the carrier density caused by LSHB leads to an inhomogeneous axial distribution of the effective refractive index [44]. Various DFB lasers with more complex grating structure have been developed in order to obtain a high yield of single-mode devices and a flat axial photon distribution with reduced longitudinal spatial-hole burning:

- $2\times\lambda/8$ phase shifts. The distance between the phase shifts, however, must be optimized to achieve a high yield [45].
- Corrugation pitch modulation (CPM). The DFB grating is divided into three sections. The corrugation period in the central section is slightly higher than in the outer sections so that the phase shift is quasi-continuously distributed along the cavity [46].
- Axial variation of duty cycle by using, e.g., a holographic double-exposure technique [47].
- Axial variation of coupling coefficient by variation of the etch depth [48] or sampled gratings [49].
- Bent waveguides superimposed on homogeneous grating fields can be used to obtain quasi continuously and arbitrarily chirped gratings with high spatial resolution [50].
- Axially inhomogeneous injection using a three-electrode structure. Spatial hole burning can be compensated for if the injected current density is higher in the central section near the peak of the photon density, thus reducing the gain of the side modes that then suffer from the lower current in the outer section [51].

There is a significant difference between gain- or loss-coupled DFB lasers and index-coupled DFB lasers: in the case of a negligible parasitic index coupling the

longitudinal photon distribution is similar to that of a diode laser based on a FP resonator. Thus, the strong inhomogeneity of the photon distribution in DFB lasers and the corresponding problem of longitudinal spatial hole burning are reduced in gain-coupled devices.

1.3. Linewidth characteristic of diode lasers

1.3.1. Schawlow-Townes linewidth

It has been known since the earliest days of the laser that spontaneous emission both initiates laser oscillation and fundamentally limits the degree of monochromaticity. Since the spontaneous emission cannot be fully described semiclassically, a rigorous theory of fundamental linewidth demands field quantization. Such a theory has been available in various versions for many years [52], [53]. Even before the first laser was experimentally demonstrated, Schawlow and Townes calculated the fundamental (quantum) limit for the linewidth of a spontaneous emission in resonance condition [54]. This lead to the familiar formula for the linewidth when the field and the gain coefficient in a saturable medium, namely *Schawlow–Townes* equation*:*

$$\Delta \nu_{ST} = \frac{4\pi h \nu (\Delta \nu_c)^2}{P_{out}} \qquad (1.23)$$

with the photon energy $h\nu$, the resonator bandwidth $\Delta\nu_c$ (half width at half-maximum, HWHM), and the total output power P_{out}. It has been assumed that there are no parasitic cavity losses.

Beyond *Schawlow–Townes*, the detail analysis has given later on another form of laser linewidth expression as following:

$$\Delta \nu_{ST} = \frac{R_{sp}}{4\pi I} \qquad (1.24)$$

where I is the average photon number in the cavity, R_{sp} is the spontaneous emission rate coupled to the lasing mode and is equal to the stimulated emission rate of one laser photon. R_{sp} is obtained from the Einstein relation:

$$R_{sp} = \upsilon_g g n_{sp} \qquad (1.25)$$

In this formula υ_g is the group velocity of light, and g is the threshold gain [55]. n_{sp} is called the spontaneous emission factor which is given by:

$$n_{sp} = \frac{1}{1 - \exp[-(eV - h\nu)/kT]} \qquad (1.26)$$

with $h\nu$ is the photon energy, and eV is the quasi-Fermi level separation.

The relation between total output power and average photon number [55]:

$$I = \frac{P_{out}}{\alpha_R \upsilon_g h\nu}. \qquad (1.27)$$

The α_R is the resonator loss, which is related to the threshold condition:

$$\alpha_R = g - \alpha_i, \qquad (1.28)$$

here α_i is the cavity loss.

Combining equations (1.25) , (1.27) to (1.24), we have:

$$\Delta\nu_{ST} = \frac{\upsilon_g^2 g n_{sp} \alpha_R h\nu}{4\pi P_{out}} \qquad (1.29)$$

With assumptions $\alpha_i = 0$, $n_{sp} = 1$, and $\Delta\nu_c = \upsilon_g\alpha_R/4\pi$ as in Ref. [56], the equation (1.29) return the form of original *Schawlow–Townes* equation (1.23).

1.3.2. Linewidth enhancement

The previous section has given the fundamental limit to the laser linewidth determined by spontaneous emission. This standard quantum theory of the laser linewidth is restricted to the case of small output couplings (i.e., laser mirror reflectivities near unity) [52]. In this limit the field and the gain coefficient are approximately spatially uniform, thus simplifying the theory and providing Schawlow-Townes linewidth. However, this straightforward theory that is useful for gas and solid-state lasers as well as microwave oscillator usually give over an order-of-magnitude too low an estimate of static linewidth and totally inadequate approximation to the dynamics linewidth, and this must be explained. Laser linewidth is normally much larger than the Schawlow-Townes limit (at least more than one order of magnitude observed in experimental results). The contribution of the other parameters and effects in the diode lasers (phase, amplitude fluctuation, spatial-hole burning,…) cause an enhancement of the linewidth. This section will consider some main influences on linewidth of diode lasers with most important approaches that represented via the enhancement factors, namely Petermann and Henry factors.

a. Petermann's "excess spontaneous emission" factor

This section introduces the first approach that deduce the correction for the broadening of Schawlow-Townes fundamental linewidth known as Petermann factor that modify the spontaneous-emission terms in standard rate equation under increasing outcoupling (in this case the spatial variation in the intracavity has to be considered) due to non-power-orthogonality of the modes. Petermann factor can be separated into two terms:

K_{tr} to account for transversely and K_z to account for longitudinal distribution of optical intensity (along z direction or cavity axial direction). The net effect is a spontaneous-emission factor $K = K_{tr}$ x $K_z > 1$. In Ref. [57], Peterman suggested an analysis formula to calculate K factor as following:

$$K = \frac{\left|\iiint |E(x,y,z)|^2 dxdydz\right|^2}{\left|\iiint E^2(x,y,z)dxdydz\right|^2}, \qquad (1.30)$$

where E is the optical fields. In practice, K factor is reduced to K_z because the longitudinal distribution of optical intensity is dominant and we can write:

$$K_z = \frac{\left|\int \left(|E^+(z)|^2 + |E^-(z)|^2\right)dz\right|^2}{\left|2\int E^+(z).E^-(z)dz\right|^2}, \qquad (1.31)$$

here E^+ and E^- are forward- and backward- fields, respectively. When the saturation and spatial hole-burning effects are included, the K factor will be modified by changing of optical fields. The spontaneous emission rate R_{SP} in equation (1.24) will be replaced by:

$$R_{SP,eff} = K_z R_{SP} \qquad (1.32)$$

Therefore the linewidth will be enhanced by:

$$\Delta\nu = K_z \Delta\nu_{ST} \qquad (1.33)$$

If the cavity loss $\alpha_m L = 1.95$ for a non-phase shifted DFB laser with $\kappa L = 2$ is considered, for example, a correction factor $K_z = 1.94$ is obtained. The enhancement factor K_z versus the cavity loss $\alpha_m L$ is shown in Fig.1.15 [57].

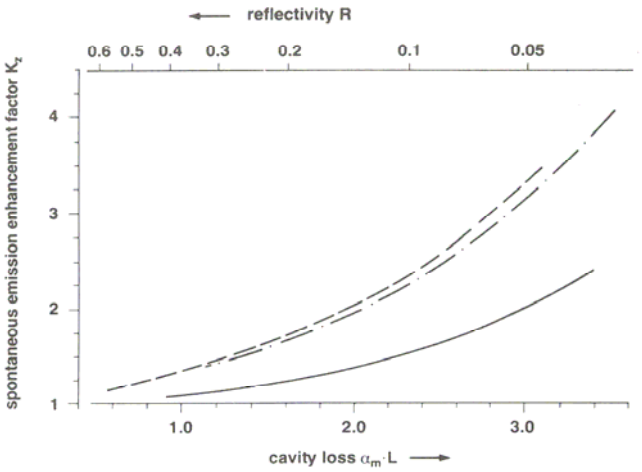

Figure 1. 15. *Axial spontaneous emission enhancement factor K_z versus the cavity loss $\alpha_m L$ or the reflectivity R: DFB without phase adjustment (dashed dot); DFB laser with $\pi/2$-phase shift (dashed); Fabry-Perot laser (solid). [57]*

b. Henry's linewidth enhancement factor

Henry had done another theoretical approach for correction of Schawlow-Townes fundamental linewidth in Ref. [54]. This section summaries some key points of his work. The width of the laser line can be thought of as due to fluctuation in the phase of the optical field. These fluctuations arise from spontaneous emission events, which discontinuously alter the phase and intensity of the lasing field.

Beside the phase change caused by spontaneous emission, there will be an additionally phase change resulting from the change in optical field intensity. The change of the optical density, which results in a change of the real part of the refractive index. The change of the real part of the refractive index can be assumed to be proportional to the change of the imaginary part of the refractive index or equivalently to change of the gain.

$$\Delta n' = \alpha\, \Delta n'' = -(c/2\omega)\, \alpha\, \Delta g \qquad (1.34)$$

The change in $\Delta n'$ results in an addition phase shift of the laser field and in additional line broadening. In general, a narrow spectral change in gain (or absorption) is accompanied by a change in n'' of the same shape and change in n' of comparable magnitude, but with a dispersive shape having two peaks of opposite sign occurring on either side of the peak in n''. For spectral hole burning, the peak in $\Delta n''$ is centered at the laser line and, therefore, $\alpha = \Delta n'/\Delta n''$ will be small compared to unity. On the other hand, the peak change in gain due to a change in carrier density occurs well above the energy of laser line, so that in this case α is large compared to unity. This is clearly shown in the results of Henry in [55]. After the analysis done by Ref. [55], for both bulk and QW laser we have an enhancement of linewidth by factor $(1+\alpha^2)$:

$$\Delta\nu = (1+\alpha^2)\, \Delta\nu_{ST} \qquad (1.35)$$

here α is called linewidth enhancement factor or Henry factor.
There have been many theoretical calculations showing that the α factor is substantially reduced in multiple quantum well compared to bulk active layer lasers [58]. In the Ref [58], α value was predicted smaller for lasers with strained quantum well structures than in conventional quantum well lasers.
In experiment, there are also several results that confirm the reduction of α in the quantum well lasers compared to bulk material lasers. Koch *et al.* in [58] demonstrated that, for similar structure of InGaAs, Henry factor is reduced from $\alpha \approx 6$ of bulk material lasers to $\alpha \approx 3$ of multiple quantum well lasers. Analogous results for InGaAsP can be found in Ref [58].

1.3.3. Linewidth floor and rebroadening effect

The analysis of previous sections shows that the laser linewidth inversely depends on optical power. Therefore, there is a great motivation to try to make the linewidth narrower by running laser at as high power as possible. Such experiments reveal additional broadening mechanisms that result in a minimum linewidth value considered as “linewidth floor” when power is increased.

For the first time, Mooradian et al. [59] had demonstrated the observation of linewidth floor for AlGaAs laser. Welfold and Mooradian, in their work [60] show that linewidth narrows in a manner that depends linearly of inverse power and consistent width theoretical formula. However, contrary to the linewidth formula the extrapolated linewidth does not go to zero at infinite power but approaches a finite value. This behavior implies a limit of linewidth reduction with increasing of optical power (Fig. 1.16). When the optical power is further increased the laser linewidth may be saturated at linewidth floor value or increased again with power for specific laser. The latter behavior is considered as linewidth rebroadening effect that was observed in calculation results and also experimental results [62]-[69].

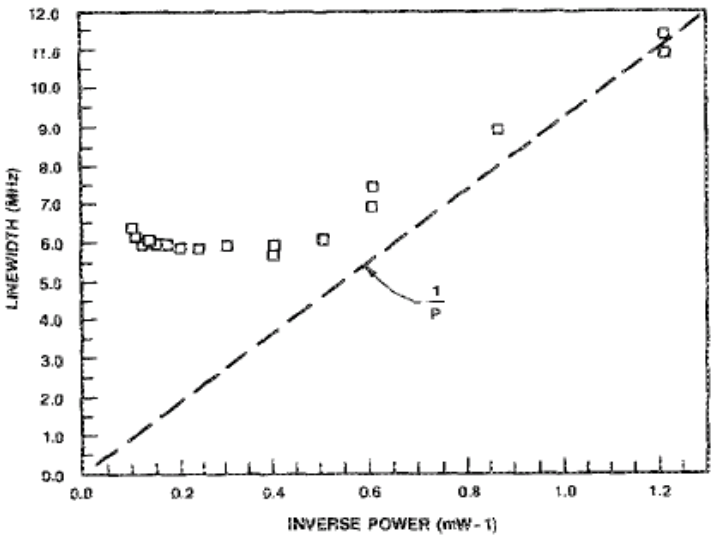

Figure 1. 16. *Linewidth versus inverse output power as measured by self-delay heterodyne. [61]*

The explanations for linewidth floor and rebroadening effect were given in several works as mention in above Ref. [59], Mooradian has suggested that the linewidth floor is due to carrier density fluctuations. Carrier number fluctuation will alter the refraction index and hence the laser frequency; however, they also alter the gain, and this lead to feedback mechanisms in a laser above threshold that suppresses such fluctuation. The linewidth rebroadening causes by several reasons and relatively complicated for a clear explanation. Generally, if the spatial hole burning increase at high power operation, the linewidth will be broadened. Beside that, the following effects were usually considered when the linewidth rebroadening was observed:

- In Ref [62], one mechanism of rebroadening was supposed by Pan et al., where the mode partition noise that relates to side mode suppression ration (SMSR) plays an important role if the SMSR is below 30 dB. When the SMSR excess 30 dB, the influence of mode partition noise into linewidth eliminates substantially. So that, another mechanism has to be taken into account.
- The results done by Agrawal in [68] show that the semiconductor lasers detuned to operate away from the gain peak, the nonlinear index changes can even lead to a rebroadening of the laser linewidth at high-output powers.
- Kikuchi's work [69] approached the explanation for linewidth rebroadening by measuring the frequency noise spectrum as well as the power spectrum. Based

on the result of the FM-noise spectrum that consists of a white-noise component and a 1 /f-noise component as following:

$$S_f(f) = C/P + K/f \qquad (1.36)$$

where C = 1.5 x 10^4 (Hz/W) and K = 5.8 x 10^{11} (Hz^2). The spectral density of the former is inversely proportional to the output power, whereas that of the latter is power independent. From these results, he concluded that the residual linewidth originated from the 1/f noise.

- By considering carrier heating effect in strained quantum well, the Ref. [63] was given a theoretical analysis as well as an experimental evidence to prove that the joint effects of nonlinear gain and nonlinear refractive index contribute to rebroadening of laser linewidth beside spatial-hole burning.
- Another idea to explain spectral linewidth rebroadening in MQW-DFB diode lasers was proposed by Yamazaki et al. in [65]. This is based on the phenomenon of spontaneous emission noise in SCH/Barrier layers that cause and an excess spectral linewidth rebroadening.

1.3.4. Simulation of linewidth of high power DFB laser diode

The spectral linewidth of DFB laser diodes is theoretically simulated in several previous works [70]-[73]. The numerical calculation shows that DFB lasers with long cavity lengths and large coupling coefficient have very narrow linewidth. The effects of phase shift and mirror facets on the spectra linewidth of DFB lasers have also analyzed [71],[74]. In this section, we present a theoretical calculation of DFB spectral linewidth at 780 nm. The simulation considers the behavior of spectral linewidth versus optical output power with the variation of some parameters, e.g. coupling efficiency, grating phase at laser facet. This work has done by H. Wenzel at Ferdinand-Braun-Institut.

According to the disscusion in Ref. [74], the contributions due to spontaneous emission noise $\Delta\nu_{sp}$, inhomogeneous carrier density fluctuations $\Delta\nu_{NN}$ and side mode partition noise $\Delta\nu_{sm}$ have been taken into account in the calculation of the linewidth of DFB laser as following formula:

$$\Delta\nu = \Delta\nu_{sp} + \Delta\nu_{NN} + \Delta\nu_{sm} \qquad (1.37)$$

In above expression, since the side mode suppression ratio (SMR) normally exceeds 40 dB for DFB lasers, $\Delta\nu_{sm}$ is almost zero and can be neglected. For contribution of inhomogeneous carrier density fluctuation, $\Delta\nu_{NN}$ is small compared to $\Delta\nu_{sp}$. Therefore, the linewidth calculation was reduced to only with spontaneous emission noise $\Delta\nu_{sp}$.

The spectral linewidth $\Delta\nu$ of laser diodes considering only spontaneous emission noise $\Delta\nu_{sp}$ is rewritten here:

$$\Delta\nu = \frac{KR_{sp}}{4\pi I}\left(1+\alpha_{eff}^2\right) \qquad (1.38)$$

The spontaneous emission rate R_{sp}, the photon number I, and the effective Henry factor α_{eff} are obtained by integrating the corresponding material functions with appropriate weighting functions over the transverse plane and the longitudinal direction as explained in [74] and [75]. They include lateral and longitudinal spatial holeburning.

The above fomulation allows for numerical calculation of spectral linewidth of 780 nm. Fig. 1.17 shows the calculation of linewidth of the 780 nm DFB lasers with cavity length of 1.5 mm for difference coupling coefficients. In this result, the linewidth is not proportional to 1/P due to spatial holeburning. It is necessary to note that when we compare the result to a previous work [76], the magnitude of $\Delta\nu_{NN}$ due to lateral hole burning in [76] was larger, because another set of parameters had been used in the simpler model. Nevertheless, both lateral and longitudinal hole burning influence $\Delta\nu$. Although the contribution of the longitudinal hole burning increases with P, mainly due to an enhancement of α. The model of the material α factor yields a somewhat smaller value for the α factor than it is usually accepted for this material system. Therefore, the calculated linewidth magnitude seems to be too small [74].

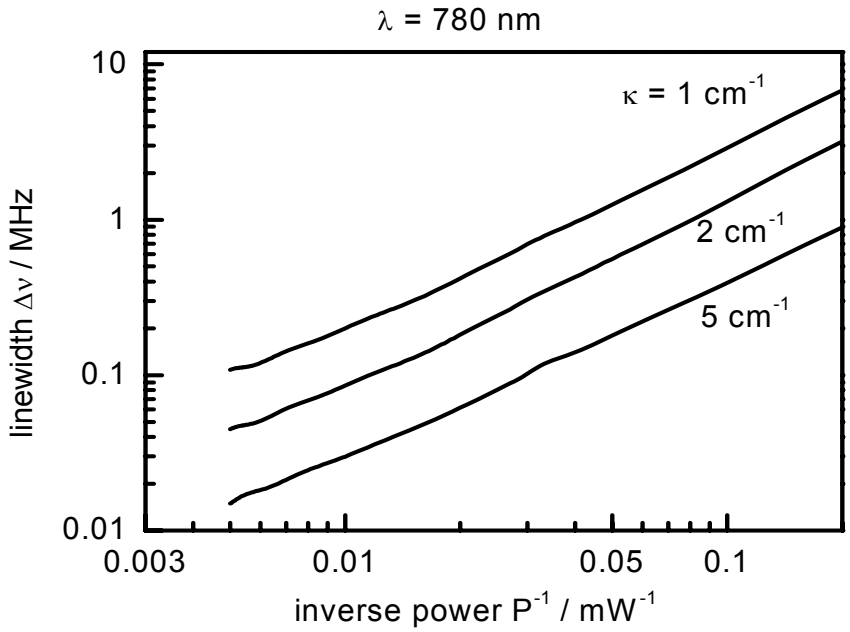

Figure 1.17. *Linewidth versus inverse output power of the 780 nm DFB lasers with various coupling coefficients.*

The linewidth of DFB lasers is proportional to the threshold field gain δ_{th} of DFB that is mainly determined by the coupling coefficient κ. According to the coupled-mode equation [42], a larger κL (where L is cavity length) gives a smaller $\delta_{th}L$. The

calculation of linewidth shown in (Fig. 1.17) was done with the cavity length of 1,5 mm and coupling coefficient κ varied with the values of 1, 2, and 5 cm^{-1}.

The linewidth of 780 nm DFB lasers were also simulated as function of phase of rear facet. The phase of front facet ϕ is defined from Fig. 1.18 and it is similar at rear facet as follow formula:

$$\phi = 2\pi\delta/\Lambda \qquad (1.39)$$

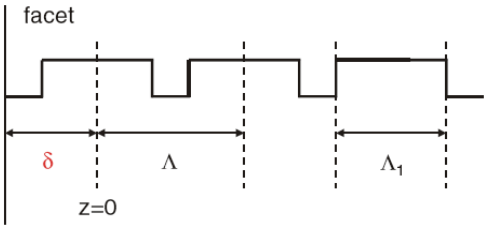

Figure 1.18. *Definition of grating phase at the front facet (similar at the rear facet). [19]*

The complex field reflectivities of the front and rear facets versus phase are expressed by:

$$r_i = |r_i| e^{j\phi_i} \qquad (1.40)$$

where $|r_i|$ is amplitude reflection coefficients at the laser facets, i = 1, 2 at front or rear facet, respectively.[36]

The threshold current I_{th} varies due to a variation of the phases of the grating [19] and the threshold gain g also changes with different value of the phases of the facets [36]. Thus, the linewidth of the DFB lasers is a function of the grating phase.

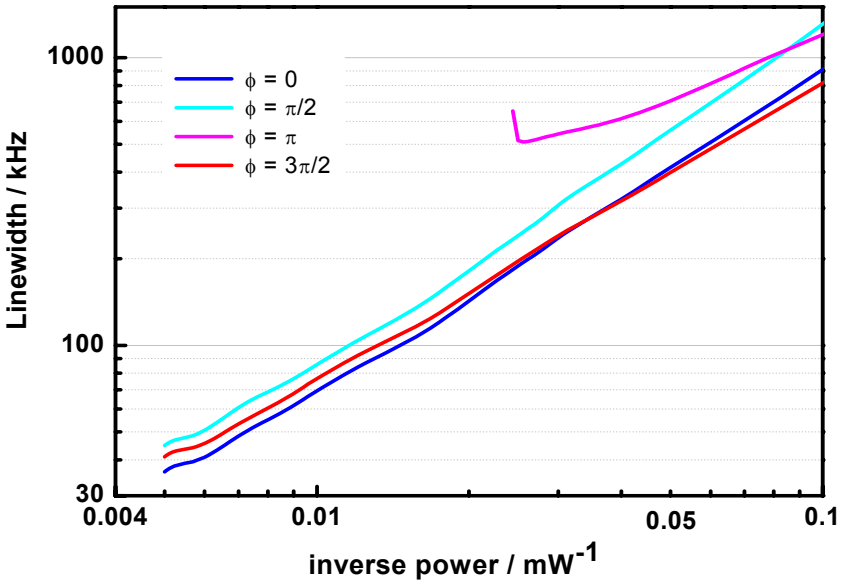

Figure 1.19. *Linewidth versus inverse output power of 780 nm DFB lasers with various phase of rear facet.*

Based on variation of the phase of rear facet of 0, $\pi/2$, π, 2π, the linewidth of 780 nm DFB lasers was calculated versus inverse output power for the lasers with the cavity length of 1.5 mm and the coupling coefficient of 2 cm^{-1}. The results are shown in Fig. 1.19.

Chapter 2.

Experiment

2.1. Device fabrication

In this section, we will describe some key points of the technological chain underlying the fabrication of solitary high power DFB diode lasers with a ridge waveguide (RW) structure. The lasers investigated within this thesis work require the following fabrication steps, namely, i) epitaxial growth of the gain medium structure on a crystalline substrate, ii) processing of the grown wafer to realize the lateral structure including the metallization of the contacts, iii) cleaving and coating of the resonator facets, and separating the individual chips for packaging on a heatsink and, finally, iv) housing in an appropriate can. The technological chain of DFB diode laser fabrication mostly obeys these steps. However, the implementation of internal gratings requires a modification of the regular RW structure fabrication process. Two-step epitaxy is required to implement a grating between the first and second phase of

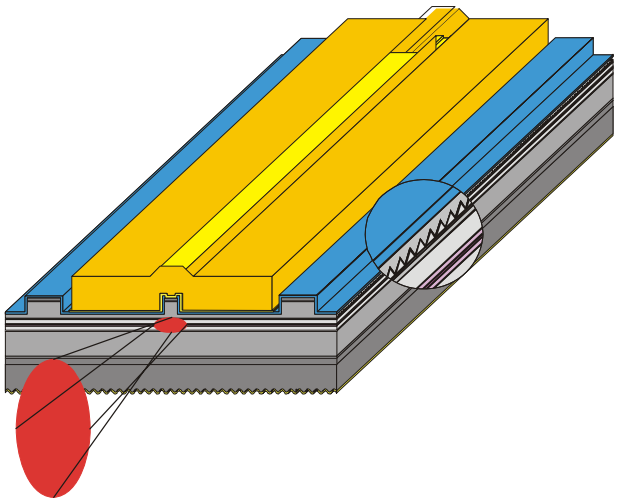

Figure 2.1. *Scheme of RW-DFB laser.[FBH internal]*

epitaxial growth. After the final step, the geometrical structure of solitary DFB laser diode resembles the one shown in Fig. 2.1.

2.1.1. Epitaxial growth and grating implementation

The vertical structure of DFB diode lasers can be fabricated either in single or multiple growth steps. The Bragg gratings in almost all DFB high power diode lasers are embedded into the epitaxial layer structure which requires a two-step epitaxy [19].

Fig. 2.2 describes the vertical structure of a DFB laser emitting at a wavelength near 780 nm. This structure design employs an AlGaAs heterostructure for the waveguide and cladding layers. The GaAsP quantum well is embedded in the AlGaAs waveguide to form the active region of the device. The grating layer is implemented within the cladding and has a spatial structure that is shown in the inset of Fig. 2.2. There are several properties of this vertical structure that deserve a brief description:

- The GaAsP QW is tensile-strained which forces the polarization of laser emission into the TM mode [77].
- Owing to the high affinity of aluminum to oxygen, an Al-containing surface exposed to air can hardly be overgrown in a conventional MOVPE reactor. Therefore, the Bragg grating is formed in an Al-free layer. Additionally, because of absorption at 780 nm of the GaAs material, a sequence of InGaP/GaAsP/InGaP embedded into the p-cladding layer must be used for the grating layer.
- The coupling coefficient κ between the forward and backward propagating waves depends on the difference between the refractive indices of the GaAsP layer and the surrounding AlGaAs layer, on the thickness of GaAsP, and on the distance d between the grating layer and the active region. The difference between the refractive indices is determined by the composition of GaAsP layer. The GaAsP layer can not be grown thicker than 20 nm due to the critical thickness of strain layer. Therefore, the coupling coefficient can be adjusted most strongly by the distance d between the InGaP/GaAsP/InGaP layer sequence and the active layer.

The epitaxial growth of a DFB diode laser vertical structure is performed by low-pressure metal-organic vapor phase epitaxy (MOVPE) methods [23]. The epitaxial procedure for the fabrication of DFB diode lasers takes place as follows. The first growth step is performed on a GaAs substrate. As depicted in Fig. 2.2, in this step n-GaAs buffer, n-AlGaAs graded index strain compensator, n-AlGaAs cladding, n-AlGaAs waveguide, active region, p-AlGaAs waveguide, the first part of the p-AlGaAs cladding, and an InGaP/GaAsP/InGaP layer sequence are deposited. The

active region includes a 14 nm GaAsP QW embedded between two thin AlGaAs layers that are typically 10 nm thick. The first growth is finished with a temporary 10 nm GaAs layer on top that will be removed during the grating implementation process [78].

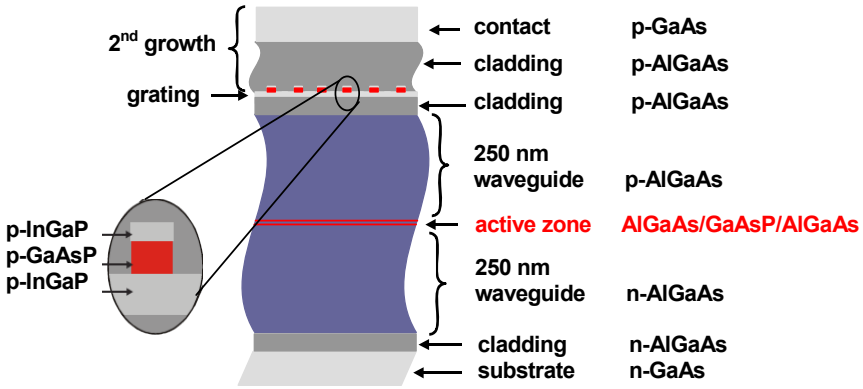

Figure 2.2. *Schematic view of epitaxial layer structure of DFB laser diodes emitting near 780 nm.*

After the first epitaxial step, the wafer is cleaned with an organic solution, e.g. ethanol, and oxides are removed from the surface. The photo-lithography is now used to imprint the grating into the laser structure. Structuring the wafer starts with depositing a thin photoresist layer. The photoresist is exposed with a UV laser in a holographic setup. This setup offers fast writing speed.

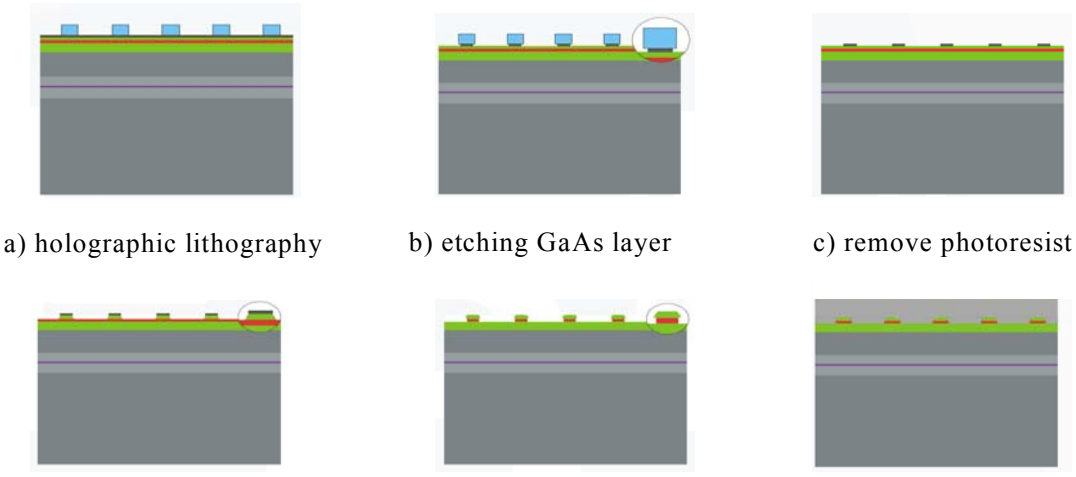

Figure 2.3. *Process technology steps for grating procreation.[FBH internal]*

Fig. 2.3a shows the surface of the wafer after the holographic lithography step. The photoresist that remains after UV exposure and development defines the grating structure for the next fabrication steps. The sample is next etched by tartaric acid to make temporary GaAs layer in the grating patterning form (Fig. 2.3b). Then, the photoresist is removed by a mixture of pure organic solvents. At the end of this step,

the wafer surface has a GaAs pattern on top as shown in Fig. 2.3c. In the next step, a $HCl:H_3PO_4$ solution is used for selective etching of the InGaP film, which will define the grating. The GaAs layer is not affected by this solution (Fig. 2.3d). In the final step, the tartaric acid removes the GaAs on top. In parallel, the GaAsP layer is etched where the InGaP is not present, see Fig. 2.3e. Now, the wafer is ready for the second epitaxial growth with a grating period Λ of about 235 nm (see Fig. 2.4) for 780 nm DFB lasers as discussed in section 1.2

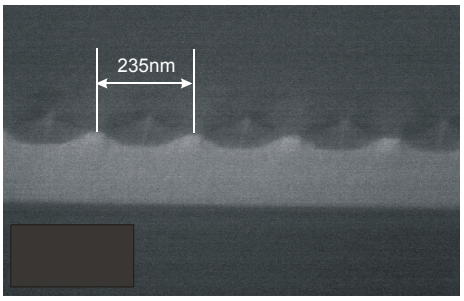

Figure 2.4. *SEM picture showing the buried second order Bragg grating Λ= 235 nm.[78]*

When the implementation of the grating is completed, the wafer surface is cleaned and the second growth can start. In this step, the growth of the p-AlGaAs cladding is continued. Finally, the p-GaAs contact layer is grown on top of the wafer.

2.1.2. RW process and metallization

After the final growth step, the wafer is ready for the RW implementation process, which will realize the lateral structure of DFB laser. For the 780 nm DFB lasers used throughout this thesis work, a ridge-waveguide with mesa widths varying between 2.2 and 3 µm were fabricated. This structure ensures single lateral mode propagation along the optical cavity. The profile of this structure is shown in the SEM picture in Fig. 2.5. This process step also includes the metallization process to provide electrical contacts and to provide a contact layer for mounting the laser chip on a heatsink.

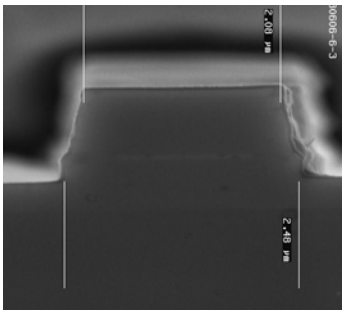

Figure 2.5. *SEM picture of the epitaxial layerstructure showing the ridge waveguide. [78]*

Lateral optical confinement is achieved with a RW structure (Fig. 2.6). First, the photoresist is coated onto the wafer surface (Fig. 2.6a). After exposure, the p-GaAs, the graded index (p - AlGaAs) and cladding layers (p - AlGaAs) are etched by reactive ion etching. The etching is stopped at the cladding layer. The photoresist is removed (Fig. 2.6b). The next step consists of depositing an insulating layer to define the spatial window for the injection current flow. SiN_x is usually used for this purpose and is deposited by plasma-enhanced chemical vapor deposition (PECVD). Carrier

confinement is realized with a SiN_x-insulation layer that is opened on top of the RW by dry etching (Fig. 2.6c) [79].

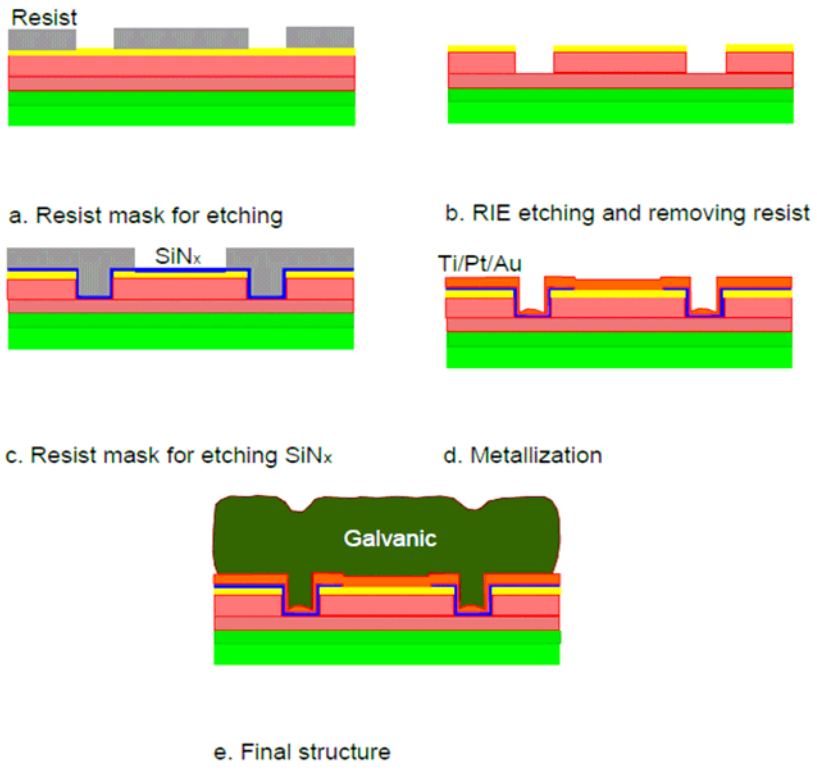

***Figure 2. 6**. Technology to fabricate a quasi-index-guided laser diode. [FBH internal]*

The wafer is now ready for the p-metallization process. The p-metallization with Ti/Pt/Au is performed inside the chamber of the electron-beam evaporator. The metallization is removed in a 20µm broad stripe between the sections using a lift-off process (Fig. 2.6d). A several microns thick gold alloy is coated onto the p-metallization to provide better heat dissipation for the chip. The final profile of p-side is shown in Fig. 2.6e.

Finally, the n-GaAs substrate is thinned from the bottom side until a wafer-thickness of about 150 µm reached. Then, a n-metallization (Ni/Ge/Au) and a strengthening (Ti/Pt/Au) layer are processed. Their contributions to the series resistance of the diode should be as small as possible. Further, the metallization provides the basis for mounting the diode laser on a heat sink. Therefore, this process should be appropriately treated to allow (i) soldering the chip on a submount for heat removal and (ii) wire bonding.

2.1.3. Coating

In order to provide a reliable resonator mirror for laser operation and to allow for efficient scaling of the output power, the output facet of the diode laser must be coated

appropriately. For all diode lasers used within this thesis work the rear facets are coated to provide a reflectivity of 95% and the front facets are anti-reflection coated so that they provide a reflectivity of 0,01%, 5%, 10%, or 30%. Adjusting the output facet reflectivity provides a means to optimize the DFB laser performance. The impact of the reflectivity on the laser characteristics will be discussed in the result section.

One of the most crucial aspects of high-power semiconductor-laser technology is the realization of long-term stable laser mirrors at the facets of the cleaved wafer. The power, that is heating the facet region, is concentrated in a small area so that the intensity easily reaches values on the order of 10 MW/cm^2, which is close to the damage threshold of a laser facet. Therefore, processing of the high-power laser facets must be carefully carried out. The laser mirrors are realized by a three-step process:

- cleaving the processed wafers into laser bars
- passivation of the cleaved surfaces
- coating to the desired reflectivity

The process has to mainly meet three requirements. First, the desired reflectivity has to be matched. A thin film of Al_2O_3 is used to coat the laser facet to a reflectivity of less than 10%, higher reflectivities are realized with pairs of thin films of Al_2O_3/TiO_2 or SiO_2/Ta_2O_5. Second, the process has to ensure a device life time of several thousand hours even under high-power operation. Third, the coating process must be a reproducible and cheap technology that is suitable for mass production [80].

2.1.4. Housing

a) 

b) 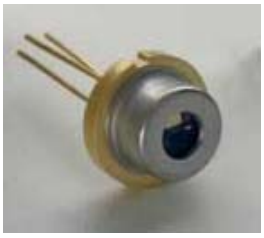
c) 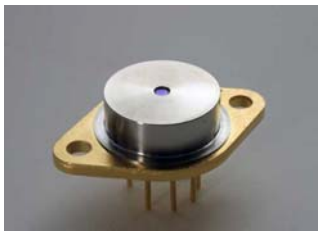

Figure 2. *7. Package of single HPDLs: (a) C-mount; (b) SOT; (c) TO 3.[FBH/schurian.com].*

In this section, we briefly describe some packaging configurations that are usually applied for DFB diode laser chips. Packaging is the final but most cost-intensive process in HPDL technology. It must fulfill two key requirements: high quality electrical contact and good heat transfer. The chip dimension is relatively small: the cavity length is typically 1 to 3 mm (6 mm at most) and the chip width corresponds to about few hundred micrometers. Hence, “packaging induced strain”, which causes mechanical strain on the active region, will be substantially eliminated (for more detail

see [81]). First, a single emitter is cleaved. The laser chip is then soldered on a submount, e.g. a CuW or AlN plate. It is oriented either p-side up or p-side down. Next, the laser with the submount is mounted on a heatsink, and wires are bonded to connect the laser chip with the housing's electrical interface. There are two classes of the packaging schemes for single emitter diode lasers, namely schemes without and with cap. An example for the first scheme is a passively cooled heatsink, the so-called C-mount, which comes in standard dimensions (see Fig. 2.7a). The lasers C-mount can be used only in the laboratory condition with limited power of about 10 W. For capping high-power single emitter lasers, the SOT (Small Outline Transistor) or TO3 housings are typically used. Both of them are suitable for laser diodes and transistors. The lasers are protected from outside damaging and can operate in the normal condition. The limited power of the SOT is few hundreds mW, and of TO3 is about 1 W. These are shown in Fig. 2.7. In this thesis work all three housing types have been used.

2.2. Experimental setups for measurement of fundamental characteristics of high power diode lasers

In this section the experimental setups used for measurements of fundamental characteristics of high power DFB lasers will be introduced. All advanced studies rely on the analysis of these characteristics. First, a detailed description of the setup applied for the electro-optical characterization will be given. The two most important characterizations, i.e. power and voltage vs. injection current, can be carried out with this setup. Second, an introduction to the equipment employed for optical spectrum analysis will be another content of this section. By using this setup, we can perform current- and temperature-dependent characterizations of the optical spectrum of the DFB lasers. Third, in the final subsection, the spatial beam property characterization setup will be described. Beside providing spatial beam profiles of DFB lasers at fixed operating conditions (constant injection current and temperature), the setup also provides the means to investigate how the spatial beam properties evolve when the operating parameters, e.g. current and temperature, are modified.

2.2.1. Optical power and voltage versus injection current (PUI characterization)

The Power-Voltage-Current (P-U-I) characteristic is one of the most important features of high power diode lasers. The optical output power and the junction voltage of the diode lasers are measured versus forward bias current. The measurement setup is

shown in Fig. 2.8 and includes the following three main parts: diode laser and diode laser mount, current and temperature controller, and various measurement equipment. The setup is controlled by a computer via GPIB interfaces.

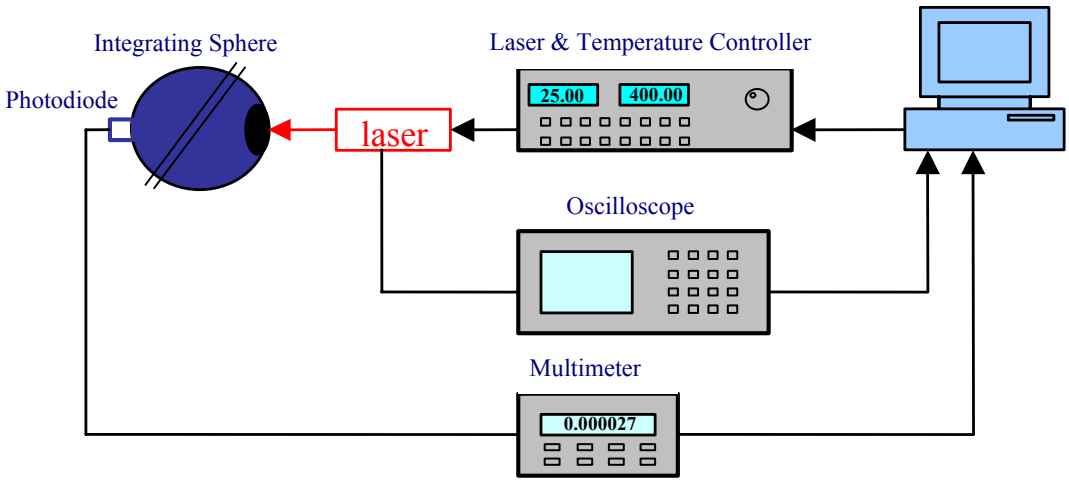

Figure 2.8. *PUI characteristic measurement diagram.*

In this setup the current-temperature controller Lightwave ILX-LDC 3724B is employed and serves two functions. It provides injection current for the diode laser with a maximum output current of 500mA and it stabilizes the diode laser mount temperature by means of a controlling the current through a thermo-electric cooler.

The diode lasers are mounted to the plate of the laser holder which is a Newport model 700 series laser diode mount. This mount comes with two 12.5 W thermo-electric coolers that can actively cool and heat the holder, and with a 10 kΩ thermistor that provides precise temperature measurement of the laser diode mount.

For optical power measurement of high power diode lasers the laser radiation is collected by an integrating sphere within the surface of which the optical power is homogeneously distributed. The photocurrent signal from a photodiode located inside the sphere is recorded by means of a digital multimeter (HP 34401A) and is then transferred to a computer. The photocurrent signal is now converted to optical power by scaling the signal with an appropriate coefficient that depends on the laser emission wavelength. Simultaneously, the voltage across the laser diode junction is determined with a digital oscilloscope and stored to the computer.

During the measurement the relevant parameters, i.e. the operating current (as set at the diode laser controller), the optical output power, and the junction voltage (both derived as described above), are recorded by the computer. The software performs all calculations and plots both, the power-vs.-current (PI) and voltage-vs.-current (UI) graphs.

Fig. 2.9 shows a typical example for the result of a PUI characterization performed on a 780 nm DFB diode laser. The solid, the dashed, and the dotted line represent the P-I

characteristics, the U-I characteristics, and the conversion efficiency as derived from the PUI characteristics, respectively.

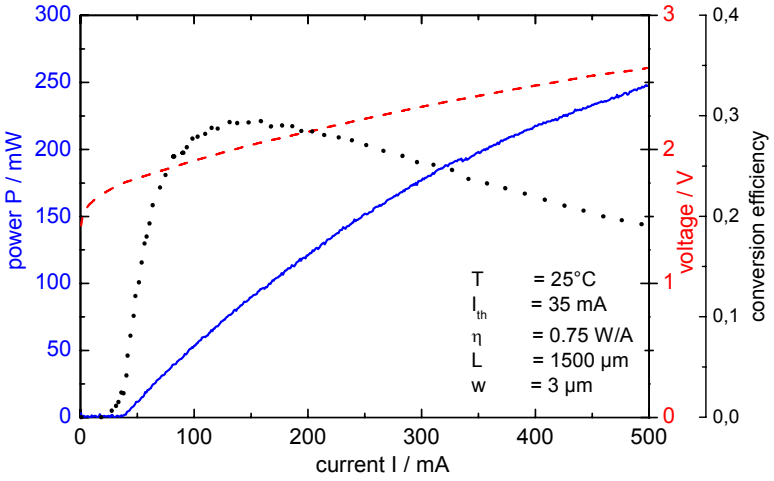

Figure 2.9. *PUI characteristic of 780 nm DFB laser.*

2.2.2. Analysis of longitudinal mode spectra

Besides analyzing the PUI characteristic it is necessary to perform a characterization of the laser emission spectrum. This delivers the center emission wavelength, single vs- longitudinal mode operation, the side mode suppression, and the dependence of these quantities on the diode laser injection current and the diode laser (mount) temperature. This measurement also provides an analysis of side mode suppression ratio (SMR) between center mode and side modes.

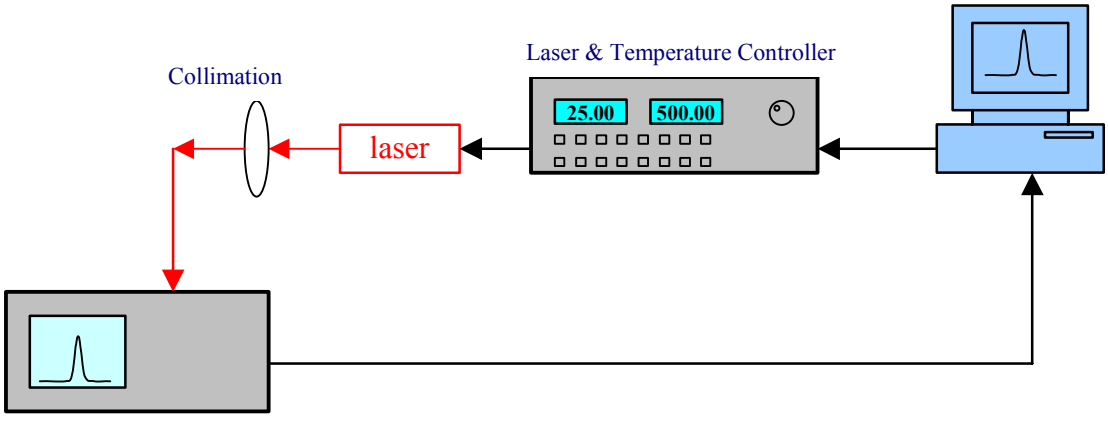

Figure 2.10. *Spectrum measurement diagram.*

The setup used to investigate the spectral emission properties of the laser diode is similar to the one used for PUI-characterization. However, now the laser emission is analyzed by means of an optical spectrum analyzer (OSA), which is an Advantest OSA model Q8384 in our case. The setup is sketched in Fig. 2.10.

To analyze the laser emission spectrum, the laser beam is coupled into an optical fiber that is connected to the entrance port of the OSA. The Advantest Q8384 provides a resolution of 10 pm or 4.92 GHz at 780 nm.

With this setup the laser spectrum is recorded at a specific injection current and diode laser mount temperature. Typically, we step-up and step-down the injection current between 0 and maximum and then record a spectrum for each current setting. The corresponding data is displayed in a 3D-graph, with the axes corresponding to wavelength, current, and intensity (spectral map). This analysis allows extraction of the wavelength shift of the laser versus the operating current. Instead of varying the injection current we can also vary the diode laser mount temperature in order to determine the temperature dependence of the laser emission spectrum. This provides useful information for the analysis of spectral characteristic of high power diode lasers, e.g. estimation of center wavelength instability under fluctuation of surrounding temperature.

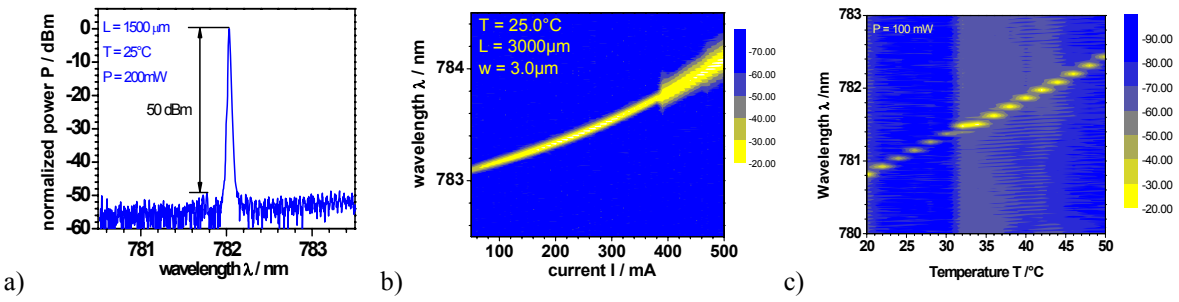

Figure 2.11. *Examples for characterization of the laser emission spectrum: a) spectrum of a 780 nm DFB at 200mW; b) the emission spectrum vs. injection current, and c) the emission spectrum vs. laser diode temperature.*

In Fig. 2.11a we show a typical spectrum of a 780 nm DFB diode laser measured at a diode laser mount temperature of 25°C and at an output power of 200 mW (drive current of 400 mA). The SMSR of the laser exceeds 50 dB. A spectral map of the other laser is shown in Fig. 2.11b, the driver current runs from 50 mA to 500 mA with step 5 mA. From 50 mA to 400 mA the spectral present a single longitudinal mode, over 400 mA the spectra show up with substantially broadening of spectral width. The temperature dependence of the laser diode spectral characteristic is shown in Fig. 2.11c. The wavelength shifts from 780.81 nm to 782.43 nm as the temperature is ramped from 20°C to 50°C.

2.2.3. Analysis of spatial beam properties

Within the framework of this thesis the vertical and lateral far-field intensity distribution is analyzed in order to characterize the spatial emission properties of high power DFB diode lasers. The measurement setup is described in Fig. 2.12. In this

setup, a CCD camera acquires the 2D intensity distribution of the beam. An analysis program normalizes the 2D intensity distribution map and then evaluates profiles by integrating along the horizontal and vertical direction to derive vertical (to pn-junction) and lateral 1D-intensity distributions. The lateral and vertical far-field profiles are usually Gaussian to good approximation because RW-DFB lasers are typically designed to only support the fundamental propagation mode. These profiles allow for determination of the vertical and lateral divergence angles. Typically, the laser is operated at various currents, and the far-field intensity distribution is investigated as a function of the injection current.

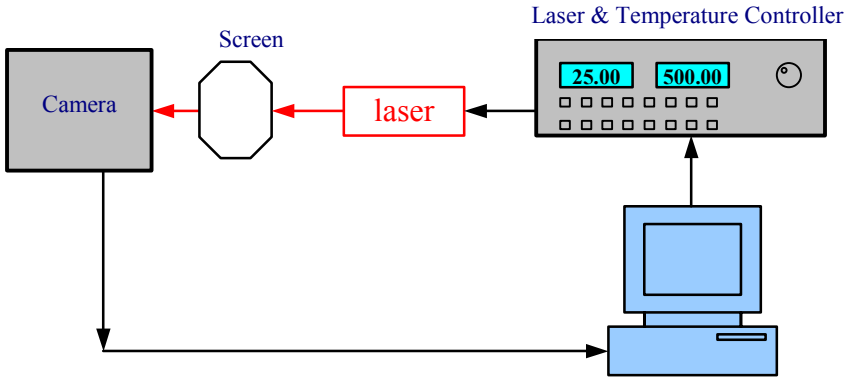

Figure 2.12. *Farfield measurement diagram.*

Fig. 2.13 shows the result of a lateral far-field analysis of a 780 nm DFB laser. The normalized lateral and vertical far-field intensity profiles are shown in Fig. 2.13a & b for an injection current of 400 mA. The nearly Gaussian profiles indicate divergence angles of 21.7° and 11° (FWHM) for vertical and lateral direction, respectively. The map in Fig. 2.13c represents the spatial intensity distribution as the injection current varies from 100 mA to 400 mA. This picture can illustrate the potential beam steering and focusing /de-focussing effects of the lasers that can occur when temperature and/or injection current are modified.

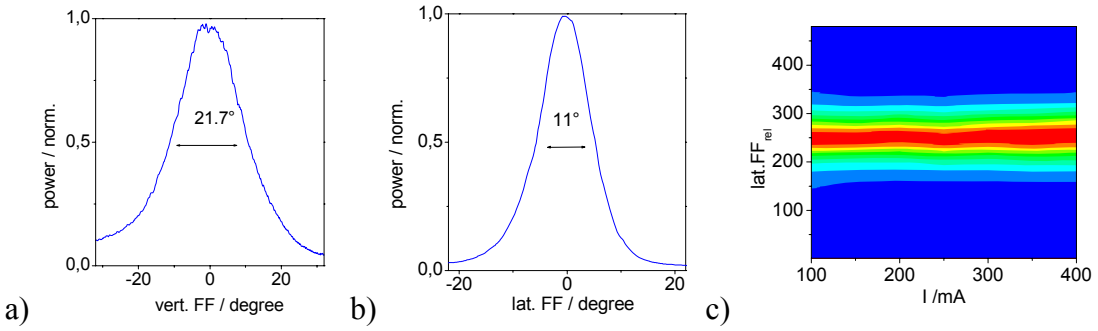

Figure 2.13. *Examples for a) normalized lateral and; b) vertical farfield profiles at a current of 400 mA for a 780 nm DFB laser operated at an injection current of 400 mA and a temperature of 25°C; c) lateral farfield of the same laser for the injection current ranging from 100 to 400 mA.*

2.3. Spectral Characteri ation of narrow linewidth HPDLs

2.3.1. Overview of spectral width measurement techniques

For many applications the precise spectral width of diode lasers (or linewidth) is essential. Atomic clock applications, for example, require high power narrow linewidth (sub MHz) or even ultra-narrow linewidth (down to the Hz range) lasers. Linewidth measurements provide the information necessary to assess whether the linewidth of a laser meets the requirements of a specific application. Several methods for laser linewidth characterization have been developed. These include interferometer-based optical spectrum analyzers (OSAs), diffraction-grating-based OSAs, Fabry-Perot resonators [82], coherent discrimination detection techniques [82], as well as self-delayed heterodyne/homodyne [83] and heterodyne [82] techniques. In this section, we will discuss different methods in use to characterize the linewidth of DFB single-frequency semiconductor lasers which nowadays is typically below 10 MHz. After giving a brief overview we will focus on the two methods that are most suitable for the spectral characterization of narrow linewidth RW-DFB lasers, namely the heterodyne and self-delayed heterodyne technique.

Interferometer-based OSAs: This spectrum analyzer is based on a Michelson interferometer. The input signal is split on two parts, which are injected into the two arms of a Michelson interferometer- one path is fixed in length and one is variable. The Michelson interferometer creates an interference pattern between the signal and a delayed version of the signal at the detector. The resolution of the instrument is determined by the path-length delay that is used to create the interferogram [82]. This type of spectrum analyzer allows for a direct measurement of the coherence-length, which is not possible with other types of OSAs. Another advantage of the instrument is that it can also provide high accuracy wavelength determination. However, the high accuracy required for optical alignment as well as the lack of true bandpass filters to pre-select a specific wavelength range are considered disadvantages of this method.

Diffraction-grating-based OSAs: The most common OSAs use diffraction gratings to realize tunable optical filters. The OSA in part (2.2.2) is one of these. The grating spatially disperses the different spectral components of the laser emission. The spectrum of the laser emission is then obtained by either rotating the grating and/or imaging the dispersed spectrum onto a 1D CCD-array. The resolution of the OSA depends on the grating parameters and on its optical setup [82].

The resolution of interferometer- and diffraction-grating-based OSAs is typically limited to the order of 10 GHz.

Fabry-Perot interferometer: The interferometer consists of two highly reflective mirrors that are aligned parallel and act as a resonator, which filters the incoming light. The configuration of the setup is shown in Fig. 2.14. Wavelength tuning of the Fabry-Perot (FP) interferometer is accomplished by adjusting the mirror spacing or by rotating the interferometer with respect to the input beam. The resolution depends on the reflection coefficient of the mirrors and on the mirror spacing. Using air-spaced Fabry-Perot interferometers (refractive index n = 1), values for mirror distance up to more than 100 mm can be easily achieved. The resolution then typically is of the order of 10 MHz [82], but could in principle be reduced to the order of 10 kHz with the best mirrors available. The potential to provide high resolution measurement is an advantage of this method. However, the repeated band pass response limits the free spectral range.

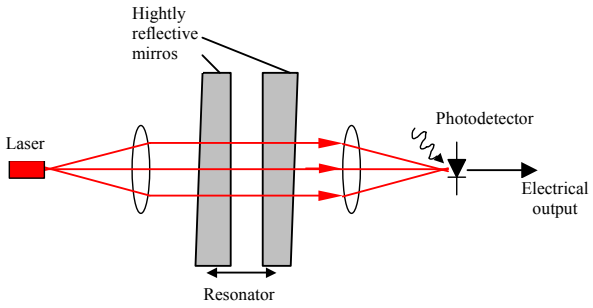

Figure 2.14. *Schematic of a Fabry-Perot interferometer [82]*

Coherent discrimination: This is another solution to reach very high resolution. The phase fluctuations of the optical field are converted into intensity fluctuations using a Michelson, a Mach-Zehnder, or a FP type interferometer. The interferometer is biased to a path length difference of $\Delta\varphi = \pi/2 + N\pi$ by inserting a phase modulator in one of its arms, so that the frequency fluctuations of the laser are converted to variations of the photocurrent that are linearly proportional to the frequency excursions [82]. Exact knowledge of the time delay and careful calibration of the linear conversion are required. The linewidth of the laser is then extracted from the RF spectrum of the photocurrent [84]. The technique can also be applied for narrow linewidth measurements. The major disadvantage is that it is a relatively complicated experimental setup as it requires constant re-biasing and very careful calibration.

Self-homodyne: The self-delayed homodyne technique offers a simple means to measure the linewidth of a laser. This technique is similar to the self-delayed heterodyne technique (described in section 2.3.2 later) but misses the optical frequency shifter. The optical implementation uses a Michelson, Mach-Zehnder or FP type interferometer as discrimination technique. The linewidth is directly obtained from the spectrum of the beat note signal displayed on an RF spectrum analyzer. In the delayed self-homodyne technique, two optical fields interfere at the photodetector The center frequency of the “beat note” signal is 0 Hz, because the two interfering fields share the same center frequencies. This causes the interference signal to strongly depend on the exact mean phase difference between the two arms of the interferometer [85]. To

overcome this problem a modified delayed self-homodyne technique has been developed [86],[87]. It includes a phase modulator that is inserted in one arm of the interferometer to average out the mean phase dependence. A significant shortcoming of this technique is that it detects the beat note signal at DC (0 Hz) where the signal acquisition is strongly affected by 1/f electronic noise.

Because of the disadvantages inherent to the above techniques, some more suitable methods should be chosen to characterize the linewidth of diode lasers. In this work, therefore, we use the heterodyne and the self-delayed-heterodyne technique for determining the linewidth of RW-DFB lasers.

2.3.2. Method for spectral characterization of narrow linewidth HPDLs and analysis of the influence of noise sources

As pointed out in the beginning of this section (2.3), the interference-based methods are methods that allow for high resolution spectral characterization of narrow linewidth diode lasers with the least experimental efforts. Therefore, in this section, an introduction to interference-based methods will be given. After that, we will briefly consider the most relevant effects that affect linewidth measurements. We finally shortly discuss the analysis methods that are used to extract linewidth information from the recorded RF spectra or time domain signals.

The interference techniques, namely heterodyne and self-delayed heterodyne technique, are the methods that are used for linewidth characterization of high power DFB diode lasers in the framework of this thesis.

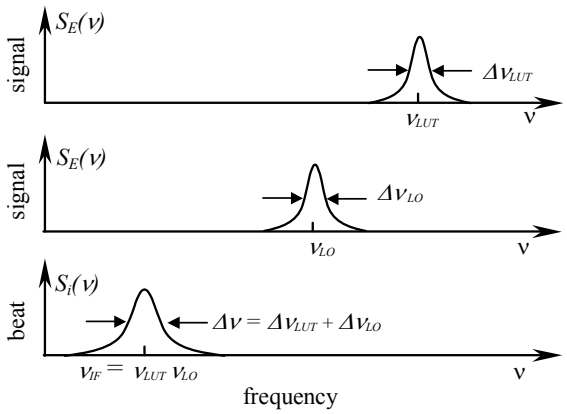

Figure 2.15. *Convolution of narrow linewidth laser translates signal spectrum to low frequencies.*

To begin with we consider the heterodyne technique. We first describe the interference of two laser fields that are superimposed on a fast photodetector. Fig. 2.15 shows a schematic description of how the interference signal ("beat note signal") is generated in the RF-frequency domain. The time-dependent laser field under test (LUT) and the local oscillator laser field (LO), i.e. $E_{LUT}(t)$ and $E_{LO}(t)$, with frequencies ν_{LUT} and ν_{LO}, and phases $\varphi_{LUT}(t)$ and $\varphi_{LO}(t)$, respectively, are represented by the following equations:

$$E_{LUT}(t) = E_{LUT} \exp\,[j(2\pi\nu_{LUT}t + \varphi_{LUT}(t)] \qquad (2.1)$$

$$E_{LO}(t) = E_{LO} \exp\,[j(2\pi\nu_{LO}t + \varphi_{LO}(t)]\,. \qquad (2.2)$$

The electric field amplitudes E_{LUT} and E_{LO} are related to the corresponding optical power P_{LUT} and P_{LO} by $E_{LUT} \propto \sqrt{P_{LUT}}$ and $E_{LO} \propto \sqrt{P_{LO}}$, respectively. It should be pointed out that the self-delayed heterodyne technique can be considered a special case of the more general heterodyne technique: in case of the self-delayed heterodyne technique the frequency difference $\nu_{LUT} - \nu_{LO}$ is controlled by the operator and hence is known [82].

The total interfering field at the photodetector is

$$E(t) = E_{LUT}(t) + E_{LO}(t). \qquad (2.3)$$

and corresponds to an optical power of $P \propto |E|^2$. The corresponding photocurrent can be described by the following expression:

$$I(t) = \eta |E(t)|^2, \qquad (2.4)$$

where η is detector responsivity (in A/W). Therefore, the electrical signal that we analyze with a RF spectrum analyzer or that we record as a time domain signal with a fast digital oscilloscope is a function of the phase difference between the two optical fields:

$$I(t) = \eta\left\{P_{LUT} + P_{LO} + 2\sqrt{P_{LUT}P_{LO}}\cos\left[2\pi(\nu_{LUT} - \nu_{LO})t + (\varphi_{LUT}(t) - \varphi_{LO}(t))\right]\right\}. \qquad (2.5)$$

In the above formula, the two first components are time independent and correspond to the individual optical power of each of the two fields. Therefore, only the third term, the "mixing-term", contains the information that characterizes the spectral stability of the laser. By defining:

$$\nu_{IF} = \nu_{LUT} - \nu_{LO} \qquad (2.6)$$

and

$$\Delta\varphi(t) = \varphi_{LUT}(t) - \varphi_{LO}(t), \qquad (2.7)$$

we obtain:

$$I(t) = \eta\left\{P_{LUT} + P_{LO} + 2\sqrt{P_{LUT}P_{LO}}\cos\left[2\pi\nu_{IF}t + \Delta\varphi(t)\right]\right\}. \qquad (2.8)$$

The characterization methods described in this thesis are based on this fundamental expression [82]. They move the ultra-high frequency of optical fields to the RF-frequency regime where the spectral (frequency) stability can be analyzed with state-

of-the-art radio frequency equipment. However, this requires the two optical frequencies to be close enough, i.e. to differ by less than a few 10 GHz which corresponds to about a few parts in 10^5 of the optical frequency.

In mathematical terms the relevant part of the time domain signal is due to the product (mixing) of the two optical fields. When RF spectra are generated either by means of an RF spectrum analyzer or by Fourier transformation of time domain data, this product transforms into a convolution of the spectra of both, the laser under test and the local oscillator laser. If the local oscillator spectrum is sufficiently narrow, the resulting RF spectrum resembles the spectrum of the laser under test.

Once the beat note signal is recorded in the time or frequency domain, the following data analysis methods can be used to extract the information regarding the spectral stability and linewidth of the diode laser:

- Spectrum analysis of the RF beat note signal either directly by means of a RF spectrum analyzer or by post-processing time domain beat note data through a fast Fourier transformation. This is the technique commonly used to determine the linewidth of diode lasers.
- Construction of the time domain "conjugate" signal from the recorded time domain data by means of the Hilbert transformation. From the conjugate signal the data set of instantaneous frequencies is derived from which then frequency noise spectra are generated by means of a Fast Fourier Transformation. This method provides detailed information about the frequency instability (noise) of lasers and also allows to separate laser power and frequency noise from each other.
- Allan variance analysis for the description of the long-term (typically > 1s) frequency stability of lasers.

These three methods will be briefly discussed.

a. Beat note power spectrum

The first method considered is RF (radio frequency) power spectrum analysis of the beat note signal by means of an electric spectrum analyzer (ESA). According to the Wiener-Kintchine theorem the power spectral density, $S(\nu)$, of the beat note signal can be considered the result of Fourier transforming the third term of the time domain signal in equation (2.8) [82]:

$$S(\nu) = 2\int_0^\infty R(\tau)\exp(-2j\pi\nu t)dt\,. \qquad (2.9)$$

Here, $R(\tau)$ is the beat note cross correlation function of the two interfering laser fields:

$$R(\tau) = \Re q\left[E(t)E^*(t)\delta(t)\right] + \Re^2\left[E(t)E^*(t)E(t+\tau)E^*(t+\tau)\right], \qquad (2.10)$$

where $\Re$ is the detector responsivity, q is the elementary charge, $E(t)$ is the total interfering field at the photodetector (see equation (2.3)), δ is the Dirac-Δ function [82]. The spectral shape of $S(\nu)$ contains the information about the spectral linewidth of the laser under test (assuming that the local oscillator is sufficiently narrow linewidth). Often, the emission spectrum of a laser is described by a Lorentzian line shape.

In case of Lorentzian lineshapes the power spectrum of the beat note signal is given by the following expression [82]:

$$S_L(\nu) \sim \frac{1}{1+\left[\frac{\nu-\nu_{IF}}{\Delta\nu_L/2}\right]^2} \qquad (2.11)$$

When $\nu - \nu_{IF}$ is zero, $S_L(\nu)$ is maximum. As the detuning form the frequency offset, $\nu - \nu_{IF}$, increases, the power spectral density of the signal falls off at 12 dB/octave which is characteristic for a Lorentzian lineshape. As we assume a Lorentzian lineshape for both, LUT and LO, the full-width-at-half-maximum (FWHM) linewidth $\Delta\nu$ of the beat note spectrum is related to the FWHM linewidth of both lasers, $\Delta\nu_{LUT}$ and $\Delta\nu_{LO}$, by:

$$\Delta\nu = \Delta\nu_{LUT} + \Delta\nu_{LO} \qquad (2.12)$$

Hence, for the self-delayed heterodyne technique ($\Delta\nu_{LUT} = \Delta\nu_{LO}$) we find:

$$\Delta\nu = 2\Delta\nu_{LUT} \qquad (2.13)$$

During the linewidth measurement, frequency jitter $\delta\nu(t)$, which is typically caused by environmentally induced fluctuations of the carrier density and/or fluctuations of the index of refraction within the active volume of one (or both) of the lasers, will be present. The frequency jitter is a random change of the operating frequency of a laser with time, it causes the RF spectrum to "jitter" in time accordingly:

$$S_L(\nu,t) \sim \frac{1}{1+\left[\frac{\nu-\nu_{IF}+\delta\nu(t)}{\Delta\nu/2}\right]^2} \qquad (2.14)$$

The frequency jitter $\delta\nu(t)$ tends to either smear out the power spectrum upon averaging over many spectra, or to distort individual spectra significantly if the jitter occurs on time scales comparable to or smaller than the sweep time of the RF spectrum analyzer. Thus, for the heterodyne technique, stringent requirements have to be posed on the stability of the laser under test and the local oscillator laser in order to suppress this

effect. In contrast to the heterodyne technique, the self-delayed heterodyne technique only requires a single laser, the laser under test. Therefore, it does not suffer from frequency jitter that is caused by DFB laser itself. An in-depth discussion of the two techniques will be presented in the next sections.

Now, we come back to expressions (2.11) and (2.14) and continue to comment on the analysis and evaluation of beat note spectra. Typically, noise, e.g. due to the diode laser current controller, causes line broadening as explained in section 1.3.3. In terms of RF beat note spectra this noise will modify the spectral line shape. In case of 1/*f* electronic noise, which one typically encounters when driving diode lasers with commercial current controllers, this modifies the Lorentzian line shape towards a Voigt profile. Generally speaking, any additional noise term that falls-off rapidly enough (faster than a Lorentzian) will modify the RF beat note spectra close to carrier but will not affect the line shape at sufficiently large detunings from the carrier. Hence, it is advisable to actually determine the Lorentzian linewidth of a laser not at 3 dB but rather at 10 dB or 20 dB. The linewidth extracted at these width levels can than be converted to the corresponding FWHM linewidth by multiplication with an appropriate scaling factor. Scaling factors for 10 dB and 20 dB below carrier are given in Tabel 2.1 [82]. For example, if the full width at 20 dB below carrier is 1 MHz, then the FWHM linewidth of the corresponding Lorentzian profile is ~100 kHz.

Tabel 2.1. *Derivation of FWHM linewidth $2\Delta\nu$ from linewidth measurements at various relative power levels.*

Full-width measured at relative power level	***Displayed width***
-3dB	$2\Delta\nu$
-10dB	$\sqrt{9}\cdot 2\Delta\nu$
-20dB	$\sqrt{99}\cdot 2\Delta\nu$

b. Beat note frequency noise spectrum

The second method used to describe laser frequency stability, namely the derivation of frequency noise spectra, is presented next. From equation (2.9), the beat note correlation function $R(\tau)$ is related to the power spectral density of frequency noise, $S_\nu(\nu)$ similar to equation (2.10). The frequency noise power spectral density is the fundamental parameter in the frequency domain measured in Hz^2/Hz. The root mean square (rms) linewidth $\Delta\nu_{rms}$ is then represented by [88]:

$$\Delta\nu_{rms}^2 = \int_0^\infty S_\nu(\nu)d\nu\,. \qquad (2.15)$$

There is no simple and generally valid relation that connects the beat note linewidth measured with an RF spectrum analyzer to the rms linewidth as defined by eq. (2.15). If the frequency noise spectrum is a delta function, the RF beat note spectrum will be approximately rectangular with width of $d = 2\sqrt{2}\,\Delta\nu_{rms}$. If the RF beat note spectrum is Gaussian, the full width at half maximum (FWHM) will be $2.35\Delta\nu_{rms}$ [89]. In case of white frequency noise the FWHM laser linewidth, $\Delta\nu$, can be estimated according to [89],[90]:

$$\Delta\nu = \frac{\pi\Delta\nu_{rms}^2}{B} = \pi S_{\nu,0}\,. \qquad (2.16)$$

where B is bandwidth used for integration of the frequency noise power spectral density and $S_{\nu,0}$ is the frequency noise power spectral density in case of white frequency noise.

We next discuss how to distinguish different sources of noise that contribute to the frequency noise spectrum. A typical frequency noise spectrum of a diode laser is shown in Fig. 2.16. In this graph, the dashed line represents quantum shot noise that ultimately limits the emission linewidth of the lasers. This shot noise level, which is known as Schawlow-Townes limit and is caused by spontaneous emission, is hardly reached under regular operation conditions of DFB lasers.

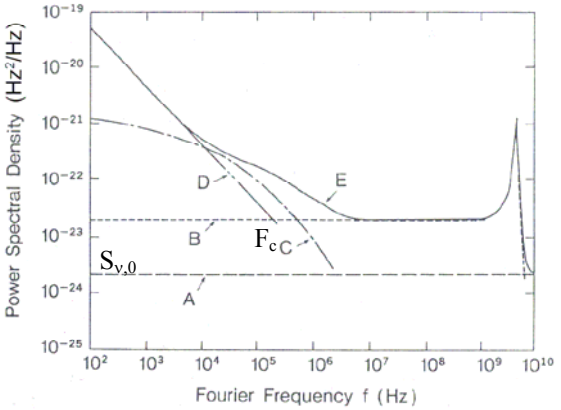

Figure 2.16. *Power density of the FM noise of a semiconductor laser induced by intrinsic noise sources. Curve A: spontaneous emission fluctuation; B: carrier-density fluctuation; C: temperature fluctuation; D: 1/f fluctuation. Curve E represents the total intrinsic FM noise by superposing the value of curve A-D. [58]*

At low Fourier frequencies, the spectrum is dominated by technical noise that is due to, for example, injection current fluctuation, temperature fluctuations, and mechanical vibrations. This type of frequency noise is usually referred to as *1/f* – noise and determines the frequency noise power spectral density at frequencies below the corner frequency F_c as shown in Fig. 2.16, which is typically of the order of 100 kHz – 10 MHz. The role of F_c can be qualitative understood as follows: because frequency noise power spectral density, which is given in units of square hertz per hertz, can be formally interpreted as a frequency, one may distinguish between two cases $F_c < S_{\nu,0}$ and $F_c > S_{\nu,0}$. For $F_c < S_{\nu,0}$, low frequency noise essentially leads to a jitter of a

Lorentzian-shape spectrum. For $F_c > S_{\nu,0,}$ the shape of the spectrum itself becomes modified towards a Gaussian [91], [89].

Another source of frequency noise is related to charge carrier density fluctuations. Spontaneous emission affects the carrier density and hence induces refractive index fluctuations which add contributions to the frequency noise power spectrum. Frequency noise caused by carrier density fluctuations has a second-order delay characteristic and therefore the frequency noise power spectrum exhibits relaxation oscillation peaks at frequencies of several GHz and multiples thereof [58], [91]. The relaxation oscillation resonance peak is clearly visible at GHz frequencies in Fig 2.16. The relaxation oscillation manifests itself in the emission spectrum as satellite peaks [92]. The ratio between the frequency noise power spectral density due to spontaneous emission and due to carrier density fluctuations can be expressed by the linewidth enhancement factor α^2 (Henry factor) [58]. Above the relaxation oscillation frequency, the frequency noise power spectral density approaches the Schawlow-Townes quantum limit.

c. Beat note Allan variance characterization

The third characterization method to be briefly discussed here is the Allan-variance. The Allan – variance may be determined from frequency noise spectrum $S_\nu(\nu)$ by the integral [93]:

$$\sigma^2(2,\tau) = 2\int_0^\infty S_\nu(\nu)\frac{\sin^4(\pi\nu\tau)}{(\pi\nu\tau)^2}d\nu\,. \qquad (2.17)$$

This parameter is a function of the interval time τ. The Allan-variance at interval time τ is a measure for the typical drift of the oscillator frequency at time scales of τ. A detailed analysis is presented in Ref. [94]. An example for the Allan standard deviation $\sigma(2,\tau)$ of wavelength-stabilized diode laser and its original power spectral density of frequency noise $S_\nu(\nu)$ is given in Fig. 2.17. The Allan variance is typically used to characterize the long term (> 1s) stability of oscillators, specifically in clock

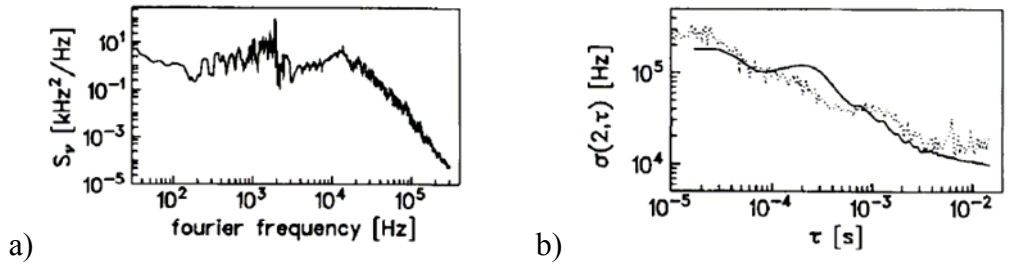

Figure 2.17*. a) Power spectral density S(ν) of frequency fluctuations of the diode laser locked to a Doppler-free rubidium resonance transition as determined from the in-loop error signal; b) Allan standard deviation σ(2, τ) calculated from the power spectral density. [93]*

applications. It provides information on which integration time provides the best stability. Allan variance graphs also provide information on the physical origin of frequency instability, which in this context are typically termed jitter or drift.

d. Voigt profile and data analysis

So far we have given an overview over concurrent methods used for the characterization of the (short-term) spectral stability of lasers. Within the framework of this thesis two of these methods, the self-delayed heterodyne and the heterodyne technique are applied. We will now explain how to analyze the data and how to extract the laser linewidth from the data recorded in the time domain with a fast oscilloscope or in the frequency domain with a RF spectrum analyzer.

As explained above the intrinsic lineshape of the emission spectrum of DFB diode lasers can be described by a Lorentzian profile, see equation (2.11). Therefore the corresponding RF beat note spectrum is also Lorentzian. However, as already explained, additional noise sources will modify the beat note spectrum. Typically, these additional noise sources can be described by a $1/f$ model to good approximation. Therefore, in practice, the Lorentzian lineshape of a beat note spectrum will be modified towards a Gaussian lineshape that represents an inhomogeneous broadening of the emission spectrum. The Gaussian lineshape function is given by [95]:

$$S_G(\nu) = \sqrt{\frac{4\ln 2}{\pi}} \frac{1}{\Delta\nu_G} \exp\left[-4\ln 2 \left(\frac{\nu - \nu_{IF}}{\Delta\nu_G} \right)^2 \right]. \qquad (2.18)$$

Here $\Delta\nu_G$ is the FWHM of the Gaussian profile. As the noise sources can be considered to inhomogeneously broaden the Lorentzian emission profile, the overall spectrum has to be described by a convolution of the Lorentzian line shape with the distribution of the emitters, which, in the simplest case, can be modeled by a Gaussian distribution. A convolution of a Lorentzian and Gaussian distribution is known as a Voigt profile, and is defined as [95], [96]:

$$S_V(\nu) = 2\int_0^\infty S_G(\nu') S_L(\nu - \nu') d\nu' \qquad (2.19)$$

The Voigt profile is not available in an analytic form; however, many useful approximations are available [97],[98]. The Voigt profile exhibits a Lorentzian behaviour in the wings and a Gaussian behaviour close to line center. Typically, the Gaussian linewidth is much larger than the Lorentzian linewidth. Then, a Gaussian approximation for the full lineshape is not accurate enough as it strongly underestimates the wings of the profile as shown in Fig. 2.18. Gaussian fits to the beat

note spectrum should therefore generally be avoided. Rather, the complete beat note spectrum is well approximated by a Voigt profile. Fig. 2.18 shows an example for the analysis of experimental data (open-circle) using a Voigt (red solid line), a Lorentzian (blue dashed line) and a Gaussian (green dotted line) profile approximation. The Voigt profile most accurately describes the beat note spectrum close to the carrier as well as far out in the wings.

Once a Voigt profile is fitted, the Lorentzian and Gaussian FWHM linewidth can be extracted from the fit. The Lorentzian linewidth is then considered to describe the intrinsic short term linewidth of the diode laser. The analysis of all data performed in this thesis is based on this procedure.

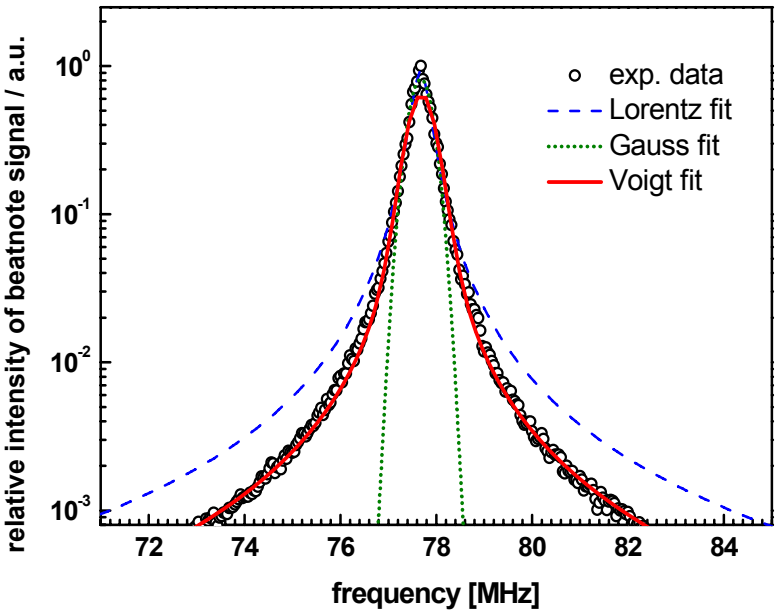

Figure 2.18. *an example of self-delayed heterodyne lineshape of 780 nm DFB laser due to 1/f compare with Lorentz, Gauss, and Voigt fit.*

As can be seen in Fig. 2.18, even a Voigt profile does not perfectly describe the beat note spectrum. One possible reason is that the additional technical noise sources can not adequately be described by a $1/f$ model. However, as long as the additional noise falls off more rapidly towards the wings of the spectrum than a Lorentzian (which is the case for electronic noise, thermal noise, acoustics, and vibrations) the Lorentzian describing the "natural" or intrinsic emission profile of the laser will always dominate the wings of the spectrum. When fitting model spectra to the data it is therefore advisable to setup the algorithm such that it is sensitive to any deviations between data and model in the wings of the spectrum but is rather insensitive to deviation close in to the carrier.

2.3.3. The Heterodyne technique

This section will introduce the heterodyne technique in detail and it will describe the experimental setup I developed.

For all of the investigations performed within this thesis, we used two lasers from the same wafer, from the same test field and from the same bar when performing heterodyne measurements. This way the two lasers are "as identical as possible". It is therefore reasonable to assume, that both lasers have very similar spectral emission properties. In this limit, two identical spectra are convoluted. In case of white frequency noise (Lorentzian line shape), the linewidth of an individual laser is half of the linewidth of the RF beat note spectrum and in case of $1/f$ frequency noise (Gaussian line shape) the linewidth of an individual laser corresponds to $1/\sqrt{2}$ of the beat note linewidth. In any case, the RF beat note linewidth determines an upper limit for the linewidth of the individual lasers.

Several effects contribute to the net frequency resolution of the linewidth measurement. The linewidth of the LO limits the minimum spectral resolution. However, in practice, as discussed in section 2.3.2, the effective resolution can be reduced by frequency jitter or 1/f frequency noise of the LUT, and possibly of the LO. The time scales for frequency jitter are typically slow, less than a microsecond, but they can still be faster than the sweep time or integration time of the RF spectrum analyzer. When the measurement averaging time is of the order of a second or longer, the effective, i.e. experimentally determined linewidth of the LO and LUT can easily

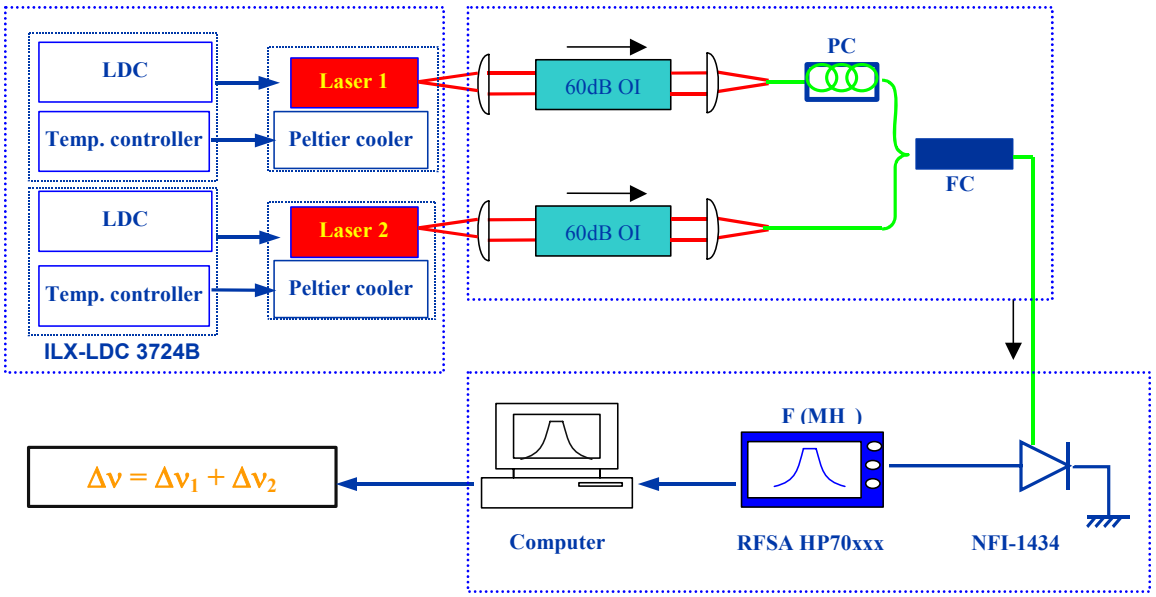

Figure 2.19. *Optical heterodyne setup for measuring laser linewidth . LDC: Laser diode controller; OI: Optical isolator; PC: Polarization controller; FC: Fiber coupler; RFSA: Radio frequency spectrum analyzer.*

be a factor of ten larger than they would be if all technical noise sources were absent. It is therefore important to reduce technical noise sources as much as possible when analyzing the "intrinsic" noise of a laser, i.e. noise caused by the lasers itself. Another factor limiting the frequency resolution is the resolution bandwidth of the RF spectrum analyzer. The resolution bandwidth filter should be set so as not to limit the desired measurement resolution [82].

Fig. 2.19 describes the heterodyne detection scheme used for laser linewidth measurements throughout this thesis. The setup includes three main parts: light sources, optical system, detection and analysis equipment.

The measurement setup utilizes two current-temperature controllers Lightwave ILX-LDC 3724B (Fig. 2.20). The current control unit of the ILX-LDC 3724B can supply up to 500 mA of injection current, where the current steps are 4 or 10 μA for output current ranges up to 200 or 500 mA, respectively. This provides wavelength fine-tuning of the DFB lasers which is required in order to spectrally overlap the two lasers used for the heterodyne linewidth measurement. The rated current stability is better than 20 ppm during an hour and better than 40 ppm over 24 hours. In the setup, two laser diode mounts (Newport model 700 series, see Fig. 2.21) are used. Inside the mounts, an efficient thermal design of thermoelectric coolers permits cooling or heating. These mounts are temperature stabilized by the temperature control units of ILX-LDC 3724B that are able to maintain a setpoint temperature to within ±0.004°C over an hour interval and ±0.01°C over 24 hours. The temperature stabilization part (mounts and controllers) has two main tasks: tuning the temperature to spectrally overlap the two lasers and then maintaining a constant laser diode operating temperature. Typically, the operating temperature can be stabilized to a value within the range from 10°C to 60°C. The lasers, which are packaged on SOT, TO3 or C-mount, are placed inside the mounts that are

Figure 2.20. *Laser diode controller ILX-LDC 3724B. [99]*

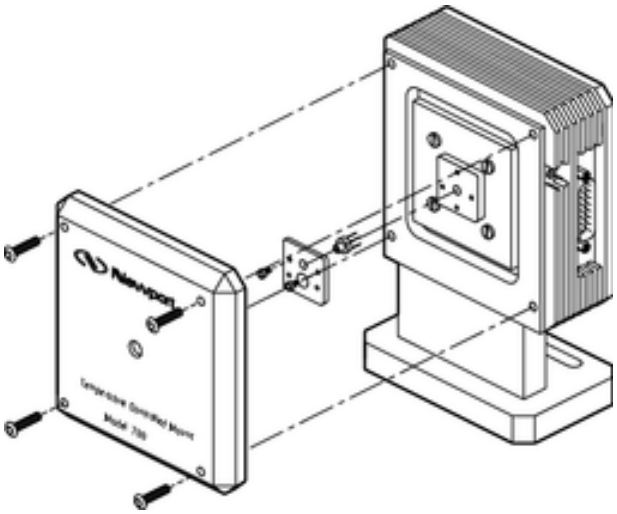

Figure 2.21. *The 700 Series temperature controlled laser diode mount. [100]*

capped to prevent external thermal interference during operation.

The second part, namely optical system, is employed to generate stable interference of two laser beams. The laser beams are firstly collimated with aspheric lenses before passing optical isolators (OI). Thorlabs A397TM-B collimation lenses with a numerical aperture of 0.3, an effective focal length of f = 11 mm, a clear aperture of 6.59 mm, AR-coated for 600 nm - 1050 nm are used. Alternatively, Thorlabs C240TME-B: with NA = 0.5, f = 8 mm, a clear aperture of 8 mm, and an AR-coating for 600 nm - 1050 nm can be used. To prevent optical feedback to the laser that causes self-interference and disturbs the spectral stability of the laser, a 60 dB optical isolator (Linos DLI-1, shown in Fig. 2.22) is inserted into each the optical paths. Optical isolators are based on the Faraday effect. The input polarizer polarizes the light travelling in the forward direction vertically. The Faraday rotator rotates the polarization by 45 degrees. The analyzer at the output is aligned so as to transmit the light. The output polarizer polarizes light travelling in the backward direction. The Faraday rotator then rotates the polarization by 45 degrees, however now into the opposite direction such that the light is rejected by the input polarizer. The operating wavelength of the isolator can be tuned between 745 nm and 890 nm. After passing the isolators the beams are coupled into single mode optical fibers by means of fiber coupling lenses (Thorlabs C260TM-B: 0.15NA, f = 15.36 mm, clear aperture 5.0 mm, AR coating range 600-1050 nm). The laser beams are guided by single mode optical fibers and interfere at a fiber-integrated Y-coupler (coupling ratio 50%, wavelength 700-1000 nm, with a core diameter of 5.9 μm; at 780 nm insertion loss of input 1 is determined to be 1.15 dB and input 2 is 2.75. At the fiber input APC (Angle polished Physical Contact) connectors are used to reduce etalon effects and optical feedback from the fiber facets. In one of the two fiber arms a fiber polarization controller (Thorlabs FPC561) is used to adjust the polarization so as to maximize the contrast of the beat note signal.

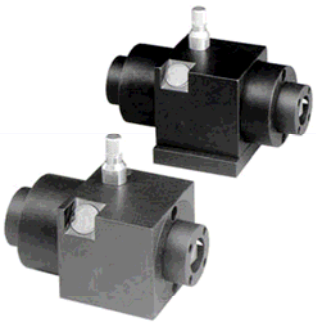

Figure 2.22. *60 dB optical isolators DLI . [101]*

In the detection and analysis part, we first use an OSA Advantest Q8347 to detect the center wavelength of each DFB lasers at the output of the Y-coupler. The center wavelength of two DFB lasers has to be overlapped to generate a stable interference signal in the RF frequency domain. Therefore, operating temperature and/or operating current will be fine-tuned to spectrally overlap the two DFB lasers, which is monitored with the OSA (see Fig 2.23). The OSA Advantest Q8347 allows setting the

wavelength of both lasers to the same value with a resolution of 2 pm (~ 1 GHz @ 780 nm). The interfering light from the output of the Y-coupler is then fed into an InGaAs broadband photodetector New Focus model 1434 (wavelength range: 550-1330 nm; 3-dB Bandwidth: 25 GHz; peak conversion gain: 5 V/W). The photoelectric signal generated in the photodetector is detected with a RF spectrum analyzer HP70 series (frequency detection range up to 22 GHz). The data recorded with the RF spectrum analyzer is dumped to the computer and then analyzed to provide beat note frequency spectra and linewidth determination for the DFB laser diodes.

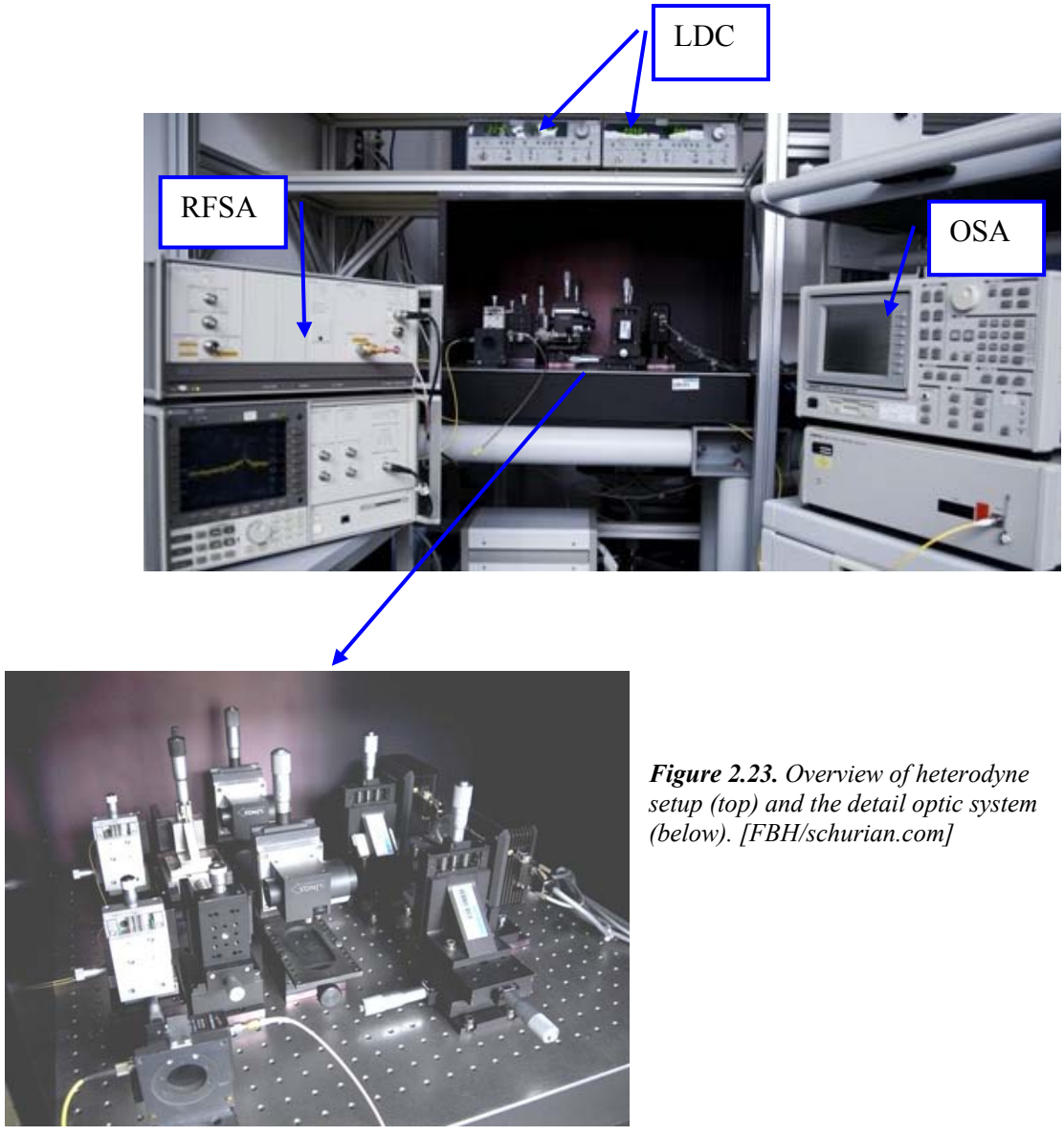

Figure 2.23. *Overview of heterodyne setup (top) and the detail optic system (below). [FBH/schurian.com]*

Finally, we would like to comment on some features of the heterodyne technique. As already discussed in detail in section 2.3.2 and at the beginning of this section, frequency jitter will strongly influence the result of a beat note measurement. The

optical frequencies of our DFB lasers are sensitive to noise present on the injection current and on the operating temperature with a typical sensitivity of 0.002…0.004 nm/mA, and 0.05 nm/°C, respectively. Therefore, the current fluctuation of the ILX-LDC 3724B current controller, which is specified not to exceed 4 µA rms, might cause a maximum rms frequency jitter of about 8 MHz. Similarly, a temperature fluctuation of 0.001°C (maximum value that was shown in specific manual) between the two lasers will lead to a relative fluctuation of the beat note frequency of about 25 MHz. Therefore, to reduce the influence of low frequency current and temperature noise onto the measurement, the RF spectrum analyzer sweep time is selected to be as short as possible (on the order of ten milliseconds). Further, in order to reduce thermal, convectional, or optical interference originating from the laboratory environment, the setup is carefully shielded by a black box (Fig 2.23). During the measurement the box is closed.

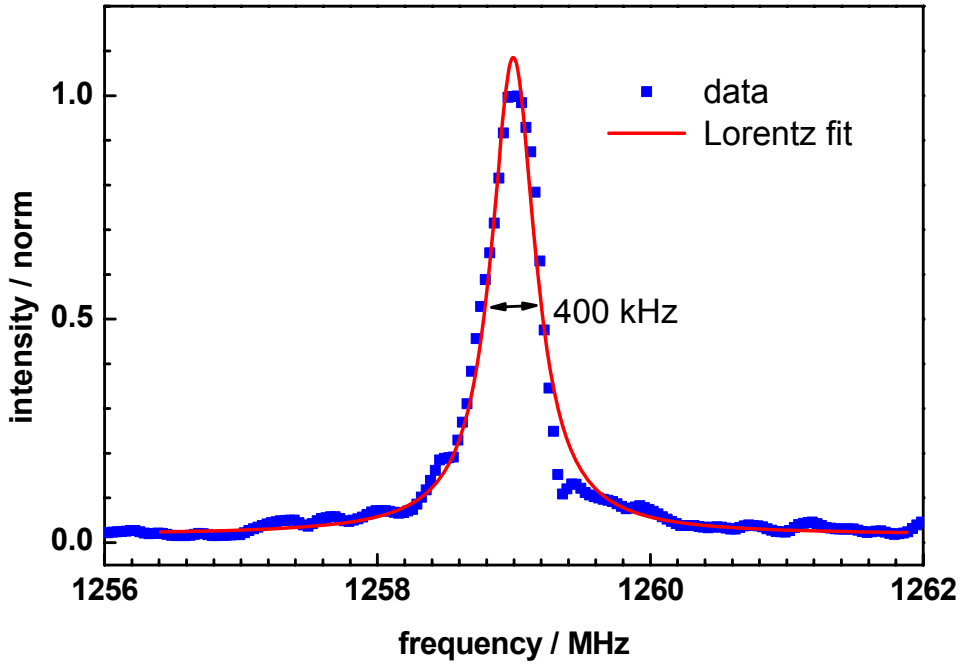

***Figure 2.24**. Linewidth of 780 nm DFB laser at 100 mW out put power and sweep time of 12 ms.*

Fig 2.24 shows the result of a beat note measurement on a pair of 780 nm DFB lasers, performed at an output power of 100 mW with sweep time of 12 ms and resolution bandwidth of 50 kHz. The beat note frequency is 1259 MHz. The beat note spectrum has a Lorentzian spectral width of about 400 kHz FWHM. Within the Lorentzian model the linewidth of an individual laser therefore corresponds to 200 kHz. In any case, independent of the exact spectral line shape, the FWHM linewidth of an individual laser is at most 400 kHz.

2.3.4. *Self-delayed heterodyne technique*

The heterodyne technique presented in the previous section allows for a characterization of the laser linewidth - in principle - with unlimited resolution. However, it features an important shortcoming, in that two lasers at similar injection current and operating temperature have to spectrally overlap to a few parts in 10^5. To overcome this problem, we alternatively employ another method, i.e. the self-delayed heterodyne technique, for linewidth measurements. This technique will be briefly introduced in this section.

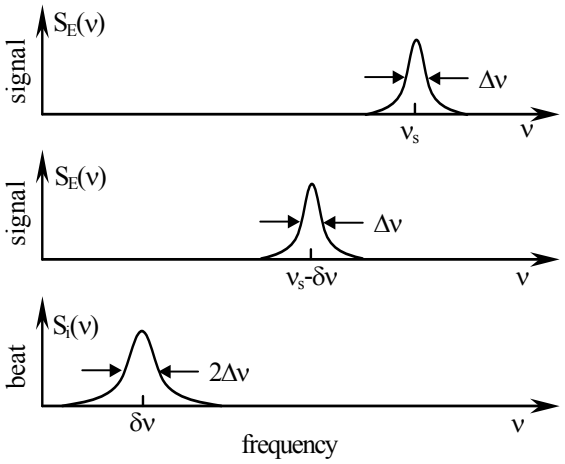

Figure 2.25. *The self-delay-heterodyne mixing of the laser field with a frequency shifted replica. [82]*

The self-delayed heterodyne technique provides a way to perform linewidth measurements without the need for a separate LO laser, see figure Fig 2.26. The first self-delayed-heterodyne setup was reported by T. Okoshi et al. [83] in 1980. Light from the LUT, which has a center frequency of ν_s, is split into two parts, which feed

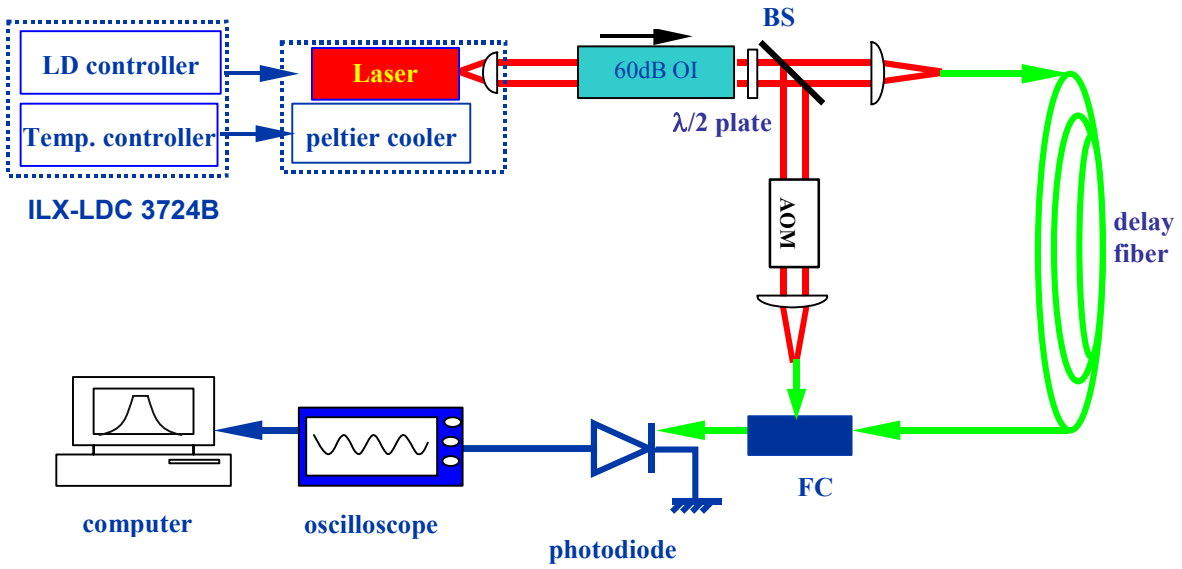

Figure 2.26. *Optical self-delay-heterodyne setup for measuring laser linewidth. OI: Optical isolator; BS: Beam splitter; FC: Fiber coupler.*

the two arms of a heterodyne interferometer. By using an optical frequency shifter for one arm, the center frequency of this arm is shifted to ν_s - $\delta\nu$ (or ν_s + $\delta\nu$). Therefore, the beat note signal generated when the light from both arms interferes occurs at a

frequency, which is defined by the frequency of the optical frequency shifter $\delta\nu$ (see Fig 2.25). The self-delayed-heterodyne technique requires a minimum delay τ_o between the two arms of the heterodyne interferometer which has to satisfy [82]:

$$\tau_o \geq \frac{1}{\Delta\nu} \qquad (2.20)$$

where $\Delta\nu$ is linewidth of LUT. This ensures that the delay exceeds the coherence time of the laser radiation so that noise present on both laser fields is statistically independent when it interferes at the photodetector. From a statistical point of view, the delay line generates an exact but statistically independent copy of the laser system [82]. As in case of the heterodyne technique the interference signal is detected with a fast photodetector and is recorded either with a spectrum analyzer in the frequency domain or with a fast oscilloscope in the time domain. As already described for the heterodyne technique (section 2.3.3) the laser linewdth is extracted from the RF beat note spectrum.

The self-delayed heterodyne setup at the Ferdinand-Braun-Institut has recently been developed by S. Spiessberger and M. Schiemangk. Fig 2.26 shows a schematic of the experimental setup. The diode laser current and temperature controller is the same as for the heterodyne setup described in section 2.3.3. The diode laser is mounted to an adapator which itself is then connected to a copper block which acts like a massive heat sink. The copper block sits on a thermoelectric cooler that provides a heat removal capacity of 60 W. The temperature of the block is measured with an AD590KF thermal sensor. This setup provides precise temperature control of the setup in the temperature range of 10°C to 60°C. The setup is placed inside a housing (Fig. 2.27) that provides thermal and acoustic isolation from in the environment. The laser emission is collimated by a collimation lens (Thorlabs C240TME-B). The collimated beam passes an optical isolator (Linos DLI) and is then split by means of an adjustable beam splitter constructed from an achromatic half wave plate (Thorlabs AQWP05M-950) and a polarization beam splitter (Linos G335-725-000). One output of the splitter is directed to the optical frequency shifter. In our setup, this is an acousto-optic modulator (AOM) by IntraAction ATM-804DA2B that is operated at 78 MHz. The first diffraction order of the AOM is then coupled into a single mode optical fiber. The second

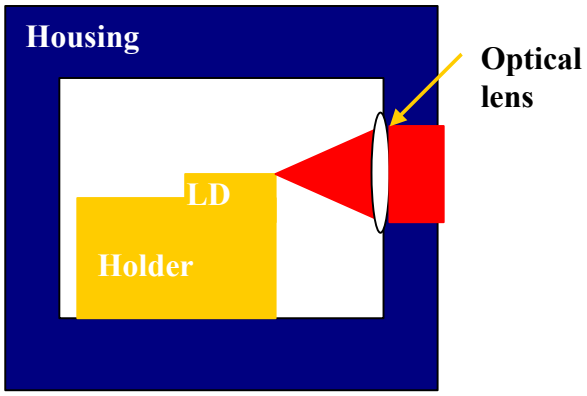

Figure 2.27. *Close housing of self-delay heterodyne setup.*

output of the splitter is launched into another optical single mode fiber that provides a delay of 2000 m (Fibercore SM-800). Light from the two the fibers is then superimposed by means of a single mode, fiber integrated 2x2 or 2x1 coupler. The beat note signal is finally detected with the fast photodetector that was already used for the heterodyne setup. The photodetector signal is recorded and analyzed by means of an RF spectrum analyzer (Rohde & Schwarz FSV30-100747) and the linewidth of the laser is extracted directly from the RF spectrum as described in section 2.3.3. Alternatively the signal can be recorded with a fast oscilloscope Agilent DS090254A. The time domain signal is the converted to the frequency domain by means of a Fast Fourier Transformation.

The minimum achievable linewidth of the self-delayed-heterodyne setup depends on the delay time of second arm. We now estimate the minimum achievable linewidth for the delay fiber parameters and the laser wavelength specific for this thesis work. Assuming a Lorentzian line shape the coherence time of the laser, τ_c, is inversely proportional to the laser linewidth, $\Delta\nu$ [82]:

$$\tau_c = \frac{1}{\pi\Delta\nu} \qquad (2.21)$$

The coherence length L_c is the product of the coherence time and the group velocity of light: $\upsilon_g = c/n_g$, where n_g is the group velocity index of the fiber [82].

$$L_c = \upsilon_g \tau_c \qquad (2.22)$$

Combining the equations (2.21) and (2.22), we find that the minimum linewidth $\Delta\nu$ that can be analyzed is inversely proportional to the fiber length L:

$$\Delta\nu_{MIN} = \frac{\upsilon_g}{\pi L_c} \qquad (2.23)$$

For a fiber length of 2000m and a wavelength of 780 nm the minimum linewidth is evaluated to 30 kHz. Therefore, the setup is suitable to analyze the linewidth of lasers down to approximately 30 kHz.

As the self-delayed heterodyne technique does not require two lasers to be matched in wavelength to a few parts in 10^5 it is easier to operate than the heterodyne setup and speeds up the experimental part of the linewidth analysis. For the investigations on 780 nm DFB-RW laser diodes, the linewidth of all lasers is first determined by the self-delayed-heterodyne technique. Those lasers, for which the self delayed measurements indicate a linewidth approaching or falling below 30 kHz, are then re-investigated by means of the heterodyne technique.

Chapter 3.

Results and Discussions

3.1. High-power narrow linewidth 780 nm lasers Update achievements

In the introduction, we already mentioned about the motivation for the research carried out in framework of this thesis. However, an overview about recent investigations of 780 nm high power lasers, which were oriented also to spectroscopic application, has not been presented. Therefore, this section now provides a short representative summary of results that where obtained by other groups in studies on 780 nm narrow linewidth high power lasers.

High power, narrow linewidth, coherent light sources for 780 nm can be implemented in various ways. All of the concepts but the one described in this thesis require optical components for narrowing the linewidth and, potentially, optical amplifiers to reach power levels of a few hundred milliwatts. In this thesis an approach is followed which relies on improving the spectral stability of high power solitary DFB diode lasers.

The most common concept is based on an external cavity setup (external cavity diode laser, ECDL). With an external blazed grating in Littrow configuration, the ECDLs reported by *Lancaster et al.* [102] deliver an output power of 30 mW at 780 nm with a linewidth of the beatnote signal between two identical lasers of 300 kHz. *Hawthorn et al.* [103] demonstrate a Littrow-type ECDL configuration that can be tuned over 10 nm

and provides an output power of 40 mW and a linewidth of less than 400 kHz. *Shvarchuck et al*. push the maximum output power of a diode laser-based laser system up to 160 mW and demonstrate a linewidth of about 1MHz by amplifying the radiation emitted by a grating stabilized master laser in a broad area diode laser amplifier [104]. The breakthrough in ECDL technology was achieved by *Stry et al.* [105] and *Gilowski et al.* [106]. In [105] the authors presented a Littrow-type ECDL setup with a tapered gain medium capable of generating up to 1 W output power with a linewidth of less than 1 MHz. In [106], *Gilowski et al.* used a narrow-band interference filter to stabilize the laser wavelength to 780 nm. The implementation of a tapered amplifier ensures that the authors can generate an optical output power of more than 1W with spectral linewidth of less than 85 kHz.

Second harmonic generation (SHG) is another technique applied for realizing high power, narrow linewidth coherent light sources emitting at 780 nm. SHG techniques benefit from achievements in fiber laser technology (Erbium doped fiber amplifiers – EDFAs) and recent progress in the production of periodically poled Lithium Niobate (PPLN) crystals. *Thompson et al.*, [107] report an output power exceeding 900 mW at 780 nm by using an EDFA laser system and a cascade of two PPLN crystals. They are demonstrated application of their laser system to absorption spectrum of rubidium. However, no specific linewidth was quoted for their system. Later, *Lienhart et al.* [9] developed a setup for laser cooling of rubidium. Their laser system provided 600 mW of optical power with a linewidth of 2.2 MHz. The most recent achievement, by the best of our knowledge, was published by *Feng et al.* [108]. In this article, the authors describe a 780 nm laser system that delivers 715 mW of optical power with the linewidth of 300 kHz. The advantage of EDFA-based SHG systems over ECDLs is that they provide higher optical power, however, only at the price of a relatively complicated setup.

An other approach, namely the Master Oscillation Power Amplifier (MOPA) configuration, combines high output power with narrow linewidth emission. It is based on a low power DFB diode laser which is optimized for minimum emission linewidth. The light of this master oscillator is then fed through a power amplifier that boosts the output power typically by 10 dB without degrading the spectral perfomance. *Sacher et al.* [109] proposed a MOPA setup that employs a DFB diode laser as the master oscillator and a tapered amplifier for power amplification. This setup is called a DFB MOPA. It is capable of delivering 1.5 W of optical power with good beam quality and a linewidth of less than 5 MHz. The linewidth of the DFB MOPA is mostly limited by background ASE generated by the tapered power amplifier.

Very recently, by using an extremly huge system based on a Ti: Sapphire tunable laser with an additional external cavity [110], *Chiow et al*. demonstrate a Ti:Sapphire laser

that is tuneable between 750 nm and 810 nm and which provides an optical power of up to 8 W with a linewidth of less than 1 kHz. However, this was only achieved with huge efforts in active laser frequency stabilization. A system like this lags all the advantages of diode lasers, namely the compactness, the mechanical stability, the reliability, and the relatively small costs.

Finally, we would like to come back the state-of-the-art results for solitary DFB diode lasers. The first high power (50 mW) 780 nm DFB diode laser was reported by *Takigawa et al*. [111] in 1989. Since then, no significant improvement on DFB laser performance has been reported until recently. *Kraft et al.* [1] present a solitary DFB diode laser with the linewidth of 2 MHz, that provides an optical power of 80 mW. This also is a typical specification for commercially available DFB diode lasers. Our group [112] very recently demonstrated DFB lasers with sub-100 kHz short term linewidth at an optical power of 100 mW.

In the next sections of this chapter, the performance of our solitary DFB laser will be discussed.

3.2. Specifications of the samples under test

This section provides an overview about the main specifications of the DFB-RW lasers that are investigated within the framework of this thesis. The samples can be categorized in three groups represented by the three different wafers they come from. Each group contains lasers with different mounting concepts: lasers mounted in a sealed SOT housing (denoted Sx, see Fig. 2.7b), lasers mounted in a sealed TO3 housing (denoted Tx, see Fig. 2.7c), and lasers mounted on an "open" C-mount (denoted Cx, see Fig. 2.7a). The cavity length of the lasers is either 1.5 mm or 3 mm. The coupling coefficient of the grating is designed to match either 1 cm^{-1} or 2 cm^{-1}. The rear facet of all lasers is coated with a nominal reflectivity of 95%, whereas the front facet reflectivity is varied between $<10^{-4}$ %, 5%, 10%, and 30%. Detailed information of all lasers available for this thesis project is summarized in Table 3.1 below.

The "matrix" of different lasers defines a basis for comparing different mounting styles, different laser lengths, different coupling coefficients, and different front facet reflectivities with respect to electro-optical properties, spectral emission, and spectral stability. When analyzing the influence of a certain parameter we only vary that parameter but - as far as possible - keep all other parameters fixed. For example, to compare the influence of front facet reflectivity we select lasers from the same wafer, that have the same grating constant, the same cavity length, and that are mounted on

the same submount as well as in or on the same type of housing. This way we decouple the different effects as much as possible. We typically analyze at least three lasers of each kind in order to provide at least some statistical basis.

Table 3.1. *Specifications of 780 nm DFB lasers under test*

Group	Batch	Package (heatsink/ submount)	Cavity length (μm)	Nominal coupling coefficient (cm^{-1})	Nominal front facet reflectivity (%)	Ref. section
01	*S1-15-2-00-1..6*	SOT/AlN	1500	2	$<10^{-4}$	3.4; 3.5; 3.7
	C1-15-2-00-1..3	C-mount/CuW	1500	2	$<10^{-4}$	3.3; 3.5
	C1-15-2-05-1..3	C-mount/CuW	1500	2	5	3.6; 3.7; 3.8
	C1-30-2-00-1..3	C-mount/CuW	3000	2	$<10^{-4}$	3.3; 3.5; 3.6; 3.8
	T1-30-2-00-1..3	TO3/AlN	3000	2	$<10^{-4}$	3.5
02	*C2-30-2-00-1..4*	C-mount/CuW	3000	2	$<10^{-4}$	3.3; 3.5; 3.7; 3.8
	C2-30-2-05-1..3	C-mount/CuW	3000	2	5	3.3; 3.8
	C2-30-2-10-1..3	C-mount/CuW	3000	2	10	3.3; 3.8
	C2-30-2-30-1..3	C-mount/CuW	3000	2	30	3.3; 3.8
	T2-30-2-00-1..4	TO3/AlN	3000	2	$<10^{-4}$	3.4; 3.5
03	*S3-15-1-00-1..5*	SOT/AlN	1500	1	$<10^{-4}$	3.7
	C3-15-1-00-1..3	C-mount/CuW	1500	1	$<10^{-4}$	3.4; 3.5; 3.6
	C3-30-1-00-1..3	C-mount/CuW	3000	1	$<10^{-4}$	3.6; 3.7

3.3. Electro-Optical and spectral characteristics of the DFB lasers

The electro-optical characteristics, i.e. power and voltage vs. current (P-U-I) characteristics, and the spectral characteristics are the basic properties that describe the performance of a device. These properties have been investigated for all of the samples

described in previous section 3.2. The study on the short-term spectral stability, i.e. the linewidth characterization, is performed in an operating regime that is selected based on the basic characterization. Therefore, the starting point for a discussion of the results derived in this thesis work is the analysis and discussion of typical experimental data for P-U-I characteristics and spectral characteristics of the DFB lasers. The corresponding data refer to samples that differ with respect to cavity length as well as facet reflectivity. The dependence of laser performance on these parameters will be now be discussed in detail.

3.3.1. Electro-optical characterization

The PUI characteristics of 780 nm DFB diode lasers are measured with the setup described in section 2.2. Optical output power vs. injection current, *P(I)*, and voltage drop across the device vs. injection current, *U(I)*, are plotted in the same graph together with the conversion efficiency *η(I)* that is deduced from *P(I)* and *U(I)* data.

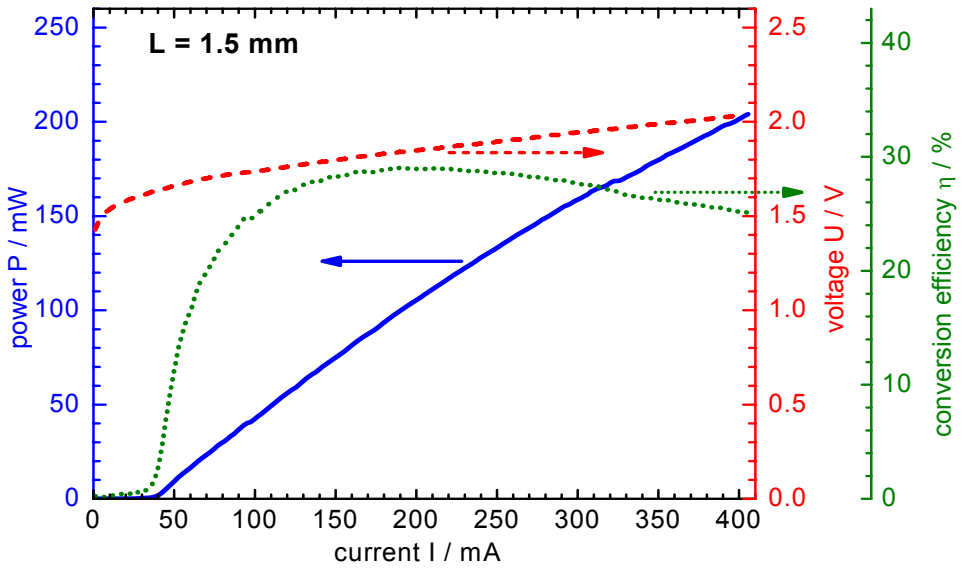

Figure 3. 1. *Optical power, voltage and conversion efficiency versus current Of a 780 nm DFB laser (device C1-15-2-00-1) at 25 °C.*

Fig. 3.1 shows *P(I)*, *U(I)* and *η(I)* of the DFB laser *C1-15-2-00-1* (cavity length 1.5 mm) recorded at 25°C. These results are typical for the DFB lasers with a cavity lengths of L=1.5 mm and a front facet reflectivity of $R_f < 0.01\%$. As can be seen in Fig. 3.1, this laser has a threshold current of about 39 mA and provides more than 205 mW of output power at an injection current of 400 mA at a forward voltage drop of 2.04 V. Up to about a current of 250 mA, the *P(I)* curve shows a slope efficiency of about 0.65 W/A. A further increase of the injection current to 400 mA reduces the

slope efficiency down to 0.56 W/A. A significant reduction of the slope efficiency is observed above 300 mA for almost all of the 1.5 mm cavity length lasers under test.

The reduction of the slope efficiency at large injection currents is mainly caused by heating of the active region, and that is referred to as Joule heating effect. This heating can be described by the effective series resistance of the diode, which includes the contact resistances as well as the bulk resistance in the heterostructure itself [114]:

$$P_{joule} = I^2 R_s = P_{total} - P_{out} \qquad (3.1)$$

where P_{joule} is the Joule heating term, I is the injection current, R_S is the effective series resistance, P_{total} is the electrical power consumed by the device, P_{out} is optical output

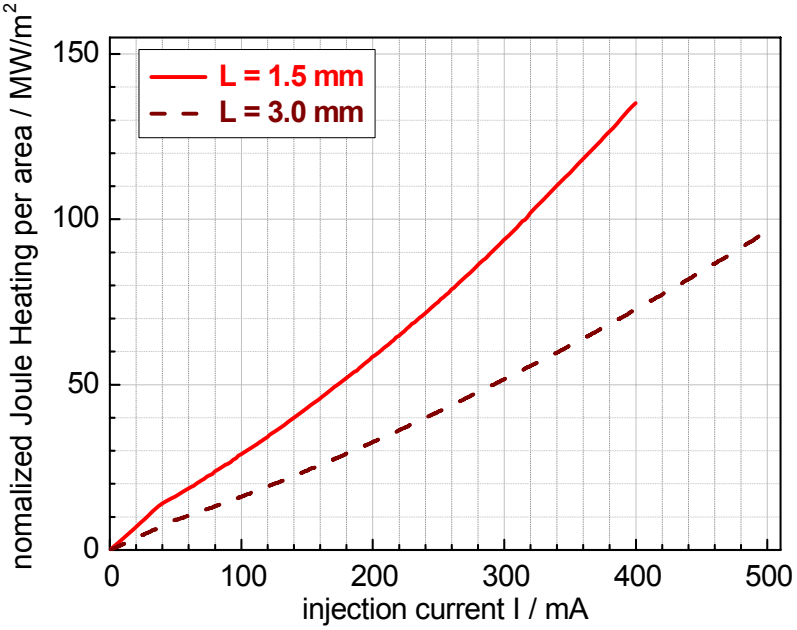

Figure 3.2. *Normalized Joule heating per area versus injection current of devices: C1-15-2-00-1 and C1-30-2-00-1.*

The Joule heating per unit area is shown in Fig. 3.2 for the device *C1-15-2-00-1*, and is extracted from data shown in Fig. 3.1. It clearly indicates that heating increases with increasing injection current thus reducing quantum efficiency of DFB laser.

The conversion efficiency calculated from the experimental data shown in Fig 3.1 reveals a maximum efficiency of about 30% that is typical for most of the 1.5 mm DFB lasers that were investigated. The measurements performed on the series of devices *S1-15-xxx, C1-15-xxx, S3-15-xxx*, and *C3-15-xxx* (see Table 3.1) revealed a behaviour similar to that of the device *C1-15-2-00-1*: the threshold currents at 25°C ranged from 30 mA to 42 mA. The maximum output power reached values between 190 and 230 mW at injection currents of approximately 400 mA. The slope efficiency of all lasers, which were calculated from threshold to 250 mA, varied between 0.55 W/A and 0.7 W/A.

We now turn to DFB lasers with 3 mm long cavities. The PUI characteristic of the sample *C1-30-2-00-1* with a front facet reflectivity of $R_f < 0.01\%$ was recorded at 25°C. The result is shown in Fig 3.3, which is similar to Fig 3.1. As expected, the threshold current is slightly increased to 45 mA compared to 39 mA of the 1.5 mm long device. The slope efficiency of about 0.63 W/A remains constant up to an injection current of 350 mA. The optical output power reaches 280 mW at 500 mA at a voltage drop of 2.21 V across the device. The maximum conversion efficiency is about 27%. This value is slightly smaller than the corresponding value for the device with 1.5 mm cavity length as a longer cavity leads to increased material loss. No roll-over can be observed but the slope efficiency is substantially reduced above 350 mA from 0.63 W/A to 0.6 W/A at 500 mA.

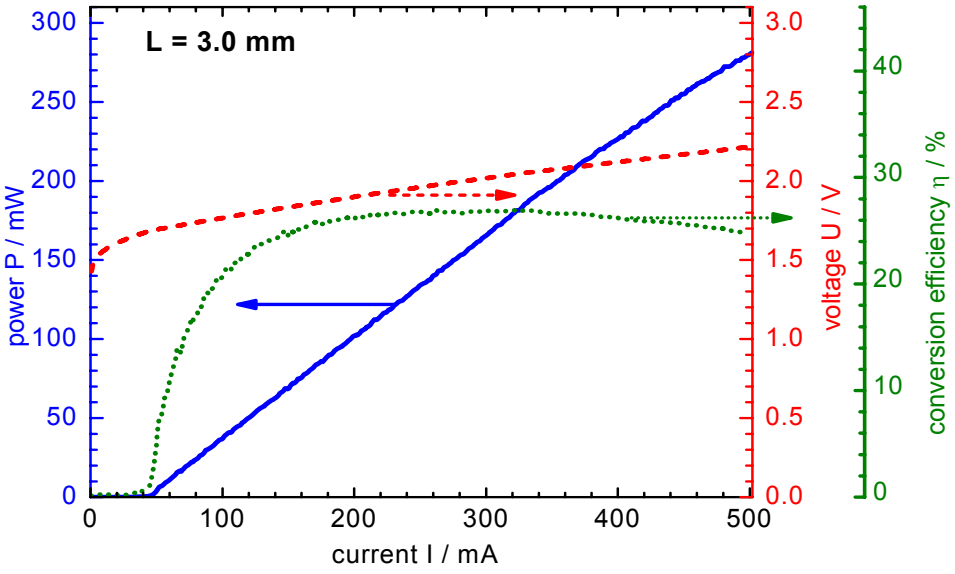

Figure 3.3. *Optical power, voltage and conversion efficiency versus current of 780 nm DFB laserv C1-30-2-00-1 with 3 mm cavity length at 25°C.*

The Joule heating of the device *C1-30-2-00-1* is described in Fig 3.2. Obviously, the heat load per unit area generated within the 3.0 mm DFB laser chip is significantly smaller than the load for the 1.5 mm chip (by a factor of 1.8). This explains why the slope efficiency at large injection currents is larger for the longer chip than for the shorter. Another advantage of longer lasers is that they can be operated more easily at high power levels than shorter lasers because of the reduced Joule heating. The analysis of all 3 mm long DFB lasers at 25°C provides the following information: the typical threshold currents ranges from 40 to 50 mA, the output power reached at 500 mA takes on values between 240 and 310 mW, and the effective slope efficiency (up to 500 mA) lays between 0.53 W/A and 0.68 W/A. The reduction of the slope efficiency at large operating currents is less pronounced for the 3.0 mm long devices. In principal, as there is no roll-over observed, the injection current may be increased to

values above 500 mA so that an output power in excess of 280 mW should be achievable. However, an output power of 300 mW emitted from the ridge-waveguide active region with dimensions of 1 x 3 μm^2 leads to a facet load of 100 $mW/\mu m^2$ (10 MW/cm^2). This is very close to COMD threshold of lasers based on GaAsP material [115]. Therefore, the output power should be limited to 300 mW for DFB lasers with a ridge wave guide width of 3 μm or less in order to ensure reliable operation and reasonable life times for these devices.

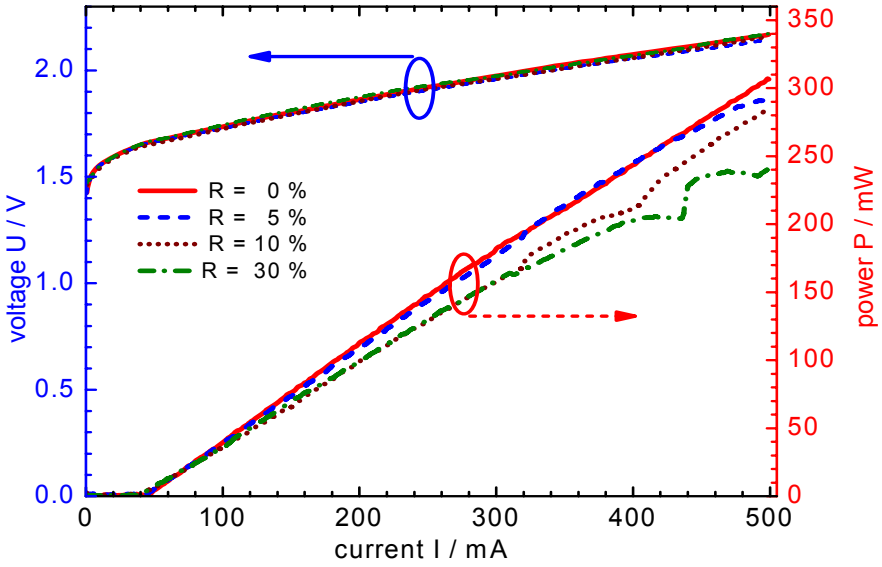

Figure 3.4. *PUI characteristics of 3 mm long 780 nm DFB diode laser, the rear facet reflectivity is 95% and the front facet reflectivity is varied: < 0.01% (C2-30-2-00-1), 5% (C2-30-2-05-1), 10% (C2-30-2-10-1), and 30% (C2-30-2-30-1).*

The last topic to be addressed in this sub-section relates to the effect of front facet coating onto PUI characteristics. While the rear facet of all lasers was coated to 95% reflectivity the out facet reflectivity way varied between R < 0.01%, 5%, 10%, and 30%. Here, we do not explain the motivation for this procedure - this will be addressed in the section 3.8. However we present PUI characteristics of these lasers. The samples: *C2-30-2-00-1, C2-30-2-05-1, C2-30-2-10-1, C2-30-2-30-1*, all packed on C-mount, were characterized at 25°C. The result is shown in Fig. 3.4. The threshold current decreases from 48 mA to 40 mA as the reflectivity is increased from < 0.01% to 30%. The output power at 500 mA ranges between 240-310 mW for all lasers. The slope efficiency is reduced from 0.67 W/A (for R < 0.01%) to 0.52 W/A (for R = 30%). As expected, the voltage drop across the device does not depend on coating.

It is important to note that lasers with front facets coated to relatively high reflectivities tend to show instabilities in the power current characteristic. At high-power operation, the P-I curves for DFB lasers with facet reflectivity above 5% show a significant

variation of the power versus current, most prominently emphasized by several kinks. This behaviour is most clearly observed with the R = 30% (*C2-30-2-30-1*) device.

The underlying phenomenon can be briefly explained as follows. The substantially higher feedback coefficient at the front facet of the lasers ensures a high photon density inside the cavity. This has the following consequences:

- The power build-up of the optical field inside the resonator spatially broadens the active region. This increases cavity loss thus causing a reduction of quantum efficiency that causes "kinks" in the PI-characteristic [116].
- If the longitudinal mode intensity distribution is nonuniform, then, as the photon density increases at large injection currents, spatial hole burning evolves and an associated longitudinal nonuniformity in the effective refractive index and gain of the mode develops. This alters the longitudinal mode intensity profile, which changes the mode gain and hence the mean carrier density and refractive index of the mode. The result under static conditions is a nonlinear light-current characteristic with increasing output power [117].

3.3.2. Spectral properties of DFB lasers

In this section, we present some fundamental spectral properties of DFB diode lasers. We first consider the emission spectrum of a DFB diode laser at a specific operating temperature and injection current. The spectrum is analyzed by a high dynamic range (> 60 dB dynamic range @ ± 0.2 nm offset) OSA described in the setup of section 2.2.2. Fig 3.5. shows the results of measurements on device C2-30-2-05-1 operated at a temperature of 25°C and at power levels of 100, 200 and 300 mW. The spectra show that the center wavelength shifts from 782.62 nm at 100mW (180 mA) through 783.10 nm at 200mW (329 mA) to 783.37 nm at 300 mW (477 mA), corresponding to a tuning coefficient of 3.75 nm/W (2.5 nm/A) The corresponding side mode suppression ratio (SMSR) reaches or exceeds 48 dB, 50 dB, and 53 dB for the values of the injection current considered. The result of the SMSR measurement is important for the discussion of the laser linewidth. In several studies ([62],[76],[118],[119],[120]), the influence of SMSR on the linewidth of the DFB lasers has already been considered. It was shown that the existence of the side modes does not significantly affect the laser linewidth via mode partition noise as long as the SMSR exceeds 40 dB. As our measurements indicate an SMSR well in excess of 40 dB for all of the lasers analyzed in this work, we conclude that mode partition noise can be neglected.

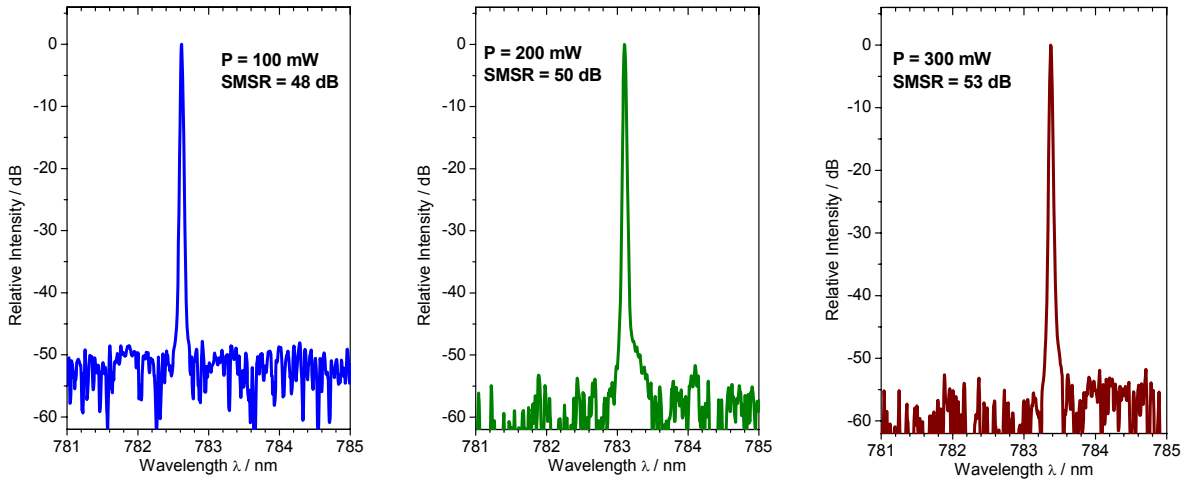

Figure 3.5. *Single spectrum of DFB laser C2-30-2-05-1. Mount temperature is 25°C.*

Spectral characterizations are also performed to analyze how the device's spectral performance depends on the injection current. Fig. 3.6 shows how the emission spectrum of two DFB lasers *C1-15-2-00-1* and *C1-30-2-00-1* depend on injection current at an operating temperature of 25°C (3D "spectral maps"). The following results are derived from the spectra:

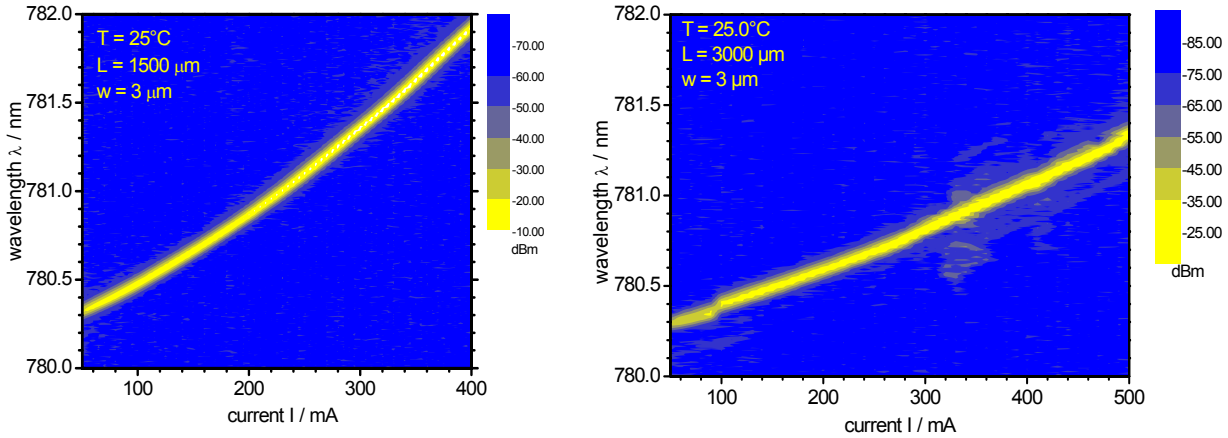

Figure 3.6. *Spectral map of 780 DFB diode lasers:*
a) 1.5 mm cavity length (C1-15-2-00-1) with Δλ/ΔI of 0.0041 nm/mA; and
b) 3 mm cavity length (C1-30-2-00-1) with Δλ/ΔI of 0.0023 nm/mA.

Both spectral maps show that single mode operation is maintained for an injection current ranging from just above threshold (50 mA) to 400 mA and 500 mA with devices *C1-15-2-00-1* and *C1-30-2-00-1*, respectively. At every current setting the spectrum indicates a SMSR in excess of 40 dB, except for injection currents close to 350 mA (*C1-30-2-00-1*), where SMSR is reduced to about 30 dB. This behaviour may

be attributed to spatial hole burning, which more likely appears in long cavity devices (see [120]).

Both spectral maps provide information about how the emission wavelength shifts with the injection current. Wavelength shifting is caused by Joule heating. Heating of the laser chip leads to a reduction of the active region band gap which causes a red-shift of operation wavelength with increasing injection current. If we compare the shift present in the two spectral maps of Fig. 3.6 to the corresponding Joule heating versus current curves in Fig. 3.2, it is obvious that they coincide (Fig. 3.7). The 1.5 mm long laser *C1-15-2-00-1* shifts at 4.1 nm/A whereas the 3 mm long laser *C1-30-2-00-1* shifts at 2.3 nm/mA, i.e. at about half the rate. These values are typical for the DFB diode laser used in this work. The smaller rate for *C1-30-2-00-1* is attributed to better heat dissipation and reduced heating load per unit length in the longer DFB laser. This result points the route to decouple the emission wavelength from injection current: longer DFB lasers have to be used to reduce the effect of Joule heating.

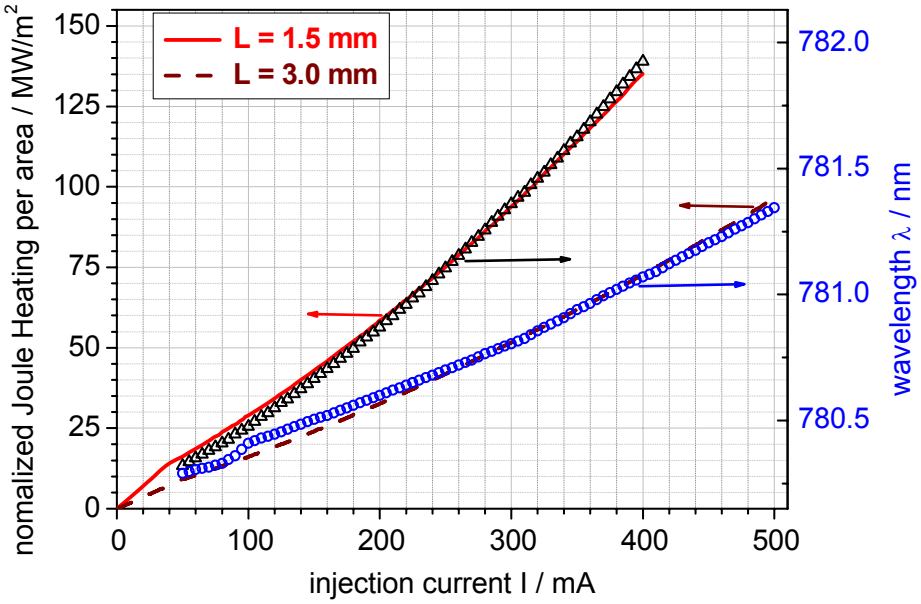

Figure 3.7. *The connection of wavelength shifts of 1.5 mm (open triangle), 3 mm (solid circle) lasers and corresponding normalized Joule Heating per area of 1.5 mm (solid line) and 3 mm (dashed line) lasers with the variation of injection current at 25°C.*

For the 1.5 mm long device *C1-15-2-00-1* the wavelength smoothly increases with injection current. In contrast, the emission wavelength of the 3 mm long device C1-*30-2-00-1* shows a discontinuity at current of 100 mA. The phenomenon is known as mode hopping. Mode hopping occurs when the two modes that provide the highest gain, exchange their roles due to a shift of the gain profile, that occurs via Joule heating when the injection current is increased. From the data of Fig. 3.6b, we deduce

a mode hopping gap of about 0.035 nm. This mode hopping behaviour occurs between the two modes adjacent to the stop band of the DFB grating (stop band modes). The same stop band width is deduced from ASE spectra (presented in section 3.4). Mode hopping is a typical signature of DFB diode laser spectra when temperature or injecton current are tuned. Typically, after a mode hop, the DFB laser emits in single longitudinal mode again with high SMSR. However, during linewidth characterization by the heterodyne technique, attention has to be paid to the operating regime of the two DFB diode lasers in order to avoid mode hopping of either of the DFB lasers.

The preceding discussion focused on the influence of the injection current on the spectral behaviour of DFB lasers. As described above, this can be considered an "internal" thermal effect. Now, we refer to "external" thermal effects, i.e. we analyze how laser mount - and therewith laser chip - temperature affects the spectral properties of DFB lasers.

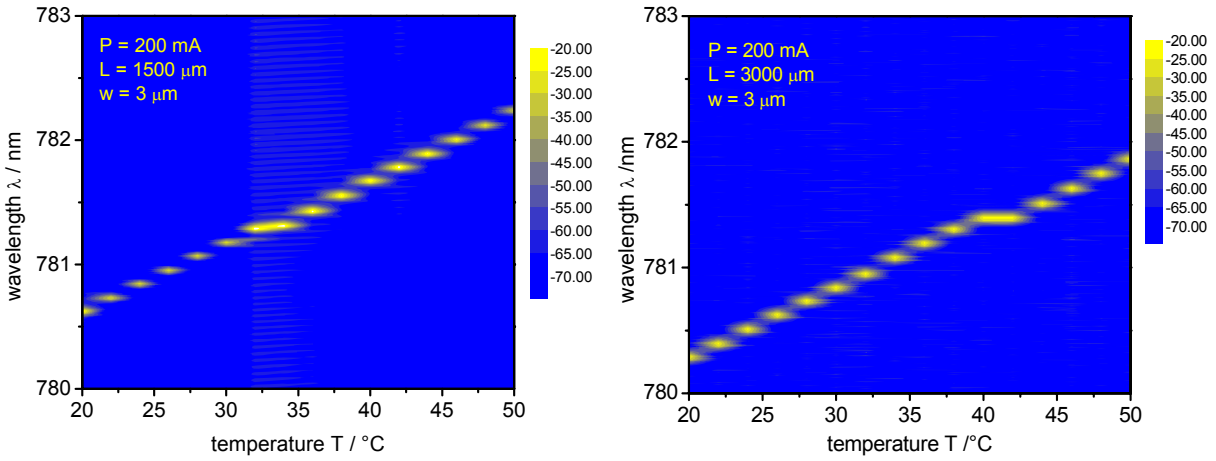

Figure 3.8. *Spectral map of 780 DFB diode lasers, wavelength versus temperature at 200 mA: a) 1.5 mm cavity length (C1-15-2-00-1;) and b) 3 mm cavity length (C1-30-2-00-1).*

Fig. 3.8 shows spectral maps of the two devices *C1-15-2-00-1* (1.5 mm length) and *C1-30-2-00-1* (3 mm length) vs. the operating temperature at an injection current of 200 mA. The operating temperature was varied from 20°C to 50°C with step size of 2°C. The SMSR of the spectrum at any temperature exceeds 40 dB. Both lasers show thermal shift rates of 0.053 nm/°C (1.5mm) and 0.052 nm/°C (3mm) (see Fig 3.9), that are identical within the uncertainty of the measurement. This is expected as the spectral characteristics only reflect the dependence of the laser material on temperature. The temperature and current tuning rates are important parameters. Their knowledge is required for heterodyne linewidth measurements, when two lasers have to be wavelength-tuned in order to match their emission wavelength to better than 1 pm.

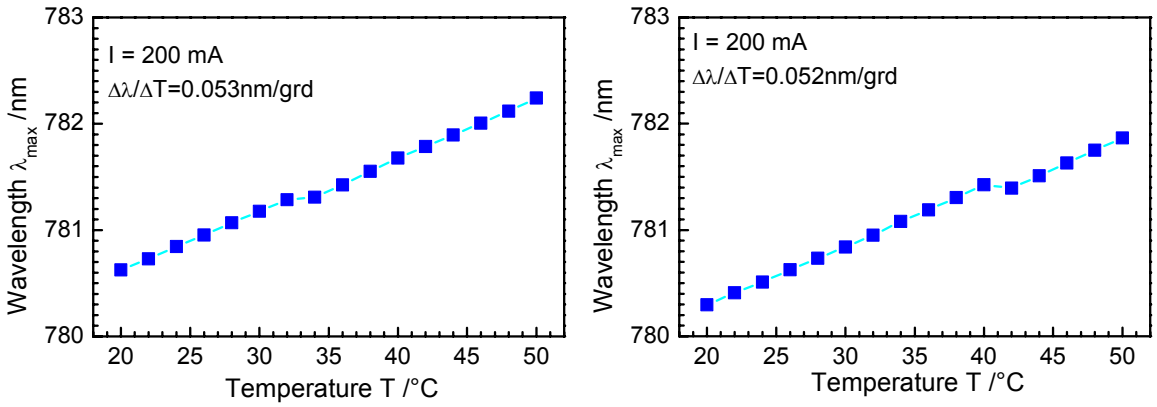

Figure 3.9. *Wavelength versus temperature of 780 DFB diode lasers at 200 mA: a) 1.5 mm cavity length (C1-15-2-00-1); and b) 3 mm cavity length (C1-30-2-00-1).*

3.4. Amplified spontaneous emission spectrum and experimental extraction of individual DFB diode laser parameters

It is well known that the performance of DFB diode lasers is sensitive to parameters that determine the optical properties of the laser cavity, e.g., the coupling coefficient and Bragg wavelength of the grating, the waveguide losses, the group velocity and the magnitude and exact positions of the reflections from the end facets. It is desirable to measure the values of these parameters of manufactured lasers to evaluate and align the manufacturing process and also at an early stage discard components that are unlikely to fulfill the specification [100], [121]. However, these parameters are usually difficult to access directly from laser spectra. To overcome this problem, determination of the amplified spontaneous emission spectrum (ASE), which contains important information about fundamental parameters of DFB lasers, is considered as alternative solution [100], [121]-[125]. From the ASE spectra, the above parameters can be estimated. Therefore, in this section, we spend time to firstly explain the ASE spectrum, and secondly to describe the procedure used to extract some parameters of individual 780 nm DFB diode lasers from the ASE spectra.

3.4.1. Amplified spontaneous emission spectra of DFB lasers

Amplified spontaneous emission in gain medium of DFB diode lasers denotes the spontaneous emission of photons into the laser mode and subsequent optical amplification by stimulated emission within the amplifier. ASE spectra can only be recorded when the laser operates at or closely below threshold. The determination of ASE spectra for the 780 nm DFB diode lasers was performed with the setup depicted in Fig. 2.10 of section 2.2.2. However, for this measurement, the OSA Advantest

Q8384 is substituted by an OSA Advantest Q8347 that provides higher spectral resolution (2 pm at 780 nm). The radiation emitted from front facet of the DFB diode lasers is coupled into a single mode optical fiber that transferred the light to the OSA. The DFB diode laser is kept at 25°C during the measurement. The injection current is adjusted to just below threshold. As the threshold current can not be defined precisely, a few ASE spectra should be recorded near the estimated threshold current (typically 2, 3 and 4 mA below the estimated threshold current).

As the accuracy and credibility of fitting results specifically rely on the spectral resolution and signal-to-noise ratio of the ASE spectrum measurement, it is important to use a highly sensitive, high resolution OSA that provides high dynamic range. Unfortunately, OSAs available do not match all of these requirements simultaneously. Therefore, we have to compromise between the resolution and sensitivity in order to ASE spectra with sufficient quality. It should be noted that shorter cavity length DFB lasers usually provide better quality ASE spectra, so that parameter extraction is more reliable for these.

First, an ASE spectrum is quickly captured with low resolution and large span. The example in Fig. 3.10a presents the data derived for the laser *S1-15-2-00-1* with the operating current set to 34 mA. The span is set to 20 nm in order to check for any unusual behaviour of ASE spectrum

Once the quick scan has confirmed the settings for laser current and temperature, ASE spectra are recorded again, now with narrow span (1 nm typ.) centered at the stop band wavelength and with increased resolution (2 pm typ.). In order to increase the signal-to-noise ratio, 20 ASE spectra are averaged. This result is shown in Fig. 3.10b.

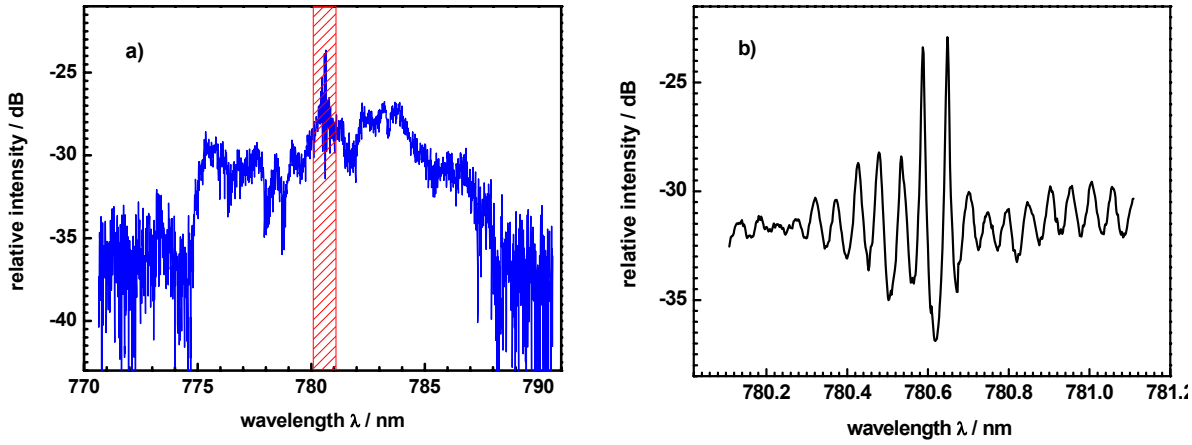

Figure 3.10. *ASE spectra of the laser S1-15-2-00-1 @ 25°C and 34 mA: a) spectral width of 20 nm; b) spectral width of 1 nm after 20 times of averaging.*

3.4.2. Determination of DFB laser parameters from ASE spectra

As mentioned in the beginning of this section (3.4), the ASE spectrum, which has been described in previous section 3.4.1, provides data that can be used to extract some parameters of DFB diode laser. In this section, we describe an algorithm to fit ASE spectra to experimental data in order to receive the following parameters: front facet reflectivity, phase of the grating at the facets (see Fig. 1.18), coupling coefficient and group index of refraction.

The theoretical basis for this extraction is described in detail in Ref. [126] with the derivation of a new Green's function based solution of the inhomogeneous coupled wave equations. The ASE spectra are described by a model that is based on some importance different laser parameters (see Table 3.2). This model is fitted to the experimental data by means of a least-squares method that varies some or all of these laser parameters.

Table 3.2. *Some importance fit parameter of the ASE spectra for 780 nm DFB lasers.*

parameter		***unit***
R_f	*the front facet reflectivity*	
φ_f	*the phase of the grating at the front facet*	2π
R_r	*the rear facet reflectivity*	
φ_r	*the phase of the grating at the rear facet*	2π
κ_r	*Rear part of coupling coefficient*	
φ	*The phase of coupling coefficient*	2π
g_p	*peak gain*	*1/m*
g_c	*curvature of gain (rsp. wavelength)*	$1/m^3$
pk_{lam}	*wavelength of peak gain*	*m*
n_g	*group index*	

The minimization can be performed on the basis of a local or a global numerical search. In contrast to a local search, a global search necessitates no guess values for the parameters to be determined, on the expense of enhanced computational time. Here, the program employs a global search using a stochastic derivative-free algorithm [126], which is combined with a local search. Usually, several minima are found. Among them, hopefully, is the global minimum.

In order to perform the minimization, the theoretical model has to be parameterized. The more parameters are known in advance, the better the fitting procedure works and the more reliable the result is expected to be.

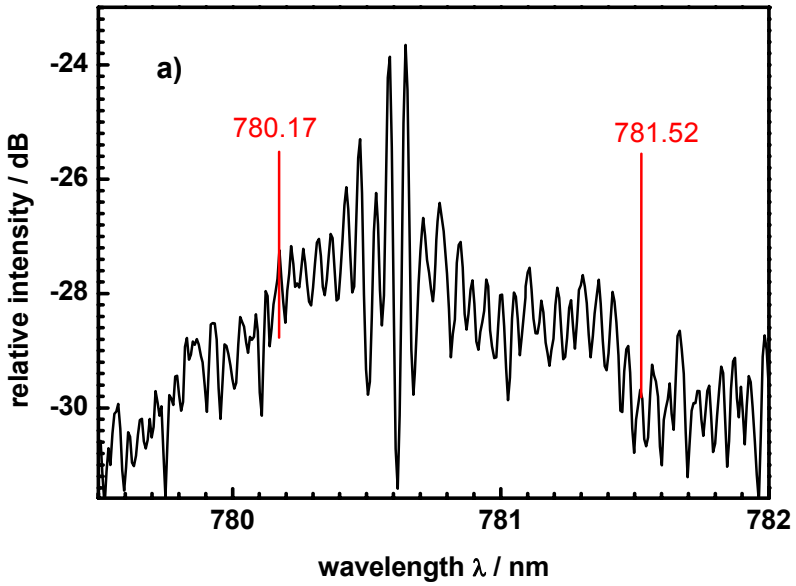

Figure 3.11. *ASE spectral of 780 nm DFB laser to calculate the group index.*

After the above general comments on the method, we know present the details of how the interesting laser parameters are extracted. First, the initial parameters must be estimated for the fitting procedure. The main input parameters include fitting range, cavity length, wavelength of maximum gain peak, Bragg wavelength (center of stop band), group index of reflection, reflectivity of facets, phase of the grating at the facets, and some other parameters (see table Table 3.2). Some of these parameters are well determined, e.g. cavity lengths, wavelength of maximum gain peak, Bragg wavelength. The others are must be estimated or calculated.

For example, the group index n_g of the laser *S1-15-2-00-1* is calculated from the 20 nm wide range spectrum. The mode spacing $\Delta\lambda$ of the ASE spectrum is derived from an average over 25 periods (as shown in Fig. 3.11) and is determined to be 0.054 nm. The cavity length of the DFB laser *S1-15-2-00-1* is 1.5 mm. Substituting these parameter into the equation (1.11) in section 1.1.3, the group index of refraction is found to be n_g = 3.76. The values of other parameters are either estimated on the basis of

experimental data or design parameters. For the fitting, the high resolution ASE spectrum recorded for a span of 1 nm (see Fig. 3.10b) is taken as experimental data input. The fitting spectral range is set to cover 780.35 nm to 780.90 nm as indicated in Fig. 3.12a). The Bragg wavelength is 780.61 nm. For the front facet reflectivity R_f and the rear facet reflectivity R_r the design values of < 0.01 % and 95% are used, respectively. The phase of the both facets, φ_f (for front facet) and φ_r (for the rear facet), are initially set to 0. To the coupling coefficient κ_r an initial value of 2 cm^{-1} is assigned. The fitting routine then evaluates a set of parameter sets for which the fit residuals take on local minima. The most reasonable parameter set for the DFB laser *S1-15-2-00*-1 and the corresponding fitted ASE spectrum are selected. The fitted ASE spectrum for *S1-15-2-00-1* is shown in Fig. 3.12a and the corresponding fitted parameters are given in the Table 3.3. In the Fig. 3.12b and c, we present two more fitted ASE spectra for devices *T2-30-2-00-1* and *C3-15-1-00-1*. The fitted parameters for these DFB lasers are also given in Table 3.3.

Table 3.3. *List of collected parameters from fitting ASE spectrum.*

Parameter / Laser	R_f	φ_f (2π)	φ_r (2π)	κ_r (cm^{-1})	n_g
S1-15-2-00-1 (group 01)	$4.47*10^{-3}$	0.50	0.12	1.98	3.81
T2-30-2-00-1 (group 02)	$5.01*10^{-4}$	-0.20	0.00	2.20	3.96
C3-15-1-00-1 (group 03)	$1.6*10^{-4}$	-0.31	0.30	0.97	3.9

The examples given above are typical for all lasers, for which ASE spectra were analyzed within the framework of this thesis. These example lasers were chosen from three different wafers different laser chip designs (corresponding to the three groups in section 3.2. We should now briefly discuss the result of the analysis, that is summarized in Table 3.3. The group index of refraction varies between 3.8 and 3.9 as expected, the coupling efficiency as well as the front facet reflectivity do not deviate much from their corresponding design values (AR coating $R < 10^{-3}$ coupling coefficient $\kappa_r = 1$ cm^{-1} for *C3-15-1-00-1*, and $\kappa_r = 2$ cm^{-1} for *S1-15-2-00-1* and *T2-30-2-00-1*).

For this thesis work, the most interesting parameters are the phase of the grating at the facets and the coupling coefficient, as these strongly influence the spectral emission properties, specifically the short-term linewidth.

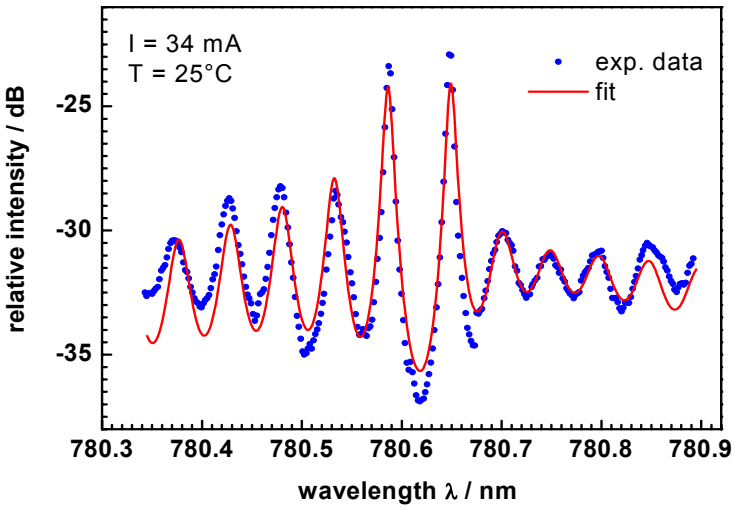

a)

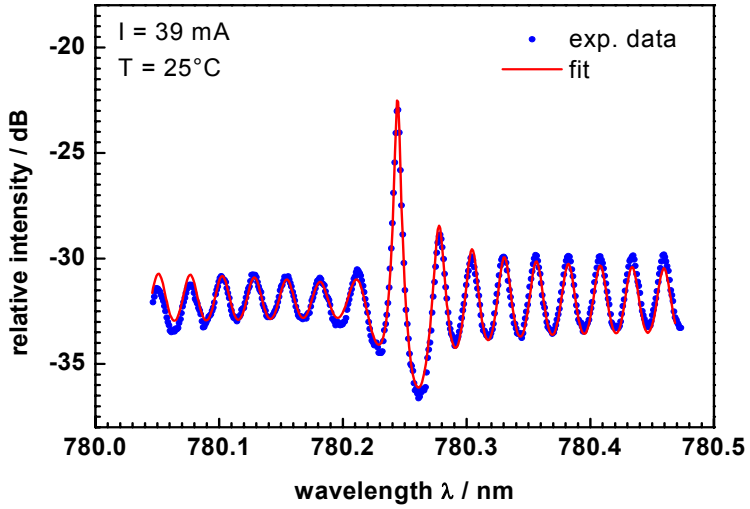

b)

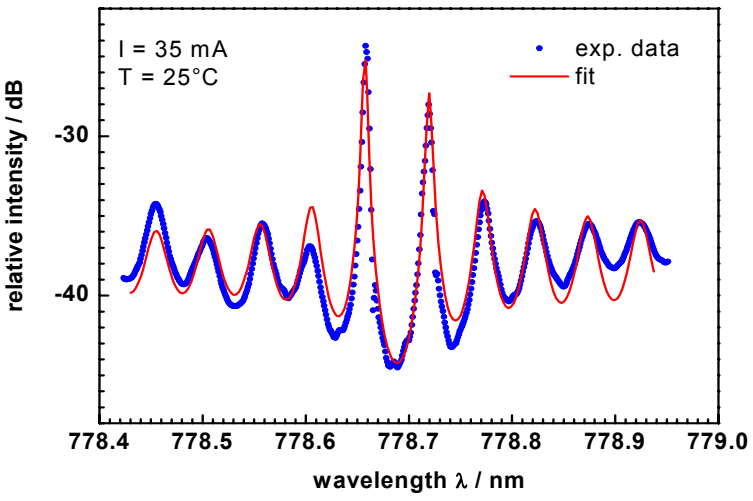

c)

Figure 3.12. *Measured (point) and fitted (solid) ASE spectrum of 780 DBF lasers: a) S1-15-2-00-1; b) T2-30-2-00-1; and c) C3-15-1-00-1*

3.5. The dependence of DFB laser linewidth on the optical output power

After the fundamental characterizations described in section 3.3, the high power DFB lasers are now investigated with respect to their spectral linewidth.

Before discussing the results we would like to emphasize the following remarks:

- The linewidth characterization are only carried out on DFB diode lasers that run single mode, i.e. they are restricted to the maximum injection current level below which single mode operation is maintained
- From heron all linewidth measurements are performed with the heterodyne and/or self-delayed heterodyne technique.
- As the spectral linewidth strongly depends on optical output power as described in section 1.3, linewidth measurements are typically performed vs. optical power.

This section is focusing on following points: first, the general behaviour of the dependence of spectral linewidth on optical power is described in section 3.5.1. Then, in the section 3.5.2, we discuss specific phenomena encountered at high current/high power operation, namely the "linewidth floor" and "linewidth-rebroadening". In section 3.5.3 compare experimental results to theoretical simulations. Finally, the effect of diode laser packaging onto the linewidth is described in section 3.5.4.

3.5.1. Linewidth vs. power dependence

Linewidth measurements can be carried out either with the heterodyne or with the self-delayed heterodyne technique. As already discussed in section 2.3, the heterodyne method is only employed for lasers the linewidth of which reaches the resolution limit (~30 kHz) of the self-delayed heterodyne setup.

First, I would like to briefly recall how the linewidth measurement is performed and the data are analyzed. After setting the DFB diode laser working parameters (e.g. temperature, current or output power) the laser beams in the two path of the setup (either self-delayed heterodyne or heterodyne) are interfered in single-mode fiber Y-coupler. The optical signal is detected with a fast photodiode, recorded with an oscilloscope or a rf-spectrum analyzer, and the corresponding data is dumped into an

ASCII file. Within the data post-processing step, a Voigt profile is fitted to the experimental spectra as described in section 2.3.2d. These measurements are carried out at different injection currents so that the linewidth can be analyzed vs output power. We should note that heterodyne measurements require additional efforts to spectrally overlap the two DFB lasers under test.

According to equation (1.38), the linewidth is proportional to the inverse of the optical output power. Therefore, the most convenient representation of the experimental results is to give the linewidth versus inverse of the optical output power (*1/P*). When the optical output power increases, the linewidth of the DFB laser will monotonically decrease. Following the model described by equation (1.38), the linewidth should linearly depend on the inverse power, i.e. in a linewidth vs. inverse power graph the data points are expected to lay on a line through origin. However, the model only approximately describes the devices's behaviour. If nonlinear effects in the DFB diode lasers, e.g. spatial hole-burning, nonlinear gain, etc. as well as noise sources or external influences can not be ignored, the experimental data are expected to deviate from this linear behaviour.

In our investigation, the linewidth measurements typically start at a power level of 10-20 mW with a step of 5 - 10 mW. The routine measurements for each individual power level setting were performed at 25°C for all DFB lasers under test. Four representative results are shown in Fig. 3.13. In all of these graphs the linewidth is plotted as a function of the optical output power. For the device *C3-15-1-00-1* (Fig. 3.13a.), the linewidth is measured at output power levels ranging from 20 mW to 200 mW. When the optical power is increased, we can see a dramatically reduction of the spectral width from about 2010 kHz (at 20 mW) to about 210 kHz (at 200 mW). A linear fit of to the experimental data, as similarly described by other authors ([58], [127]-[132]), reveals a slope of (41.6 ± 2.0) MHz · mW ("linewidth-power product" $\Delta\nu \cdot P_0$) which performed, This concept provides us a quantitative value to compare different lasers with respect to how there linewidth develops with increasing output power. To compare the experimental linewidth of different lasers in the next sections we apply this simple model to estimate the linewidth at a given power level, if no experimental data exist for that power level.

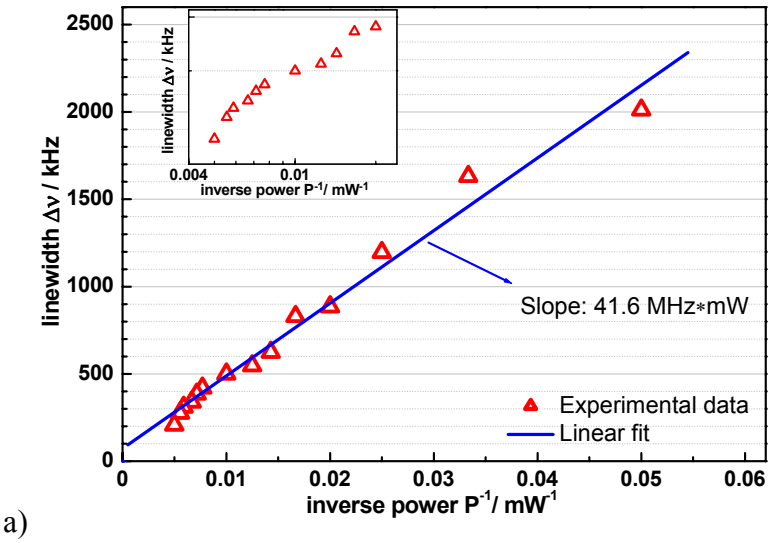

a)

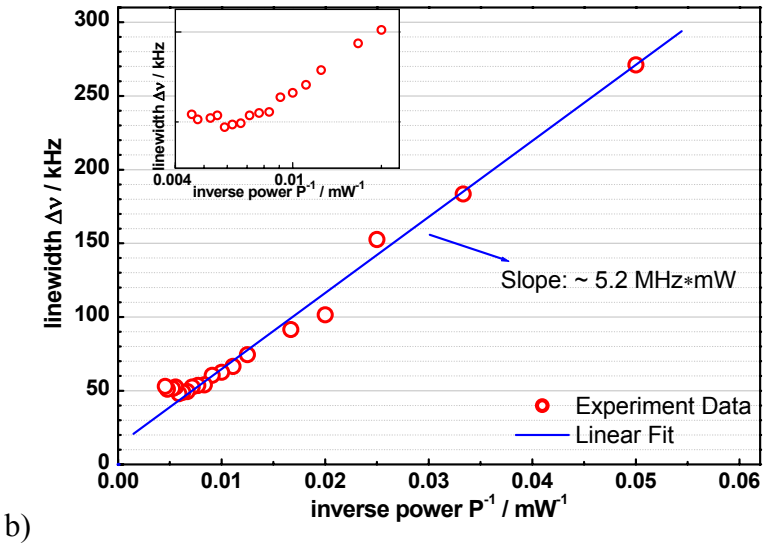

b)

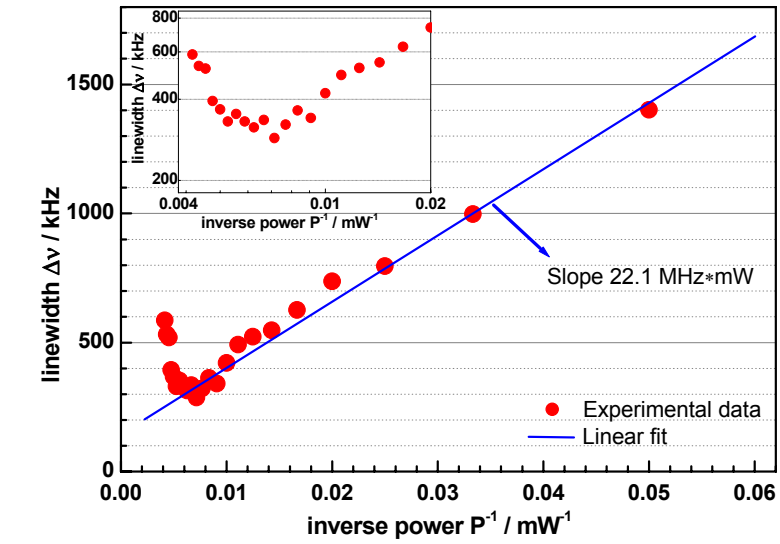

c)

Figure 3.13. *Linewidth versus inverse output power of DFB laser diodes: a) C3-15-1-00-1; b) C2-30-2-00-1; c) C1-15-2-00-3*

We finally want to comment on a specific issue related to the data analysis. In practice, the relation linewidth - inverse power is nonlinear, because the spontaneous emission rate R_{sp}, the effective Henry factor α_{eff} and Petermann factor K are power dependent [133]. However, comparing the result of the simulations described in section 1.3.4 with a linear fit in $1/P_{out}$ we find that for power ranging from 20 mW to 200 mW the deviation between linear fit and experimental data is less than 10%. This allows us to use the linear fit to compare the linewidth and its dependence on output power among various devices. Further explanation and a detailed comparison of different devices are given in the subsequent sections. However, we would like to emphasize that fitting of the $\sim 1/P_{out}$ model must be restricted to a minimum optical power of 10-20 mW and to a maximum power level which is determined by the inset of linewidth broadening effects discussed in section 1.3.3.

Two more representative results are shown in Fig. 3.13b, and Fig. 3.13c. The device *C2-30-2-00-1* (Fig. 3.13b) achieves a minimum linewidth of about 50 kHz (at 170 mW) that corresponds to a linewidth-power product of (5.2 ± 0.2) MHz·mW, starting at about 270 kHz at 20 mW. The asymptotic levelling of the linewidth is observed beyond 230 mW of optical power after reaching the minimum. The last example, device *C1-15-2-00-3* (Fig. 3.13c), shows minimum linewidth of 290 kHz at 150 mW. At an output power of 20 mW the linewidth corresponds to 1800 kHz. Fitting the data yields a linewidth-power product of (22.1 ± 1.5) MHz·mW. The result of this DFB laser illustrates linewidth broadening at high output power. The linewidth increases from 290 kHz at 200mW and reaches 590 kHz at a power of 250 mW.

The above analysis results (i.e. linewidth-power product, minimum measured linewidth) are directly extracted from three DFB lasers that differ with respect to the coupling coefficient, the cavity length, the facet reflectivity, the phase at rear facet. It is therefore not surprising that these lasers show quite different behaviour. Typically, higher power levels potentially yield narrower linewidth, however, this linewidth reduction is limited by the complex behaviours of the lasers at high power levels, as mentioned already. A detailed analysis of the linewidth-power dependence is the aim of all of the following section of this thesis

3.5.2. The spectral linewidth at high power operation

In the previous section, we discussed the linewidth-power dependence of DFB diode lasers at low and medium power levels, i.e. up to 50 mW. We found that the linewidth is proportional to the inverse output power to a good approximation. The observed behaviour is concluded based on statistically analysing of all experimental data.

However, at high power operation a linewidth floor or rebroadening effects mentioned in section 1.3.3 may show up. This section concentrates on discussing the linewidth at high power of DFB lasers, which differ with respect to coupling coefficient, cavity length, and front facet reflectivity. This will allow us to identify several different phenomena that set in at high out power.

The first example in Fig. 3.13a (*C3-15-1-00-1*) shows a monotonic reduction of laser linewidth versus inverse power. We conclude that for the range of optical power analyzed, no linewidth floor or rebroadening effect is observed. This conclusion can also be drawn for another device (*C2-30-2-00-2*), the analysis result of which presented in Fig. 3.14. However, we would like to point out that linewidth floor and linewidth rebroadening most likely could also be observed for these devices, if the linewidth would be investigated at larger power levels. However, at larger output power reliable single mode operation cannot be achieved, which is why the analysis could not be carried out at power levels larger than the ones shown in Fig. 3.13.

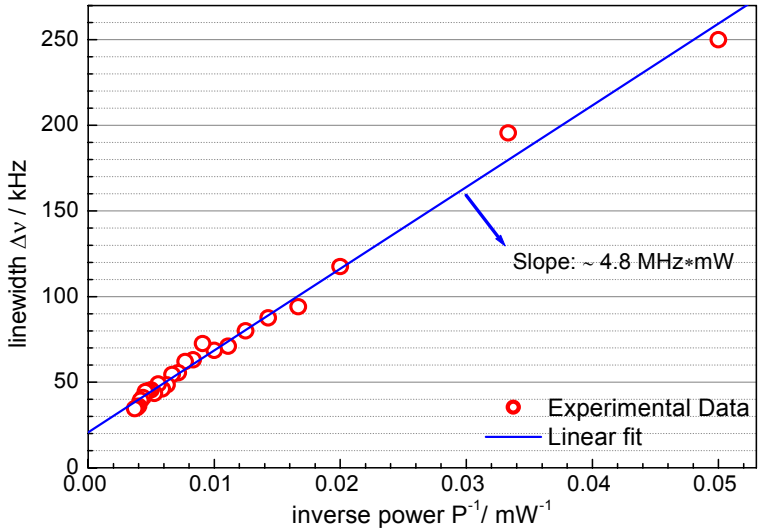

Figure 3.14. *Linewidth versus inverse power of the laser C2-30-2-00-2, upto 270 mW output power without linewidth floor and rebroadening.*

The second example of lasers shows behaviour similar to the one shown in Fig. 3.13b, i.e. a linewidth floor evolves at large output power levels. This effect describes a saturation of the linewidth reduction setting in at sufficiently high power levels. The linewidth saturation effect causes a minimum of linewidth that is considered the linewidth floor. For this particular device, the linewidth does not vary any more beyond a power level of 150 mW. For another device (*T1-30-2-00-1*) shown in Fig. 3.15, the linwidth floor is reached at 130 mW.

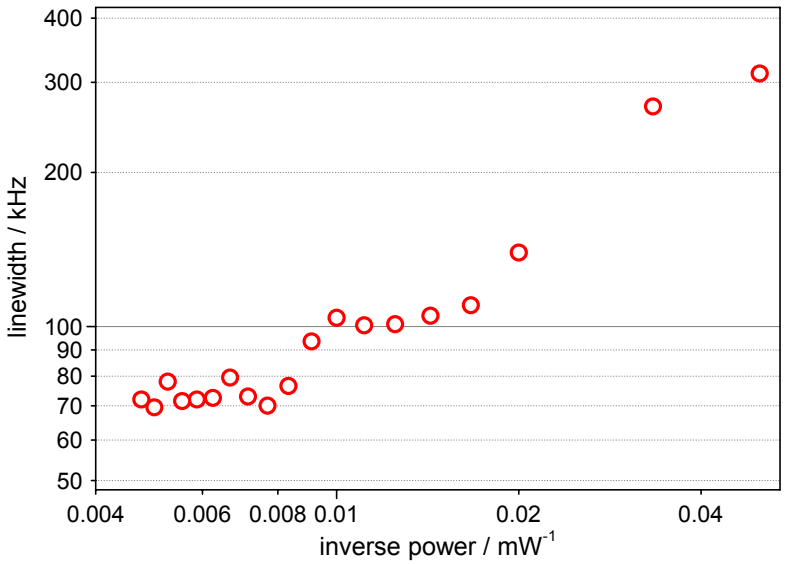

***Figure 3. 15**. Linewidth versus inverse power of the laser T1-30-2-00-1, the linewidth floor start from 120 mW output power.*

The third example of lasers, see Fig. 3.13c and Fig. 3.16, shows linewidth rebroadening. First, the linewidth of the device *C1-15-2-00-3* (Fig. 3.13c) is levelling off in the range of power of 150-190 mW at a linewidth of 290 ÷ 320 kHz. Beyond 200 mW of output power, the linewidth dramatically increases and reaches about 590 kHz at 250 mW. For *C1-30-2-00-1* (Fig. 3.16), a rebroadening occurs at a smaller output power of 120 mW. Beyond 120 mW the linewidth slightly increases.

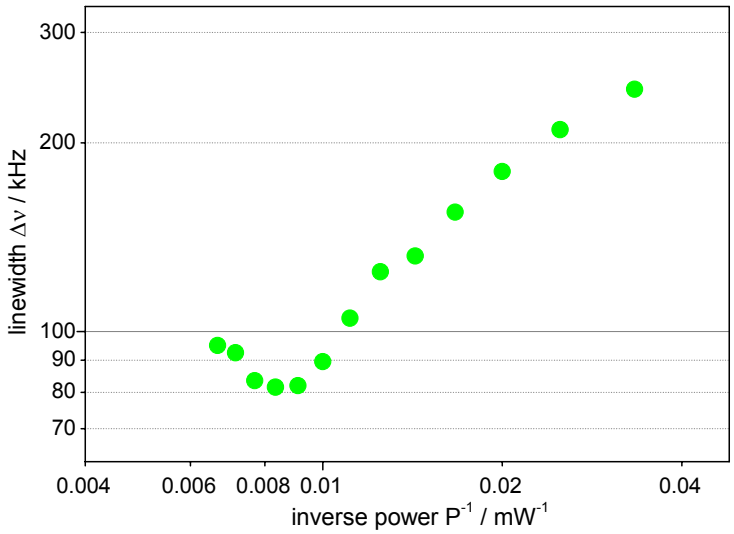

***Figure 3.16**. Linewidth versus inverse power for the laser C1-30-2-00-1, the linewidth floor and rebroadening set in at 120 mW of output power.*

We next would like to give a short summary on the linewidth-power dependence of all DFB lasers investigated within this thesis work. In general, the behavior at high power depends on the structure (e.g. epitaxial layers, grating parameters, etc), configuration

(e.g. cavity length, facet reflectivity, etc) of under test lasers as well as external noise sources. The first group consists of lasers for which the linewidth is monotonically decreasing with increasing output power, i.e. these can be considered the high performance DFB lasers. Only few of the investigated devices belong to this group. Most lasers belong to the second group. There are some lasers show linewidth rebroadening effect (third group). The minimum linewidth achieved varied from 20 kHz to about 300 kHz when the parameters cavity length, coupling coefficient, front facet reflectivity, and packaging configurations were varied.

A complete understanding of the linewidth at high output power is given in detail in the next section where we describe further investigations carried out to clarify the external and internal influences onto the laser linewidth. As already discussed in section 1.3.3 and 1.3.4, the different mechanisms that cause for the linewidth floor and rebroadening phenomena can not be separated well experimentally. Thus it is impossible to precisely determine the degree to which the different effects contribute to linewidth floor and rebroadening. For our DFB lasers, the evolution of a linewidth floor and rebroadening should hence rather be considered a consequence of the following effects:

- The most important effect is spatial hole burning [74], [134]-[136] It directly affects the linewidth enhancement factor. If the spatial hole burning is taken into account, the effective linewidth enhancement factor depends on the optical field intensity in the cavity hence the power. Thus the effective Henry factor increase with increasing power. At low power the influence of spatial hole burning is weak but at high power it competes strongly with the Schawlow-Townes narrowing mechanism. When the increase of the effective enhancement factor at high power balances narrowing, the “linewidth floor” shows up. Further increasing the output power increases of the linewidth enhancement factor so that rebroadening can be observed. The Fig. 3.17 shows a simulation result that takes into account spatial hole burning for our type of DFB lasers. The figure shows a substantial modification of the slope of linewidth-$1/P_{out}$ curve that is attributed to for the increase of the linewidth enhancement factor at high output power. Within the marked areas the reduction of the linewidth with power corresponds to less than 10 kHz which is about the experimental uncertainty of our linewidth measurements. Thus, the simulation results are consistent with the experimentally observed results. Therefore, we consider spatial hole burning to be the main reason for the evolution of a linewidth floor and linewidth rebroadening. The fact that the linewidth floor sets in at lower power than predicted by theory is attributed to details of the DFB lasers that are not included in the model.

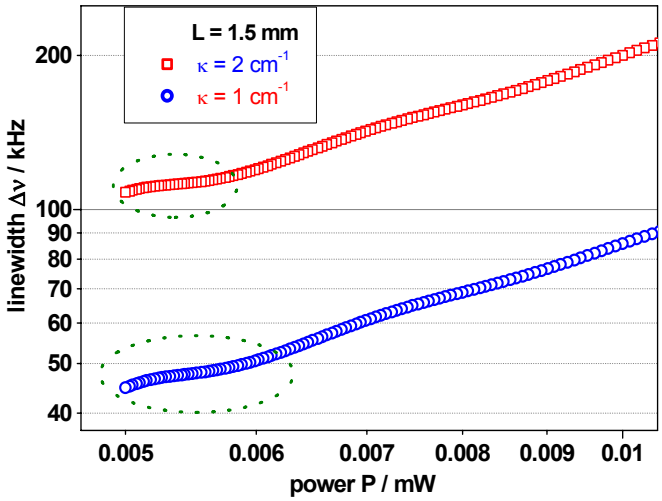

a)

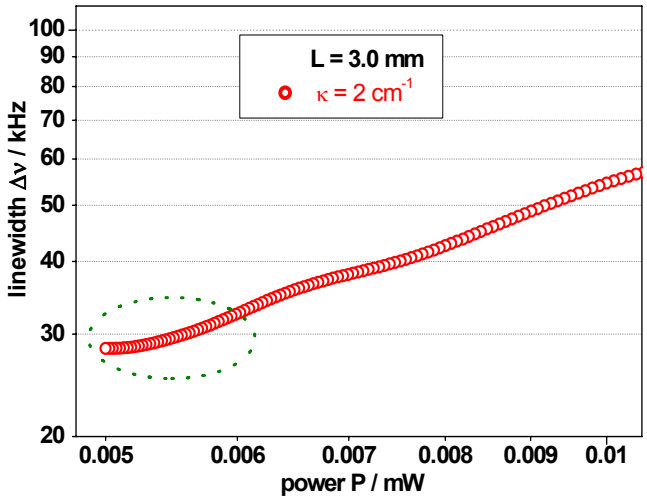

b)

Figure 3.17. *Linewidth simulation results of 780 nm DFB lasers with influence of spatial hole-burning effect at high power (marked areas) for difference cavity length and coupling coefficient.*

- The second phenomenon that in principle contributes to the linewidth floor and linewidth rebroadening is the presence of weak side modes at high power. This has been explained as being due to partition noise between main and side modes associated with cross-saturation from nonlinear gain [137]. Without nonlinear gain, the influence of side modes on linewidth has been shown to be negligible for a Fabry-Perot laser [138]. However, this is not necessarily the case for DFB lasers where longitudinal intensity distributions have shown to play a significant role [139]-[141]. For our lasers, as these matches the criteria formulated by *Pan et al*. in Ref. [62], [136] (single mode operation and SMSR > 40 dB) the side mode effect can be neglected.

- The third phenomenon, namely nonlinear gain, also contributes to the linewidth floor and linewidth rebroadening. In the Ref. [63], a numerical analysis of nonlinear gain effects onto the linewidth floor and the rebroadenning effect is given. The authors came to the conclusion that nonlinear gain effects strongly dependent on the structure and material of active layer (see [63], [142]). Since the design and fabrication of our DFB lasers were optimized with respect to suppression of nonlinear gain effects, the latter may play a secondary role.
- The last contribution to the linewidth floor and linewidth rebroadening that we would like to consider is electronic 1/f noise as well as other sources of technical noise. In the section 2.3.2d, the algorithms using Voigt profile fitting was shown to separate technical noise from white laser frequency noise, that latter of which corresponds to a Lorentzian lineshape. *Mercer* [96] carefully analyzed this algorithm when it is applied to the self-heterodyne measurement technique. They found that any Voigt fitting procedure would in practice ultimately be limited by a deviation of the technical noise spectrum from a perfect *1/f* distribution. This may cause a residual linewidth that limits the linewidth reduction.

We finally conclude this subsection by summarizing its main results. The main cause for the linewidth floor and linewidth broadening is spatial hole burning. Secondary contributions come from weak side mode partition noise and nonlinear gain effects. The extrinsic influences, namely *1/f* and other technical noises, can be separated well from intrinsic noise sources by fitting a Voigt profile to the rf beat note spectra derived in self-delayed heterodyne and heterodyne measurements.

3.5.3. Comparison between experimental results and theoretical simulation

The theoretical analysis of the linewidth of the high power DFB laser was carried out along the lines described at section 1.3.4. The design-parameters of the DFB lasers under test were uses as input parameters for the simulation. A comparison between experimental results and numerical simulations can therefore provide valuable information for improving the performance of the existing devices. It is the aim of this section.

Fig. 3.18 shows the experimental result of a linewidth measurement for the laser *C3-15-1-00-1* (open triangles). It is typical for the DFB laser that belongs to group 03 with cavity length of 1.5 mm (see Table 3.1). The result of the numerical simulation of the laser linewidth (open squares), which was calculated for a coupling coefficient of $\kappa = 1$ cm^{-1}, a cavity length of L = 1.5 mm, an AR-coated (R < 0.01%) front facet, and a grating phase at the rear facet of $\varphi_r = 0$, is also plotted in the same graph. The comparison between experimental and theroretical data shows an agreement at low to medium output power. The small systematic deviation (experimental linewidth

approximately 1.5 times larger than predicted linewidth) may be attributed to feedback from the front facet the location of which with respect to the grating, phase φ_r, is not under control and unknown, see section 1.3.4 and Fig. 1.19. The analysis of the ASE spectrum of this laser yields a grating phase at rear facet of approximately 0.6π rad (see section 3.4, Table 3.3). It is therefore expected that the experimental linewidth is slightly larger than the therotical linewidth that is predicted for a grating phase of φ_r = 0.

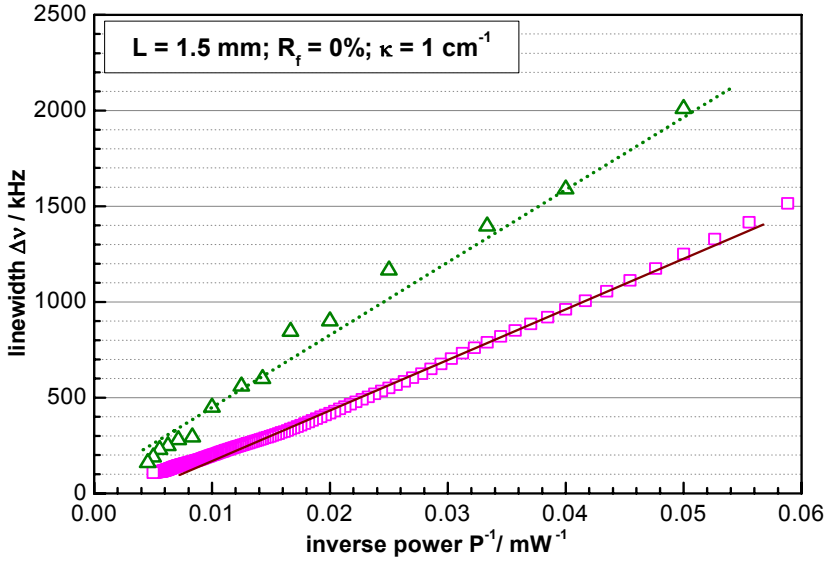

Figure 3.18. *Comparison between simulation (open squares) and linewidth of the device C3-15-1-00-1 (open triangles), The dotted line and solid line are linear fit of the data.*

We would now like to compare the experimental to the theoretical linewidth-power product. To extract the linewidth-power product, as introduced in previous section, we fit a linear model $\Delta\nu = c \cdot 1/P_{out}$ to the experimental and to the theoretical data. In order to exclude linewidth floor and linewidth rebroadening to affect the fit we restrict the input data to a power range of 20 mW to 100 mW. The linewidth-power products for several devices belonging to the same laser configuration are given in Table 3.4.

Table 3.4. *Linewidth power product and linewidth at 100 mW output power of the lasers in the group 03 (L = 1.5 mm, κ = 1 cm^{-1}, R_f < 0.01%).*

Device	SOT					C-mount			*Simulation*
	S3-15-1-00-1	*S3-15-1-00-2*	*S3-15-1-00-3*	*S3-15-1-00-4*	*Average*	*C3-15-1-00-1*	*C3-15-1-00-2*	*Average*	
Δν*P$_o$ *(MHz*mW)*	37.8±1.8	40.8±1.4	48.1±2.3	37.1±1.8	40.9±1.8	48.1±2.3	70.0±2.2	59.0±2.2	32.1±0.3
Δν@100mW *(MHz)*	0.37	0.41	0.42	0.35	0.39	0.40	0.81	0.60	0.20

Looking at Table 3.4, we first recognize the unusual behaviour of the device *C3-15-1-00-2* that we will discuss in the subsequent section 3.6. The linewidth-power products of all other devices are averaged to a value of (40.3±1.7) MHz·mW. This value is in good agreement with the linewidth-power product of (32.1±0.3) MH·mW derived from the simulation data.

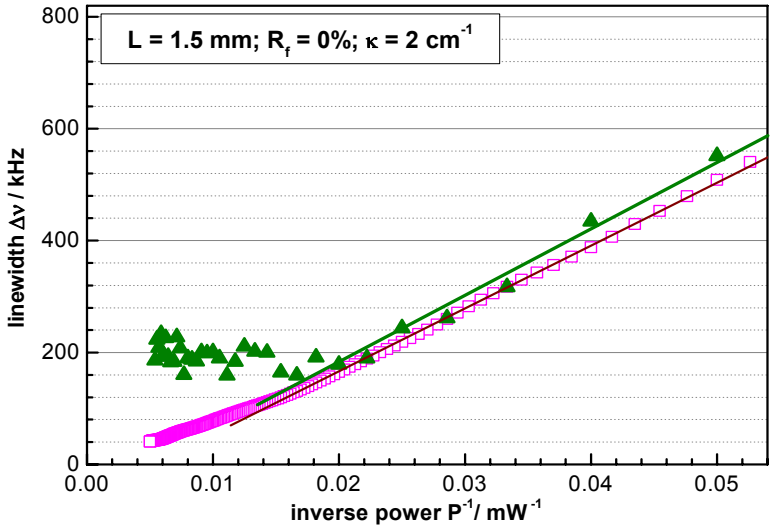

Figure 3.19. *Comparison between simulation (open squares) and linewidth of the device S1-15-2-00-1 (solid triangles), the solid lines are linear fit of the data .*

Fig. 3.19 shows us the result of a comparison between experimental data and simulation result for another device, *S1-15-2-00-1*, with all design parameters identical to *S3-15-1-00-1* but the coupling coefficient set to $\kappa = 2\ \mathrm{cm}^{-1}$. The simulation result derived for the group 01 (see Table 3.1) when assuming a grating phase at rear facet of $\varphi_r = 0$, agrees very well with the experimental data for low to medium output power. Beyond 90 mW, a linewidth floor shows up and even linewidth rebroadening may be observed as the power increases to 200 mW. The linewidth-power product corresponds to (14.7±0.4) MHz·mW, which is in excellent agreement with the value of 14.1 MHz·mW derived from the simulation (fitting of experimental and theoretical data includes linewidth values only up to 80 mW of power). Table 3.5 provides a set of linewidth-power products for several devices belonging to this group. Obviously, two out of the three C-mount devices show a linewidth that exceeds the simulation result by 60%. See section 3.5.4 for an explanation.

Table 3.5. *Linewidth-power product and linewidth at 100 mW output power of the lasers in the group 1 (L = 1.5 mm, $\kappa = 2\ cm^{-1}$, $R_f < 0.01\%$).*

Device	SOT				C-mount				*Simulation*
	S1-15-2-00-1	*S1-15-2-00-2*	*S1-15-1-00-3*	*Average*	*C1-15-2-00-1*	*C1-15-2-00-2*	*C1-15-2-00-3*	*Average*	
Δν*P *(MHz*mW)*	14.7±0.4	12.0±0.3	14.5±1.6	13.7±0.7	20.1±0.8	15.1±0.7	22.1±1.5	19.1±1.0	14.1±0.3
Δν@100mW *(MHz)*	0.22	0.17	0.19	0.19	0.50	0.41	0.40	0.43	0.09

We finally address DFB lasers with 3 mm long cavity. These devices belong to group 01 and group 02 of Table 3.1 with a coupling coefficient of 2 cm^{-1}, i.e. *C1-30-2-00-1* and *C1-30-2-00-2* of group 01, and *C2-30-2-00-1* and *C2-30-2-00-2* of group 02. The linewidths of these DFB lasers at a given optical power level are listed in Table 3.6 together with the corresponding value provided by the simulation. Table 3.6 shows that for a power below 100 mW the experimental linewidth of the DFB lasers belonging to group 02 (i.e. *C2-30-2-00-1* and *C2-30-2-00-2*) agrees well with the simulation results while the results for the devices belonging to group 01 are about 1.6 times larger than the corresponding simulation results. At higher output power (above 100 mW) the linewidth of all four devices is dispersed the narrowing tendency of simulation results. Two devices of group 02 are slightly levelling with power increasing above 100 mW and showing floor signature from 150 mW. The devices *C1-30-2-00-1* and *C1-30-2-00-2* show linewidth rebroadening beyond 140 mW. Beyond 160 mW linewidth measurements cannot be performed because the devices go multi mode. Additionally, the linewidth-power product parameters given in Table 3.7 show relatively small values, which indicates very narrow linewidths. The poorer performance of the devices from group 01 can be attributed to the poorer quality of fabrication process. Although both charges have the same design and fabrication process, the slope efficiency of the devices from group 02 (0.68 W/A) is higher than that of group 01 (0.6 W/A). The PUI characteristics show that, above 350 mA, the slope efficiency of group 1 degrades faster than that of group 02.

The simulation was carried out for an output power of up to 200 mW. However, the DFB laser *C2-30-2-00-2* can be operated at even higher output power. When we increase the current so as to reach 300 mW, the linewidth continues to decrease and reaches the minimum of 30 kHz at 270 mW. Beyond 270 mW substantial rebroadening sets in and a linewidth at the MHz level is reached. This behaviour of the specific

device *C2-30-2-00-2* confirms the competition between narrowing and rebroadening at high power operation.

Table 3.6. *Linewidth versus output power of the lasers in the group 01 and 02 (L = 3 mm, κ = 2 cm^{-1}, R_f < 0.01%).*

Power *(mW)* / ***Device***	***20***	***50***	***80***	***100***	***125***	***150***	***200***
C1-30-2-00-1	410	170	120	90	80	100	rebroadening
C1-30-2-00-2	360	160	110	90	80	80	rebroadening
C2-30-2-00-1	270	120	80	70	60	50	50
C2-30-2-00-2	250	100	70	60	60	50	50
Simulation	260	110	65	55	45	38	29
Inverse power *(mW^{-1})*	***0.05***	***0.02***	***0.0125***	***0.01***	***0.008***	***0.0067***	***0.005***

Table 3.7. *Linewidth-power product and linewidth at 100 mW output power of the lasers in the group 01 and 02 (L = 3 mm, κ = 2 cm^{-1}, R_f < 0.01%).*

Device	C1-30-2-00-1	C1-30-2-00-2	C2-30-2-00-1	C2-30-2-00-2
Δν*P *(MHz*mW)*	7.34±0.40	6.80±0.37	4.58±0.10	3.90±0.12
Δν@100mW *(MHz)*	0.09	0.09	0.07	0.06

In the above paragraph, we have already commented on the comparison between simulation results and experimental data on the linewidth-power product. Experimental results and theoretical prediction qualitatively agree very well, but show a quantitative disagreement at the level of typically a couple of 10 %. The difference of own noise characteristic plays important role that yield a different residual linewidth and deteriorating the linearity of the linewidth - inverse power relation. Additionally, the linewidth and linewidth-power product of nominally identical lasers, even when fabricated on the same wafer, typically differ by a couple of 10%. This is due to the fact that the linewidth strongly depends on the DFB laser parameters. Therefore, only lasers that were fabricated in a process where all process parameters are very precisely under control and do not vary much across a wafer will show better agreement

amongst each other and better agreement with the theoretical predictions. For the batch of devices presented in Table 3.4 we found that the experimental linewidth data exceeds the theoretical predictions by at least 60%. Similar behaviour was found for the devices summarized in Table 3.5, which indicates experimental values that exceed the simulation results by about a factor of 2. The 3 mm long devices presented in Table 3.6 and Table 3.7 show a similar behaviour. Nevertheless, we have seen good qualitative agreement between experimental results and theoretical calculation at least for small to medium output power. At high power operation we still lag a detailed understanding of the effects that determine the short term frequency stability (linewidth) of the lasers. Therefore, further theoretical and experimental investigations are required to resolve this issue.

3.5.4. The influence of packaging on spectral characteristics

Packaging is a key process in diode laser fabrication. Besides enhancing the laser chip quality by improving the growing and processing steps, efforts are undertaken to eliminate any detrimental effects packaging has on the device performance. There are three main aspects of a high quality packaging process: (i) the electrical aspect, (ii) thermal management, and (iii) reduction or suppression of mechanical interference. The first aspect is important only for lasers that are used in high-speed applications. In section 3.3 we already discussed the relation between thermal management and DFB laser performance: highly efficient heat removal reduces the temperature inside the active region and hence improves the laser performance, e.g. the slope efficiency and reliability of the device. The heat sink thermal resistance may lead to a linewidth floor [147]. Regarding the mechanical aspect, packaging induced strain critically affects the emission characteristics, e.g. it shifts the emission wavelength when the laser chip experiences packaging related compressive/tensile strain. This is attributed to a modification of the QW bandgap, to deformation introduced to the grating altering the spectral properties of ASE [144]. Strain also affects the reliability of the diode lasers, especially of long cavity DFB lasers [81], [144]-[146]. References [147],[144],[146], [146] specifically report on the influence of thermal and strain effects onto the spectral properties of DFB diode lasers. Packaging can also generate an inhomogeneous strain along the laser [146], which leads to an inhomogeneous gain effect that causes a rebroadening of the laser linewidth at high injection currents.

The DFB lasers were packaged in C-mount, SOT and TO3 configurations (see section 2.1.4). It is beyond the scope of this thesis work to carry out a detail analysis of the influence different packaging options have onto the laser performance. The results reported in this section should rather be considered a very simple and preliminary

guideline with respect to the packaging configuration for the DFB diode lasers, when devices with high spectral performance are requested.

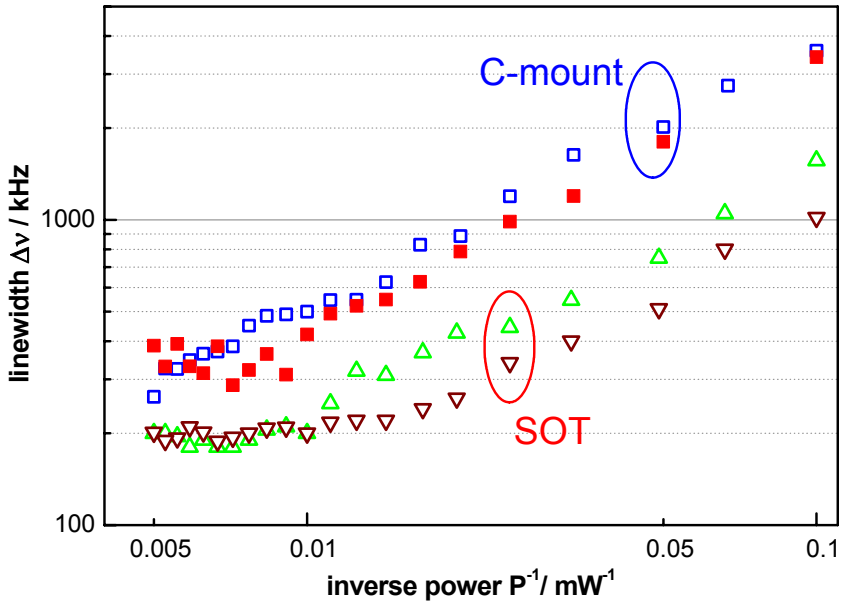

Figure 3.20. *Comparison of the linewidth of 780 nm DFB laser diodes mounted on different submounts and different packages: AlN/SOT (triangles), and CuW/C-mount (squares).*

Fig 3.20 provides a comparison between 1.5 mm long DFB lasers of group 01 (see Table 3.1) packaged on AlN/SOT (closed packaging) and CuW/C-mount (open packaging). The results show a systematic difference between these two packaging configurations. We can observe that the AlN/SOT devices show clearly smaller linewidth than the devices mounted on CuW/C-mount. Additionally, Table 3.8 provides linewidth data for some representative devices from both packaging configurations. The data confirms that the AlN/SOT devices provide better performance than the CuW/C-mount devices. The differences have to be attributed mostly to the following two effects:

- The grating phase at the facets of the devices are likely to be similar among the device on AlN/SOT and among the devices on CuW/C-mount, but are likely to differ between AlN/SOT and CuW/C-mount packaged devices. This could explain up to a factor of two difference in the linewidth, as shown by the simulations in section 1.3.4.
- The linewidth of devices packaged on open mounts (C-mount) and closed mounts (SOT, TO3) differs by more than a factor of two. It is therefore likely, that packaging in an open or closed mount has a significant effect, which however does not amount to a factor of two in linewidth.

However, a reliable conclusion on the performance of AlN/SOT devices vs. CuW/C-mount devices requires further experiments with the DFB laser chips that are as identical as possible, i.e. come from the same laser bar and are closely neighbored.

Table 3.8. *Comparison of the linewidth of lasers mounted on SOT and C-mount.*

Deveice	S1-15-2-00-1 (Bar 01)	S1-15-2-00-2 (Bar 01)	S1-15-2-00-3 (Bar 02)	C1-15-2-00-1 (Bar 03)	C1-15-2-00-2 (Bar 03)	C1-15-2-00-3 (Bar 03)
Δν @ 100 mW *(kHz)*	220	170	190	450	410	500
$\Delta\nu_{minimum}$ *(kHz)*	180 (@ 200 mW)	150 (@ 150 mW)	170 (@ 170 mW)	260 (@ 200 mW)	230 (@ 200 mW)	290 (@ 150 mW)

A comparison for DFB lasers packaged on AlN/TO3 (another sealed packaging configuration) and on CuW/C-mount was also carried out. In Fig 3.21, a representative result is shown, whereas Table 3.9 summarizes the details of this analysis for the whole batch of devices. We find that for an output power below 150 mW the linewidth does not significantly depend on the mounting type (C-mount vs. TO3). We should note that all DFB diode laser chips listed in Table 3.9 and presented in Fig. 3.21were taken from the same bar. All chips can therefore be considered identical, specifically

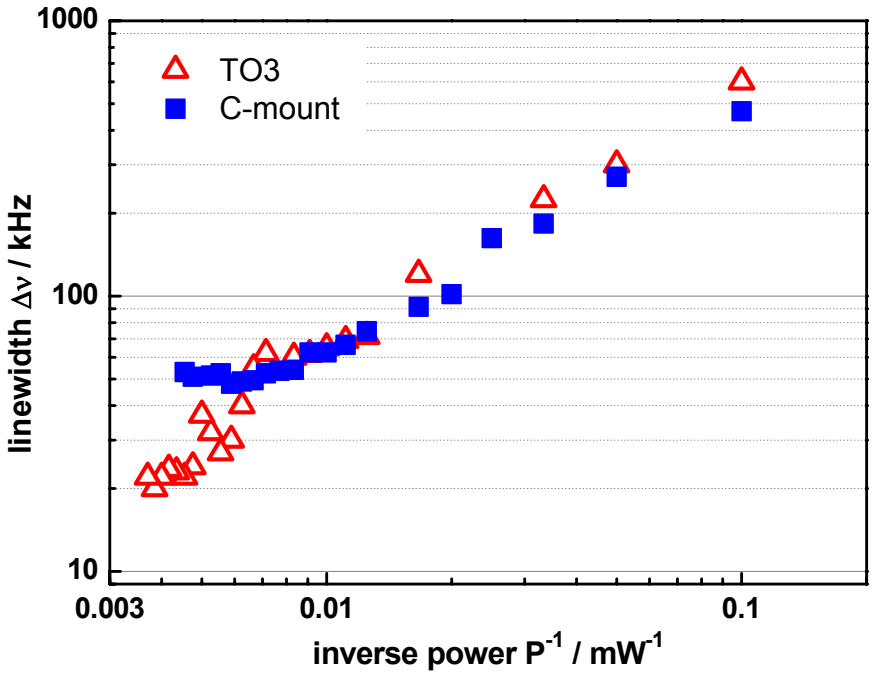

Figure 3.21. *Comparison linewidth of 780 nm DFB laser diodes on difference submounts and headsinks: AlN/TO3 (open triangle), and CuW/C-mount (solid square).*

including the phase of the grating at the facets which explains why the lasers in TO3 and on C-mount show very similar performance in the low to medium power range. At high power, beyond 150 mW of output power, the linewidth of lasers packaged on C-mount and in TO3 differs: the linewidth of lasers on C-mount reaches a linewidth floor at about 40 kHz to 50 kHz while the linewidth of the TO3 devices is further reduced to

a minimum of 20 - 30 kHz as the output power is increased, see Table 3.9. Further, the C-mount devices tend to be harder to operate in single mode at a power level beyond 200 mW; only one of the lasers on C-mount reaches this power level. The difference between the linewidth of CuW/C-mount and AlN/TO3 devices at high power may be attributed to the packaging scheme. However, this conclusion needs further experimental support.

Table 3.9. *Comparison linewidth of TO3 and C-mount lasers.*

laser	T2-30-2-0-1	T2-30-2-0-2	T2-30-2-0-3	T2-30-2-0-4	C2-30-2-0-1	C2-30-2-0-2	C2-30-2-0-3	C2-30-2-0-4
$\Delta\nu$ ***@ 100 mW*** *(kHz)*	65	65	50	50	70	60	60	60
$\Delta\nu_{minimum}$ *(kHz)*	20 (@ 270 mW)	20 (@ 270 mW)	30 (@ 240 mW)	30 (@ 300 mW)	35 (@ 270 mW)	50 (@ 200 mW)	40 (@ 190 mW)	40 (@ 170 mW)

The experimental results presented above suggest that devices mounted in a sealed package (SOT or TO3) tend to achieve better spectral short-term stability (linewidth) at high output power than lasers packaged on an open C-mount. However, it should be emphasized that the current experiments do not provide a sufficiently broad statistical basis to come to a general conclusion. Nevertheless, in general sealed cap configurations (TO3 and SOT) suppress convection and acoustic and mechanical interference from the environment, so that sealed cap configurations are generally speaking expected to provide smaller linewidths than open configurations. We will come back to this point in the outlook.

3.6. Linewidth reduction by extension of resonator length

In the previous section, we analyzed the linewidth of DFB lasers versus optical output power. When the output power increases the linewidth decreases until it hits the linewidth floor or linewidh rebroadening occurs. However, the output power can only be increasing to a certain maximum level, at which the lasers go multimode or COD occurs. It is therefore worthwhile to optimize the DFB diode laser design parameters for high power, narrow narrow linewidth emission. The current section addresses this topic.

First of all, the influence of the resonator length on the DFB laser linewidth is investigated. In theoretical description of DFB diode lasers the product κL is preferably considered as it specifies the confinement of light within the laser resonator. However, in this thesis, the influence of κ and L are discussed separately because they

correspond to two independent parameters of the process technology. This section starts by giving a short description of the realization of the different cavity length DFB diode lasers. Then, the spectral linewidth is compared between DFB laser with different cavity length.

3.6.1. Realization of DFB lasers with difference cavity length

The motivation for manufacturing DFB diode laser chips with different cavity length comes from the theoretical argument according to which the linewidth of a DFB laser depends on threshold gain that is related to the cavity length *L* (see Ref. [42] and [71]). This section presents all of the experimental details of the analysis that aims at optimizing the cavity length for minimum linewidth at high output power.

a) 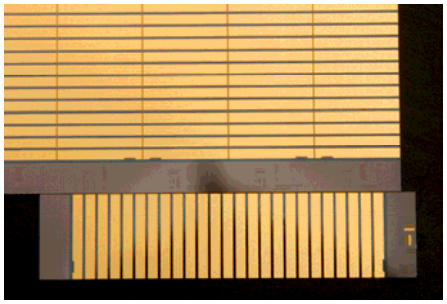 b) 

Figure 3.22. *High power diode lasers: (a) Cleaving of the bar ; (b) Single emitter on CuW submount and C-mount packaging. [FBH/Schurian.com]*

After the RW process and metallization, the next step of laser preparation, is done directly on the metalized wafer. The single bars are cleaved, which creates the cavity mirrors and hence the laser cavity. From a complete wafer that contains all oriented RW laser structures, a single laser bar is cleaved perpendicularly to the crystallographic planes. The cleaving step determines the cavity length of the DFB laser chip. For this thesis work, the wafer was cleaved into bars so as to yield a cavity length of 1.5 mm and 3 mm. The process is started by diamond scribing the wafer surface to determine the crystallographic planes along which cleaving has to take place. Fig. 3.22a shows a part of the wafer of DFB lasers and one cleaved bar with 25 single 1.5 mm cavity length laser chip. A cavity length of 3 mm is realized by cleaving two bars at the same wafer area immediately after the separation of 1.5 mm bar is complete. After the passivation of the facets, both, the front and rear facets of these bars are coated to < 0.01% and 95%, respectively. After coating, the bar is split into single laser chips. These single laser chips are then mounted on CuW submount before being packaged on a C-mount heatsink. Fig. 3.22b shows a 3 mm single emitter laser on C-mount.

3.6.2. The resonator length - a key factor to improve the spectra linewidth

All DFB diode lasers considered in this section were characterized as described in section 3.3. Linewidth measurements were performed as described in section 3.5. In this subsection, we first present and then explain the experimental results of the linewidth measurements.

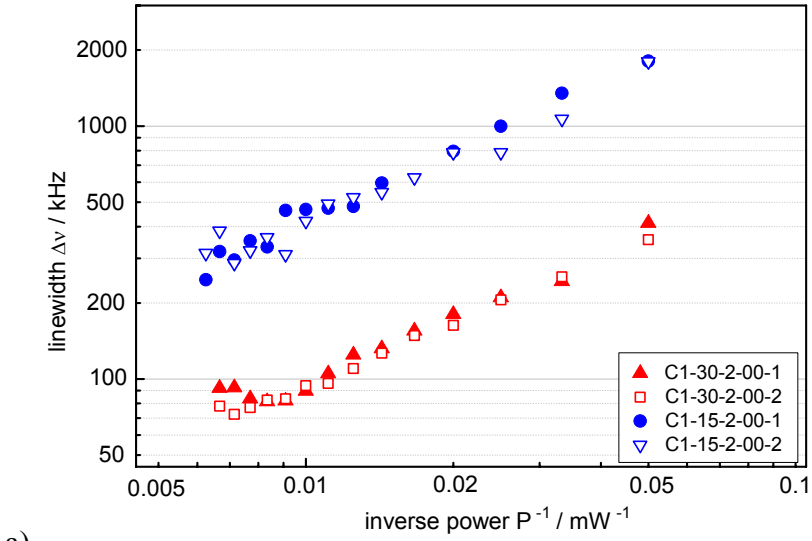

a)

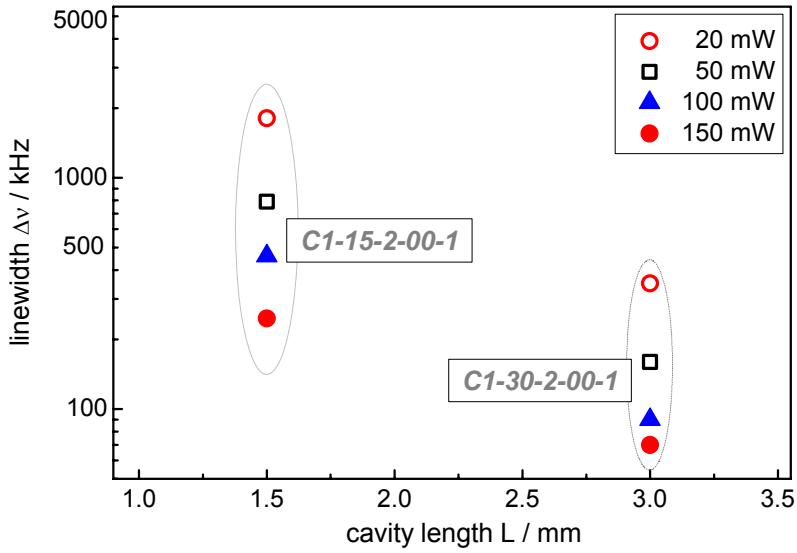

b)

Figure 3.23. *a) Linewidth - inverse power behaviour of the DFB laser diodes from the group 01 with cavity length of 3 mm: C1-30-2-00-1 (solid triangles), C1-30-2-00-2 (open squares); and 1.5 mm: C1-15-2-00-1 (solid circles), C1-15-2-00-2 (open triangles).*

b) Linewidth at different power levels depend on cavity length: C1-30-2-00-1(3 mm) and C1-15-2-00-1 (1.5 mm).

Fig. 3.23a presents the measured linewidth data for four devices of group 01 with coupling coefficient of 2 cm^{-1}. Two DFB lasers, namely *C1-30-2-00-1* (solid triangles)

and *C1-30-2-00-2* (open squares), represent the group of 3.0 mm long devices. The other lasers, i.e. *C1-15-2-00-1* (solid circle) and *C1-15-2-00-2* (open triangle), are typical for the 1.5 mm long devices. The linewidth measurements were carried out for a power ranging from 20 mW to 200 mW (250 mW) for 1.5 mm (3.0 mm) long lasers. A linewidth floor and linewidth rebroadening set in for all of these lasers at an output power between 130 mW and 160 mW which is why the data range has been restricted to 160 mW in Fig. 3.23. In Fig. 3.23a. the data for the 1.5 mm long DFB lasers show the monotonic reduction of linewidth with increasing power starting from 1800 kHz at

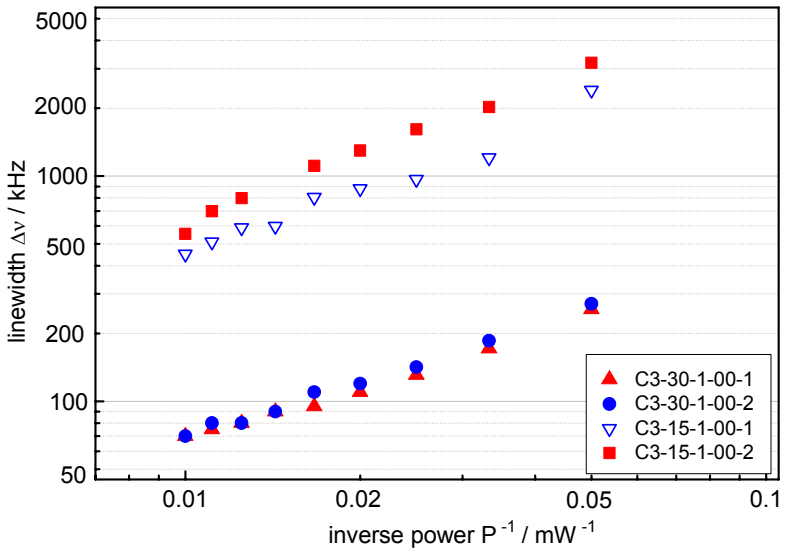

a)

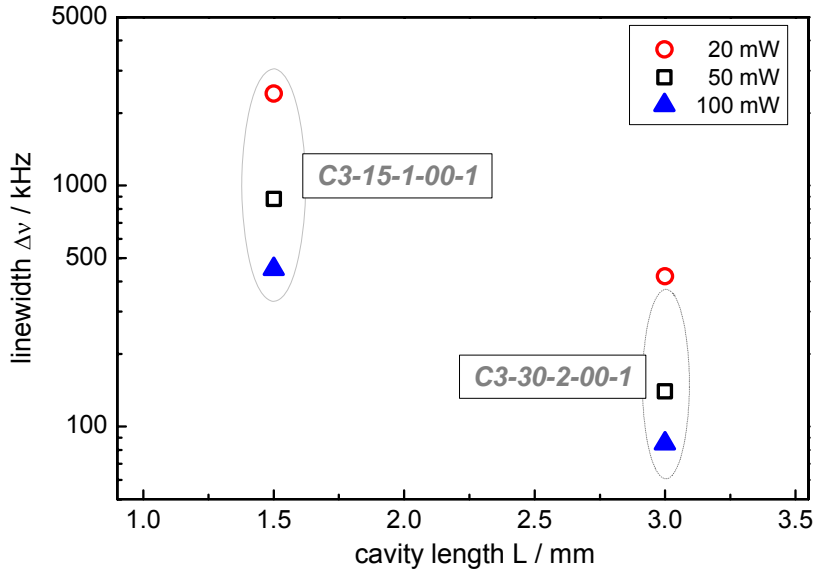

b)

Figure 3.24. *a) Linewidth - inverse power behaviour of the DFB laser diodes from the group 03 with cavity length of 3 mm: C3-30-1-00-1 (solid triangles), C3-30-1-00-2 (solid circles); and 1.5 mm: C3-15-1-00-1 (open triangles), C3-15-1-00-2 (solid squares)*

b) Linewidth at different power levels depend on cavity length: C3-30-1-00-1(3 mm) and C1-15-2-00-1 (1.5 mm).

20 mW to about 300 kHz at 150-160 mW. Similar behaviour is observed for the 3.0 mm devices, the linewidth of which decreases from 400 kHz at 20 mW down to about 70 kHz at 150 mW.

Fig 3.23b shows the comparison between *C1-30-2-00-1* (3.0 mm) and *C1-15-2-00-1* (1.5 mm). The linewidths of the laser change vs. the cavity length at different output power. The other devices *C1-30-2-00-2* and *C1-15-2-00-2* behave very similarly and are thus shown in the graph.

In Fig 3.24, we provide the corresponding results on DFB diode lasers belonging to group 03, the design of which differs from the design of group 01 lasers with coupling coefficient of 1 cm^{-1}. The devices *C3-30-1-00-1* and *C3-30-1-00-2* are 3 mm cavity length lasers and the *C3-15-1-00-1* and *C3-15-1-00-2* represent 1.5 mm devices. Linewidth data are given for an output power ranging from 20 mW to 100 mW. Some of these lasers could be operated in single mode at even higher power but showed strong rebroadening or a linewidth floor at high output power. The results of 1.5 mm long devices (*C3-15-1-00-1* and *C3-15-1-00-2*) show (Fig 3.24a) that the linewidth is reduced from 3200 kHz and 2450 kHz at 20 mW to 560 kHz and 440 kHz at a power of 100 mW. Similarly, the 3.0 mm long lasers *C3-30-1-00-1* and *C3-30-1-00-2* show a linewidth reduction from 270 kHz at 20 mW to about 70 kHz (at 100 mW). In Fig 3.24b, the results of two lasers *C3-30-2-00-1* (3.0 mm) and *C3-15-2-00-1* (1.5 mm) represent for the lasers of group 03.

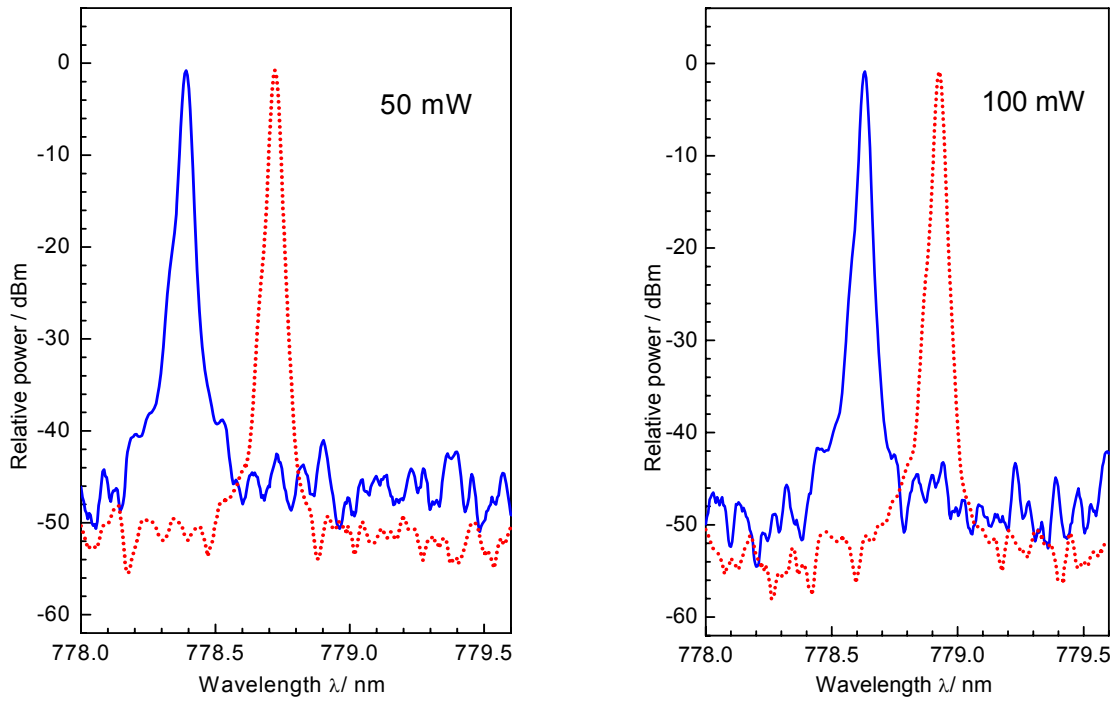

Figure 3.25. *Emission spectra of C3-15-1-00-1 (dotted line) and C3-15-1-00-2 (solid line) at 50 mW and 100 mW output power.*

Based on these results we can now discuss the dependence of the laser emission linewidth on laser cavity length. First, we would like to comment on the data shown in Fig 3.23 and Fig 3.24. The linewidths of pairs of devices that share the same device parameters are very similar except for the 1.5 mm devices *C3-15-1-00-1* and *C3-15-1-00-2* of group 03 in Fig 3.24. The main reason for this difference can be found in the fundamental characterisation, which shows relatively poor spectral performance for the device *C3-15-1-00-2*. Fig 3.25 gives a comparison of the emission spectra for the two devices at an optical output power of 50 mW and 100mW. The device *C3-15-1-00-1* clearly shows an SMSR outperforming the SMSR of device *C3-15-1-00-2* by at least 8 dB. This poorer performance of *C3-15-1-00-2* leads to a larger linewidth. The unusual linewidth-power product of this device in the Table 3.4 is now explained.

The dependence of the laser linewidth on the cavity length for DFB diode lasers with a coupling strength $\kappa L > 1$ was first presented by *Kojima et al.* [70], [71]. It was then verified experimentally by several groups [131], [148], [149]. Up to now, to the best of our knowledge, there is no corresponding theoretical description for the weak-coupling regime $\kappa L < 1$. As all lasers analyzed within the framework of this thesis work belong to the weak-coupling (κL = 0.15 .. 0.6) regime none of the theoretical predictions available can be quantitatively applied. However, as similar physical phenomena apply to lasers in the weak as well as in the strong coupling regime, the behavior of lasers in the strong-coupling regime can qualitatively be described by the strong coupling model.

In both figures (Fig 3.23 and Fig 3.24) we can see that the spectral linewidth is substantially reduced when the cavity length is increased. This finding is representative for all lasers analyzed. The corresponding results are shown in Table 3.10 and Table 3.11 where the ranges of experimental linewidth reduction factors at different power levels are collected.

Table 3.10. *Experimental linewidth reduction factors of the lasers belonging to group 01 (κ = 2 cm^{-1}, R_f < 0.01%).*

		Power levels (mW)					
		20	***50***	***80***	***100***	***120***	***150***
$K_L = \frac{\Delta\nu(1.5mm)}{\Delta\nu(3mm)}$	***min***	4.4	4.4	4.2	4.3	4.1	3.5
	max	5.2	5.0	4.9	5.1	4.6	4.5

Table 3.11. *Experimental linewidth reduction factors of the lasers belonging to group 03 (κ = 1 cm^{-1}, R_f < 0.01%).*

		Power levels (mW)				
		20	***30***	***50***	***80***	***100***
$K_L = \frac{\Delta\nu(1.5mm)}{\Delta\nu(3mm)}$	***min***	8.4	7.1	7.2	7.3	6.9
	max	12.3	11.9	11.8	10.6	11.0

To discuss the results given in the Table 3.10 and Table 3.11, we return to the theoretical description of linewidth reduction presented in section 1.3.2, 1.3.3, specifically to equations (1.33) and (1.38), where the Petermann factor K was introduced.

First, linewidth reduction is considered that follows from the reduction of "excess spontaneous emission" when the cavity length increased. The impact of spontaneous emission relates to K factor that was described in section 1.3.2a. For RW DFB lasers, the Petermann factor K is dominated by K_z, that is by the longitudinal component of K. Therefore, we use K_z only for the discussion presented in the following. When the cavity length increases, the index coupling becomes stronger which in turn decreases K_z leading to a reduction decreasing of K [150]. Consequently, the linewidth is reduced according equation (1.38). The longitudinal component of the Petermann factor K, K_z, versus the coupling strength κL is given in Fig 3.26 [150]. Although the predictions do not quantitatively apply to the regime κL < 1, the extrapolation from the strong coupling strength into the weak coupling strength predicts larger values of K_z. The following summarizes the result of our analysis:

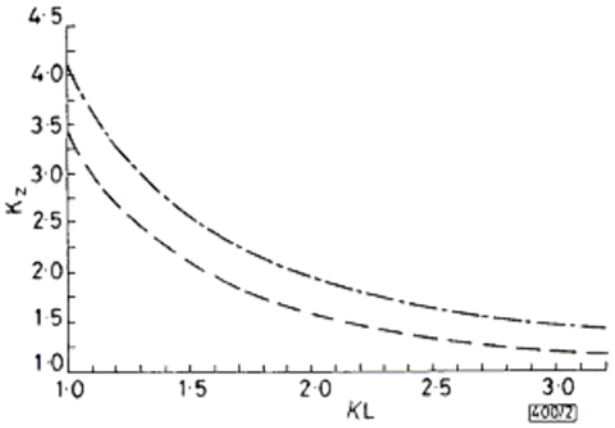

Figure 3.26. *Longitudinal component K_z of the Petermann factor versus coupling strength κL for non-phase-shifted DFB laser (solid dotted line), and phase-adjusted ($\lambda/2$ phase shift) DFB laser (dashed line). [150]*

- For the devices of group 01, the coupling strength κL nominally corresponds to 0.3 and 0.6 for L = 1.5 mm and 3.0 mm, respectively. If we extrapolate K_z in Fig 3.26 to values of κL<1 we find that the ratio K_z (L = 1.5 mm)/K_z (L = 3.0 mm) approaches values that are larger than 2. The factor of 2 corresponds to the ratio K_z (κL = 1)/ K_z (κL = 2) taken from Fig 3.26. Due to the fact that $\Delta\nu(L) \sim K_z(L)$, a linewidth reduction factor larger than 2 is expected when the cavity length increases by a factor of 2. This agrees with the experimental results summarized

in Table 3.10. These show an average reduction factor of about 4.1 (minimum is 3.5 at 150 mW).

- For the devices of group 3, a similar behaviour is found. Here, the coupling strength κL corresponds to 0.15 and 0.3 for L = 1.5 mm and L = 3.0 mm, respectively.The minimum linewidth reduction factor (at 100 mW) is 6.9. The factors in Table 3.11 (κL =0.15, 0.3) exceed those given in Table 3.10 (κL =0.3, 0.6). This supports the validity of extrapolating the longitudinal component of the Petermann K-factor, K_z towards smaller κL beyond κL=1. It further supports the hypothesis that K_z increases more rapidly as κL approaches zero. The larger difference between minimal and maximal values in Table 3.11 as compared to Table 3.10 is attributed to the fact, that device *C3-15-1-00-2* shows poorer-than-average performance.

Next, linewidth reduction is discussed, that follows from a reduction of the effective linewidth enhancement factor α_{eff} (effective Henry factor, see equation (1.38)) when the cavity length is modified. Although the reduction of K_z is considered the main mechanism of linewidth reduction linewidth, when the cavity length is increased, the contribution of α_{eff} should not be completely neglected as the square dependence of the linewidth on α_{eff} may lead to a substantial effect. The dominant role of the longitudinal component K_z of the Petermann K-factor is anticipated because for small coupling coefficient κ and at moderate output power spatial hole burning leads to only a small dependence of α_{eff} on cavity length. This assumption is supported by:

- Results of the simulation for 780 nm high power DFB lasers with weak-coupling strength ($\kappa L < 1$) [133].
- Calculations and experimental results published in [129] and [151], that show a minor variation of effective linewidth enhancement factor with cavity length.

Finally we want to refer to a work by *Liou et al.* [152]. In this work the authors present a rough estimate on how the laer linewidth depends on the cavity length. They proposed that the linewidth – cavity length relation $\Delta\nu \sim \alpha_0/\kappa^2 L^3$ (with α_0 being the sum of absorption and scattering loss) given by *Kojima et al.* [70], [71] only applies to ideal DFB lasers with large coupling strength κL. *Liou et al.* showed that, in practice, the linewidth rolls-off slower than ($1/L^3$) but faster than ($1/L$). Their DFB lasers with index coupling configuration showed a $1/L^2$ relation between linewidth and cavity length. We expect a similar behaviour for our DFB lasers.

For the 780 nm DFB lasers investigated within the frame work of this thesis none of the devices with a length of 6 mm and κ of 2 cm^{-1} could be operated successfully. Fig. 3.27 shows PUI characteristics and spectra behavior of a 6 mm laser. The slope efficient of the laser, which is shown in Fig. 3.27a of 0.24 W/A, is very small compare with 3 mm laser. Due to spatial hole burning, almost all devices with 6 mm cavity

length were emitting multi longitudinal mode even at very low power (typically 30 mW) (Fig. 3.27b). Therefore the linewidth inverstigation of 6mm were not performed.

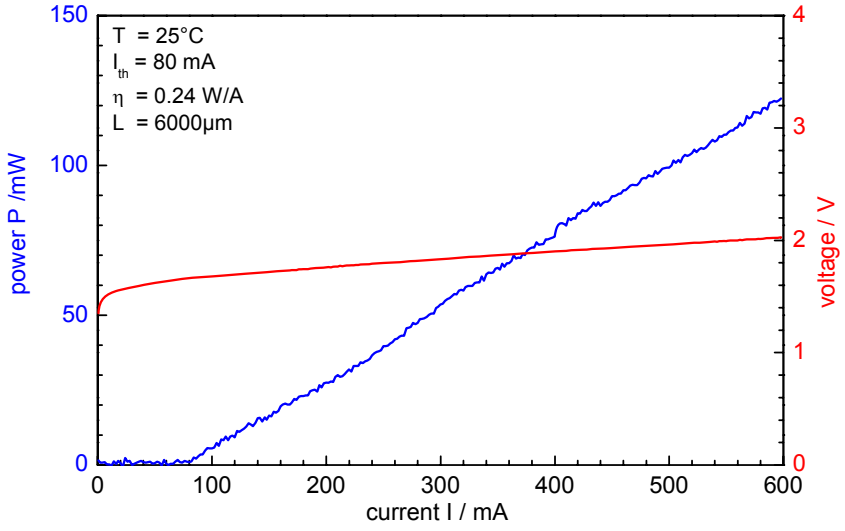

a)

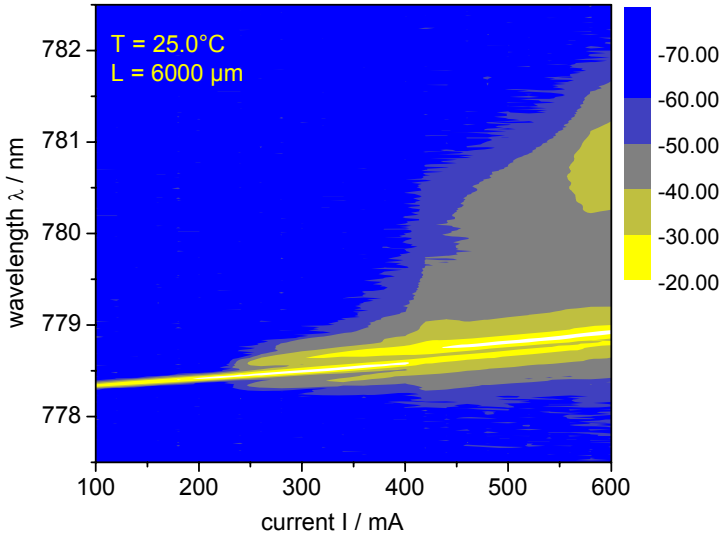

b)

Figure 3.27. *PUI characteristics and spectra behavior of 6 mm DFB laser. Slope efficient of 0.24 A/W and multi mode operation above 30 mW output power.*

We summarize the main findings of this section as follows. The main mechanism of linewidth reduction is an enhancement of index coupling effect with increasing cavity length that directly reduces the longitudinal component K_z of the Petermann K-factor. At high output power, due to a substantial increase of spatial hole burning, the contribution of effective linewidth enhancement factor α_{eff} should not be neglected.

3.7. The dependence of the DFB laser spectral linewidth on the coupling coefficient

The coupling coefficient is a key parameter of DFB diode lasers. It plays an important role for many effects observed in high power DFB diode lasers, e.g. spatial hole burning, side mode suppression, and others. As mentioned in the previous sections, the coupling coefficient κ and cavity length L together define the coupling strength κL that is typically considered a fundamental parameter of a DFB diode laser. In this thesis, we rather separate the influence of κ and L onto the linewidth because these parameters are defined separately by the process technology. The experimental results in previous section have shown the influence of L onto the DFB laser linewidth. In this section, the role of the coupling coefficient is discussed in detail. First, we briefly explain how to realize DFB diode lasers with different coupling coefficients. Then, the experimental results of the linewidth measurement on lasers with different coupling coefficient are demonstrated.

3.7.1. Design and fabrication of higher coupling coefficient DFB lasers

In section 2.1, a general approach for fabrication of DFB diode lasers with integrated gratings has been described. However, the design of gratings was not specifically addressed. In this section, we present in detail the design approach to provide material and geometrical parameters for the fabrication step.

The coupling coefficient is defined by the configuration of the Bragg grating that is monolithically integrated with DFB diode laser. There are several parameters that can be adjusted to find the optimum design including:

- The order of the grating. Higher order gratings provide weaker coupling than lower order gratings for otherwise identical design parameters.
- The refractive index contrast of the corrugation pitch and the surrounding, i.e. of a InGaP/GaAsP/InGaP layer sequence and a AlGaAs cladding layer (see again Fig. 2.2). The coupling coefficient will be the larger the larger the refractive index contrast.
- The duty-cycle of grating (ratio between corrugation width and grating period). The coupling coefficient periodically depends on duty-cycle and order of grating.
- The distance between the grating layer and the active layer. A larger distance results in a lower coupling coefficient.

For the 780 nm DFB diode lasers used for this thesis work, the following design approach was used:

- A second order grating was employed that shows certain advantages over first order gratings [153], [154].
- The refractive index contrast was chosen according to section 2.1 and according to technological feasiblility in-house.
- The coupling coefficient of a second order grating has maxima at a duty cycle of 0.25 and 0.75. The lasers are designed so as to match a duty-cycle of 0.25 because of this has proven to provide better device performance [155].
- The distance from grating layer to active layer is adjusted to set the desired coupling coefficient (typically to a value between 500 nm and 1000 nm).

Our design approach mainly focusses on varying the distance between the grating and active layer, all other parameters are optimized and then fixed for a specific wavelength. The duty-cycle was varied only by small amounts around 0,25 to ensure that the optimum duty cycle is hit during device fabrication. Two groups of wafers were fabricated for 780 nm DFB diode lasers, one with a coupling coefficient of $\kappa = 1$ cm^{-1} and and one with a coefficient of $\kappa = 2$ cm^{-1}.

3.7.2. Dependence of the DFB laser spectral linewidth on the grating coupling coefficient – experimental results and discussion

This section focuses on analyzing the dependence of the DFB laser linewidth on the coupling coefficient. The devices for investigation with 1.5 mm and 3.0 mm cavity length were selected from the wafers that designed for the coupling coefficients of $\kappa = 1$ cm^{-1} and $\kappa = 2$ cm^{-1} (see Table 3.1). The standard optical and electro-optical characterisation was carried out as described in section 3.3. The linewidth measurements were performed at 25°C. In this section, we first present typical experimental results. Then, we give a detailed overview about all results, we discuss these results and draw conclusions for design and fabrication of narrow linewidth DFB lasers.

In Fig. 2.28, we present the result of a linewidth measurment for two 1.5 mm long DFB lasers with coupling coefficients of $\kappa = 1$ cm^{-1} (*S3-15-1-00-2*) and $\kappa = 2$ cm^{-1} (*S1-15-2-00-3*), which clearly demonstrates that the spectral linewidth decreases with increasing coupling coefficient. The linewidth of *S3-15-1-00-2* drops down monotonically from 2100 kHz at 20 mW to about 420 kHz at output power of 100 mW (reduction by a factor of 5). The linewidth-power product for this device is about 40.8 MHz·mW. For the device with larger coupling coefficient (*S1-15-2-00-3*), essentially

the same reduction with power is observed (from 940 kHz at 20 mW to 190 kHz at 100 mW corresponding to a factor of 4.9) at a linewidth-power product of 14.5 MHz·mW which is smaller by a factor of 3 than the corresponding product of the first device.

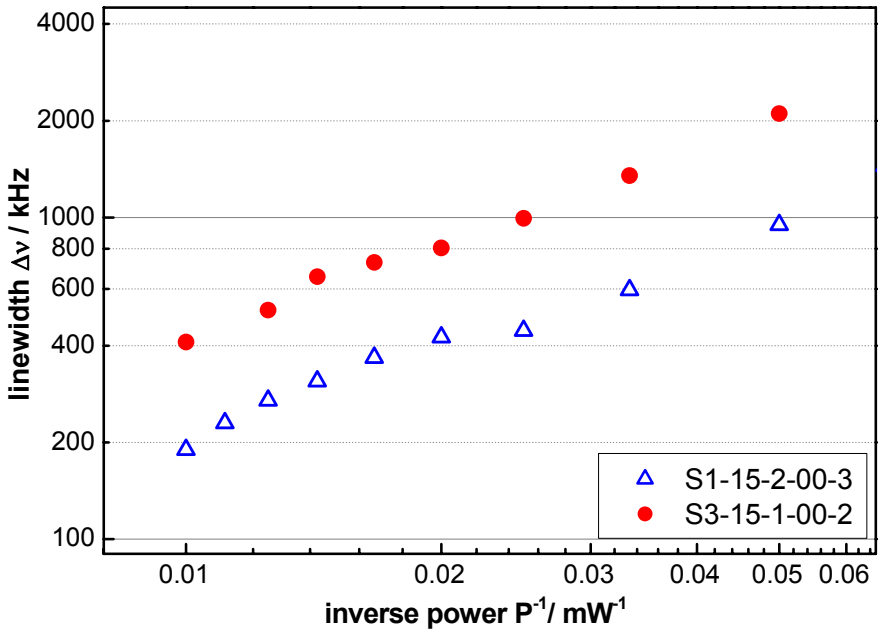

Figure 3.28. *Linewidth comparison of two 1.5 mm DFB laser diodes with a coupling coefficient of 1 cm^{-1} (S3-15-1-00-2) and 2 cm^{-1} (S1-15-2-00-3).*

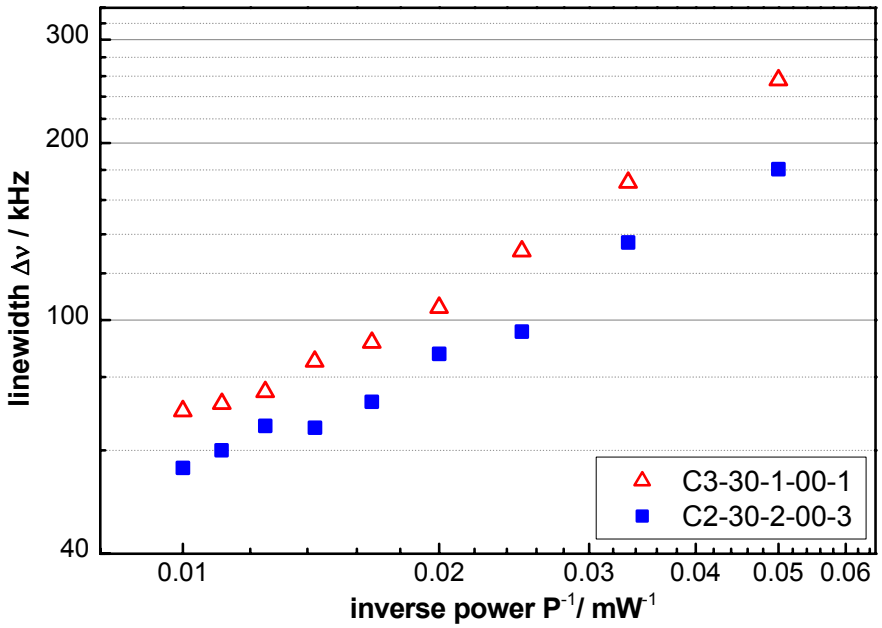

Figure 3.29. *Linewidth comparison of two 3 mm DFB laser diodes with a coupling coefficient of 1 cm^{-1} (C3-30-1-00-1) and 2 cm^{-1} (C2-30-2-00-3).*

The second example is shown in Fig 3.29. This figure shows the result of a linewidth measurement on two 3.0 mm long DFB lasers with coupling coefficients of 1 cm^{-1} (*C3-30-1-00-1*) and 2 cm^{-1} (*C2-30-2-00-3*). As for the first example,

increasing the coupling coefficient tends to reduce the emission linewidth. For this particular case, linewidths of 270 kHz (*C3-30-1-00-1*, $\kappa = 1$ cm^{-1}) and 180 kHz (*C2-30-2-00-3*, $\kappa = 2$ cm^{-1}) are found at an output power of 20 mW. With linewidth-power product of 3.3 MHz·mW (device *C2-30-2-00-3*) and 4.9 MHz·mW (device *C3-30-1-00-1*), the linewidths of these devices is reduced to 70 kHz (device *C2-30-2-00-3*, reduction by a factor of 3.9) and 60 kHz (device *C2-30-2-00-3*, reduction by a factor of 3.0) when operated at 100 mW. Hence linewidh reduction with increasing coupling coefficient is less pronounced for the 3 mm long devices than for the 1.5 mm devices.

For convenience, we summarize the linewidth reduction factors for the two pairs of the DFB lasers discussed in Fig 3.28 and Fig. 3.29 in Table 3.12 and Table 3.13. Table 3.12 additionally contains the results of a simulation for a 1.5 mm long devices.

Table 3.12. *Linewidth reduction factors for two lasers with L = 1.5 mm and coupling coefficients of 1 cm^{-1} and 2 cm^{-1}.*

		power level (mW)					
		20	***40***	***50***	***60***	***80***	***100***
$K_\kappa = \frac{\Delta\nu(1cm^{-1})}{\Delta\nu(2cm^{-1})}$	***S3-15-1-00-2/ S1-15-2-00-3***	2.2	2.2	1.9	2.0	1.9	2.1
	Simulation	2.2	2.3	2.3	2.3	2.3	2.3

Table 3.13. *Linewidth reduction factors of two lasers with L = 3 mm and coupling coefficient of 1 cm^{-1} and 2 cm^{-1}.*

		power level (mW)					
		20	***40***	***50***	***60***	***80***	***100***
$K_\kappa = \frac{\Delta\nu(1cm^{-1})}{\Delta\nu(2cm^{-1})}$	***C3-30-1-00-1/ C2-30-2-00-3***	1.4	1.4	1.2	1.3	1.2	1.3

We now describe the results in detail and comment on them. Then, we discuss the mechanisms that lead to linewidth narrowing when the coupling coefficient is increased.

The linewidth reduction factors of individual, nominally identical device pairs are typically not identical. Further, in some cases the reduction factor is close too or even smaller than 1. Nevertheless, we can conclude that lasers with a coupling coefficient of 2 cm^{-1} will provide narrow spectral emission than nominally identical DFB lasers with a coupling coefficient of 1 cm^{-1}. The result presented in Fig. 3.28 is typical for the results found in this thesis work. A linewidth reduction factor of about 2 was found for this particular case as well as for some other device pairs that were nominally identical

(i.e., similar DFB laser chip parameters as well the same packaging procedure). As shown inTable 3.12, these results agree very well with the simulation results.

We now explain the observed experimental behaviour in terms of mechanisms that cause linewidth narrowing when the coupling coefficient is increased.

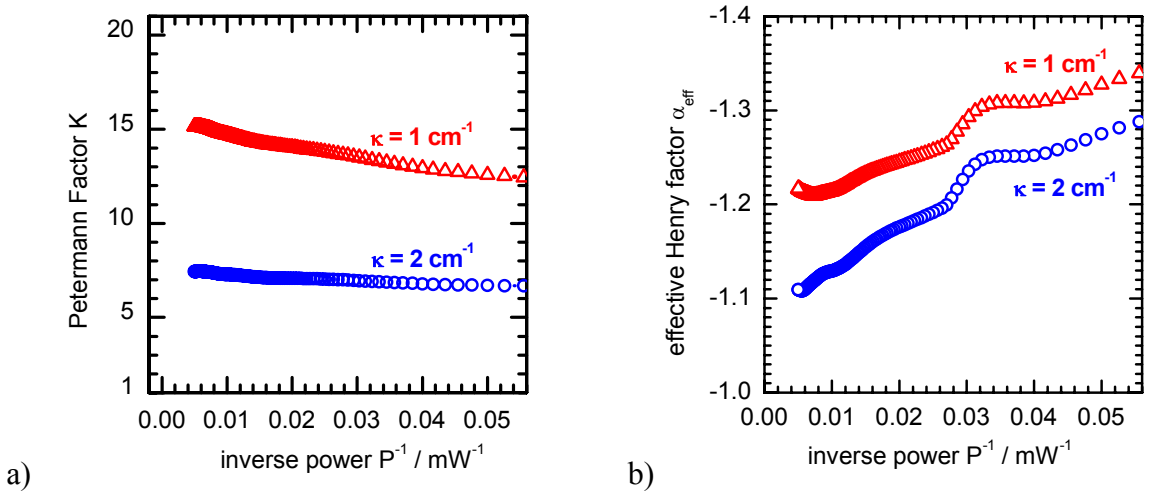

Figure 3.30. *Simulation of the (a) Petermann factor and (b) of the effective Henry factor vs. inverse output power of 780 nm DFB lasers for two coupling coefficients $\kappa = 1\ cm^{-1}$ and $\kappa = 2\ cm^{-1}$.*

First, as already discussed in the previous section (3.6), we consider the reduction of "excess spontaneous emission" to be the main mechanism for linewidth narrowing with increasing coupling coefficient. Again, we refer to the Petermann factor *K*. When the coupling coefficient is increased, *K* is also reduced. An increase of the coupling coefficient is hence similar to an increase of the cavity length. Therefore, we would expect to see the reduction of linewidth if other linewidth enhancement mechanisms were not dominant effect. The simulation carried out by H. Wenzel for a 1.5 mm long 780 nm DFB laser [133] shows that the Petermann factor varies slowly with optical power, see Fig. 3.30a. Based on this result, the reduction factors of *K* are in the range from 1.9 - 2.0 comparison from the coupling coefficient 1 cm^{-1} to 2 cm^{-1} when power varied from 20 mW to 100 mW. The reduction factor derived theoretically and given in Table 3.12 includes the dependence of the Petermann factor and of the linewidth enhancement factor on the coupling coefficient. From Fig. 3.30b, the square Henry factor decreases with increasing the coupling coefficient, but its value stays close to 1 so that no significant linewidth narrowing is expected from the dependence of the Henry factor on coupling coefficient.

However, except for the devices analyzed in Fig. 3.28 and Table 3.12, all other devices yielded a smaller linewidth reduction factor as already pointed out, i.e. these devices do not exactly follow the explanation given above. There are several arguments that might explain this deviation between the experimental findings and the theoretical predictions.

- For all devices, the grating phase at the rear facet strongly affects the linewidth, see section 3.6, but is not under control in the manufacturing process and hence is random. Depending on the actual grating phase at the rear facet the linewidth may vary by a factor as large as 2. Therefore, if the lasers, that were analyzed, posses grating phases that strongly vary, a significant deviation between experimental findings and predicted linewidth is to be observed.

- Inhomogeneity of the laser chip quality across a wafer also contributes to differences between the linewidth of various nominally identical devices. Firstly, this has was already been considered to be the reason for the development of a linewidth floor and for linewidth rebroadenning at modest currents observed for devices of group 01 (κ = 2 cm^{-1}) as compared to the devices of group 2 (κ = 2 cm^{-1}, see again Table 3.1, section 3.5.3). Secondly, if we compare the data of linewidth-power product of the devices from group 03 in Table 3.14 (L = 3 mm, κ = 1 cm^{-1}) to the corresponding data of the devices from group 01 and 02 in Table 3.6 (L = 3 mm, κ = 2 cm^{-1}), we will clearly see a smaller linewidth-power products of group 03 compare to group 01 that proves for the negative impact from laser material onto linewidth behaviour; for the group 02, a slightly lower of linewidth-power product results a narrower linewidth compare to group 03.

Table 3.14. *Linewidth-power product and linewidth at 100 mW output power of lasers in group 03 (L = 3 mm, κ = 1 cm^{-1}, R_f < 0.01%).*

Device	C3-30-1-00-1	C3-30-1-00-2
Δν*P *(MHz*mW)*	4.90±0.11	5.26±0.09
Δν@100mW *(MHz)*	0.07	0.07

- The lag of perfect reproducibility of the packaging process may also detoriate the spectral performance as already discussed in section 3.5.4.

To close this section, we summarize our findings. First, the experimental data presented in this section suggest that linewidth reduction can be achieved by implementation of gratings with larger coupling coefficients. However, a strong linewidth reduction could not be demonstrated, most likely because an increase of the coupling coefficient from 1 cm^{-1} to 2 cm^{-1} is not sufficient to dominate performance differences at the device level, that are due to fabrication tolerances. Second, the random grating phase at the rear facet is critical for the linewidth and can mask any linewidth reduction due to an increase of the coupling coefficient by a factor of 2. This

applies specifically to high power operation and devices with modest or weak coupling strength κL. To overcome this limitation the manufacturing technology has to be refined. Third, the imperfection laser material reduces laser performance, specifically with respect to the spectral linewidth. Finally, we comment on the theoretical description of the spectral linewidth of DFB lasers. According to Kojima et al. [71], an ideal DFB laser with $\kappa L > 1$ is expected to show a linewidth that follows $\Delta\nu \sim \kappa^2 L^3$. A strongly coupled laser should hence less depend on the coupling coefficient than on the cavity length. Although a correct theoretical description is yet not available for our weakly coupled DFB lasers, our experimental data clearly support this prediction.

3.8. Optimi ing output facet reflectivity for minimum spectral linewidth

Sofar we we have discussed in detail the two most important parameters that determine the laser linewidth, namely the cavity length and the coupling coefficient. Once the laser has been processed and has been cleaved from the wafer, the final optimization step is to apply the appropriate output facet reflecitivity. In this section, we report on experimental investigations that aim at an optimization of the output facet reflectivity of DFB diode lasers. To this end DFB diode lasers with various front facet reflectivities are optically and electro-optically characterized and their linewidth is determined. First, we discuss about the motivation behind this investigation and about the technology steps necessary to realize a desired facet reflectivity. Second, the experimental results are presented. The dependence of laser performance on output facet reflectivity is discussed

3.8.1. DFB laser diodes with facet coating

The variation of the facet coating of diode lasers is expected to alter the spontaneous emission and hence the Petermann factor, which leads to a modification of the spectral linewidth Therefore, it is worthwhile to experimentally investigate how the spectral linewidth varies with the facet reflectivity. Typically, to efficiently extract the power from the laser chip, the so-called rear facet is coated with a highly reflective coating after cleaving. The reflectivity of the other facet, the so-called front facet, is then optimized for best laser performance. The dependence of the spectral linewidth of DFB lasers on the facet reflectivity was analyzed theoretically by *Kojima et al.* [155], *Agrawal et al.* [156], and *Adams et al.* [157]. However, this work does not address the question of how to obtain stable single-longitudinal-mode operation Later, *Ogita et al.*

[158] analyzed theoretically and experimentally the dependence of the spectral linewidth of DFB lasers on the facet reflectivity. This work shows theoretically that higher facet reflectivity leads to narrower spectral linewidth, but at the same time provides smaller yield of single-longitudinal-mode emitters. Their experimental investigations on 1300 nm DFB lasers with the rear facet cleaved showed that the spectral linewidth takes on its minimum value at a front facet reflectivity of about 5%. The result of the analysis presented by Re*dolls et al*. [159] for 1550 nm DFB lasers disagreed with the findings of Ogita: the authors concluded that a reduction of the front facet reflectivity from a value of 32% for the uncoated facet to about 5% caused linewidth broadening.

To resolve the disambiguity and to investigate quantitatively the effect of partially coating the front facet of 780 nm DFB lasers, specifically in the high power regime DFB lasers were prepared with front facet reflectivities of R<0.01%, 5%, 10%, and 30%. Coating of the facets is carried out as follows.

- The surface of cleaved DFB laser bars is cleaned to remove thermodynamically unstable species that can cause gradual facet degradation, eventually leading to COMD. Then the facets are coated with a passivating layer preserving the clean state of the facets. The material typically used for this process step is ZnSe (see detail in [160]). The reflectivity of pure cleaved facets is close to 30%.
- After passivation, the laser bars are coated to adjust the facet reflectivity. The desired reflectivity is achieved by coating the facets with an appropriate layer or an appropriate stack of appropriate layers. First, to increase the reflectivity of the rear facet, pairs of quarter-wavelength layers are processed, where the first and second layer of a pair correspond to the lower and higher index of refraction, respectively. This process is repeatedly applied for the rear facet to achieve a reflectivity of 95%. Thin film materials used are Al_2O_3/TiO_2, Al_2O_3/Si, and Al_2O_3. The front facet of DFB laser is coated up to 30% with Al_2O_3 and TiO_2 layers. To minimize the reflectivity with a single layer, the coating material should have a refractive index close to the geometric mean between the effective index of the waveguide and the index of air. Typically a single layer of Al_2O_3 is used. To coat the front facet to R<0.01%, 5%, and 10%, the thickness of the film has to be selected appropriately. All these materials are deposited by ion beam sputtering (ISSA-03-00).

Since rear facet remain the same high reflectivity, the influence of the non-zero facet reflectivity on spectral characteristic only defined by front facet reflectivity. The 780 nm DFB diode lasers with various front facet reflectivities and 95% rear facet reflectivity are now ready for the experimental investigation.

3.8.2. The dependence of the spectral linewidth on the front facet reflectivity

The DFB diode lasers with various front facet reflectivities are subsequently characterized with respect to optical and electro-optical properties as well as spectral

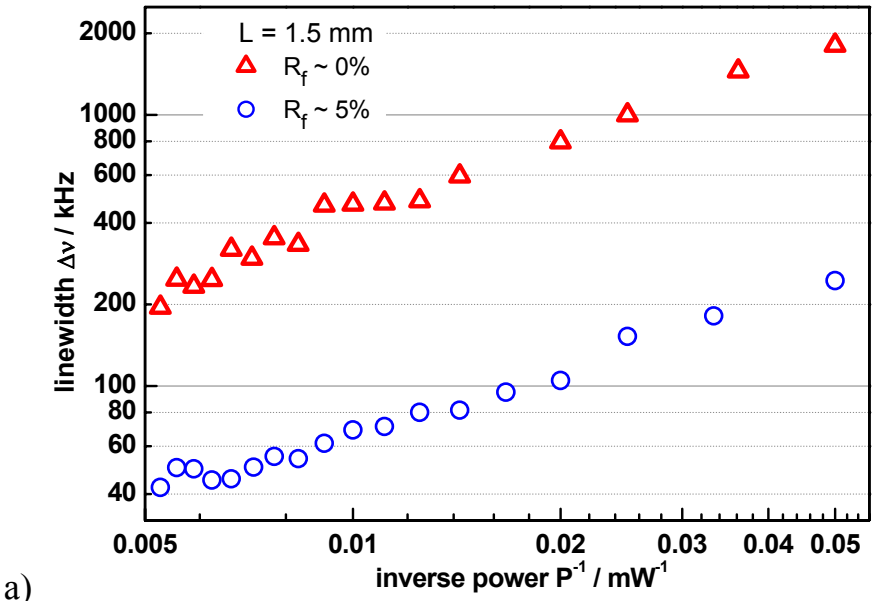

a)

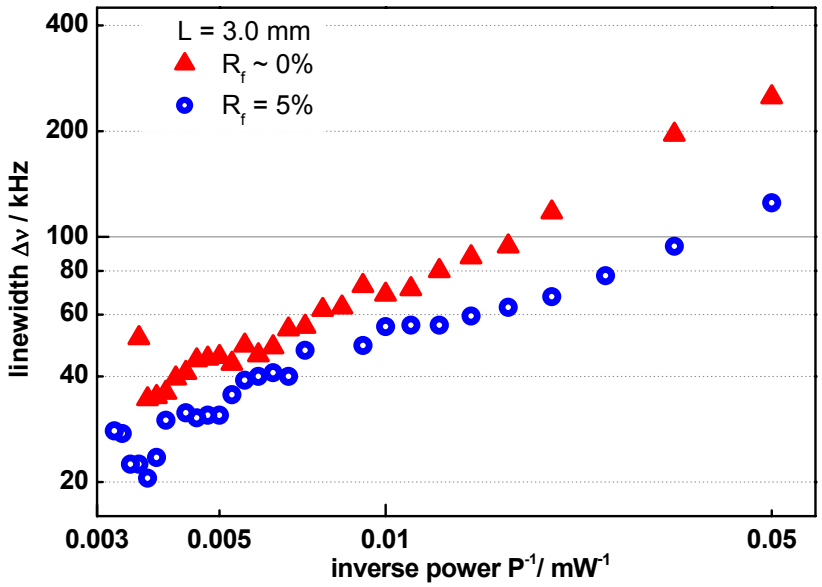

b)

Figure 3.31. *Linewidth comparison for 780 nm DFB diode lasers that differ with respect to front facet reflectivity:*

a) 1.5 mm long lasers: C1-15-2-00-1 with R_f = 0.01% (open triangles), and laser C1-15-2-05-1 with R_f = 5% (open circles), κ = 2 cm^{-1}.

b) 3 mm cavity length lasers: C2-30-2-00-1 with R_f = 0.01% (solid triangles), and laser C2-30-2-05-1 with R_f = 5% (open circles), κ = 2 cm^{-1}.

linwidth. In this section, we present the experimental results, which indicate better spectral performance for DFB lasers with the front facet partially reflective. We discuss the results and give a recommendation for optimum front facet coating.

First, we compare the AR-coated (<0.01%) DFB lasers to the devices with 5% front facet coating. In Fig. 3.31, the spectral linewidth vs. output power is shown for a pair of 1.5 mm and a pair of 3.0 mm long devices. Each pair consists of nominally identical chips that only differ with respect to the front facet coating which corresponds to $R_f <$ 0.01% and 5%. Fig. 3.31a presents the behaviour of 1.5 mm long devices, namely *C1-15-2-00-1* and *C1-15-2-05-1*, with reflectivity of $R_f < 0.01\%$ and R = 5%, respectively. The device *C1-15-2-05-1* shows a linewidth of about 300 kHz at an output power of 20 mW. When the output power is increased to 190 mW the linewidth of this device reaches its minimum value of about 40 kHz (linewidth reduction by a factor of 7.5 for a power ratio of 9.5). Its linewidth is substantially smaller than the linewidth of the device with $R_f < 0.01\%$ (*C1-15-2-00-1*) which provides a linewidth of about 1800 kHz and 200 kHz at these power levels (linewidth reduction by a factor of 9 for a power ration of 9.5). The linewidth of partially reflective and of the AR-coated devices differ by a factor of about 5-6.
The second example is shown in Fig. 3.31b. For the 3.0 mm device coating to R=5% also reduces the linewidth. However, the reduction is less pronounced than for the 1.5 mm devices. The device *C2-30-2-00-1* with $R_f < 0.01\%$ shows a linewidth reduction of 250 kHz at 20 mW to a minimum of 35 kHz at 270 mW (factor of 7.1 for a power ratio of 13.5). At the same power levels, the 5% device (*C2-30-2-05-1*) demonstrates a linewidth of only 120 kHz and 20 kHz (linewidth reduction by a factor of 6 for a power ratio of 13.5). The linewidth of the partially reflective and of the AR-coated devices differ by a factor of 1.8-2.1.

Besides the reduction of the linewidth we also see a substantial modification of the linewidth-power product when the front facet reflectivity is changed from R < 0.01% to R_f = 5%. The linewdth-power product is reduced from 20 MHz·mW to 4.71 MHz·mW for 1.5 mm DFB lasers and from 4.58 MHz·mW to 2.10 MHz·mW for 3.0 mm devices. This results show that the feedback yield from front facet plays a role to eliminate spontaneous emission thus reduces Petermann factor hence the linewidth. The effect caused by increasing of the front facet reflectivity is quite similar to the increasing of coupling strength (κL) which was studied experimentally in Ref. [161]: both, coating of the front facet to achieve partial reflectivity and increasing the coupling strength reduce threshold gain by increasing optical feedback. The result in Ref. [161] agrees with the theoretical prediction by *Kojima et al*. [155] and *Agrawal et al.* [156], that shows a substantial reduction of the Petermann factor *K* when the facet reflectivity is increased. Since we lack numerical simulations for the weak coupling case $\kappa L < 1$, a quantitative comparison between this theoretical work and our experimental findings is not possible. However, the tendency is clear: for 3.0 mm devices, a coating of the front facet to 5% does not reduce the linewidth by the same factor as coating of the 1.5 mm devices. This suggests that some kind of saturation will

occur when the front facet reflectivity is further increased. The same behaviour was observed when the cavity length was increased (see section 3.6.2): when a short cavity length is doubled, the coupling strength κL is doubled and the Petermann factor is reduced at least by factor 2. A smaller reduction of Peterman factor is expected at higher coupling strength. Analogously, we expect that increasing the reflectivity by another 5% to 10% leads to a less pronounced reduction of the Petermann factor and hence of the linewidth. To clarify this prediction, DFB diode lasers were also coated to a front facet reflectivity of 10% and 30% while the rear facet was kept at high reflectivity (95%). All devices are 3.0 mm long and coupling coefficient of $\kappa = 2\ cm^{-1}$.

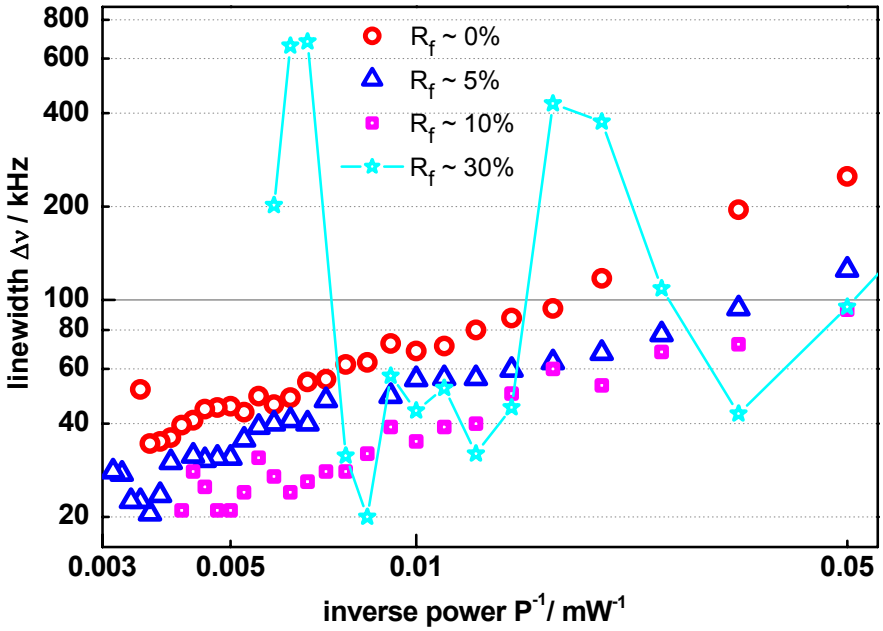

Figure 3.32. *Linewidth of 3 mm 780 DFB laser depends on front facet reflectivity: Laser C2-30-2-00-1 with R_f < 0.01% (open circles), C2-30-2-05-1 with R_f = 5% (open triangles), C2-30-2-10-1 with R_f = 10% (solid squares), C2-30-2-30-1 with R_f = 30% (stars).*

The experimental results for coatings of R_f = 10% and R_f = 30% are shown in Fig. 3.32. The data for R_f < 0.01% and 5% are added for comparison. The device *C2-30-2-10-1* (R_f = 10%) can be operated single mode up to an output power of 240 mW and hence linewidth measurements can be carried out up to this power level. At 20 mW, we find a linewidth of 90 kHz which is the smallest value of all DFB lasers analyzed within the framework of this thesis at this power level. Other devices with 10 % front facet reflectivity yield a similar linewidth with the values ranging between 90 kHz – 100 kHz. When the optical power is increased, the linewidth is reduced. At 200 mW and 240 mW it reaches the minimum linewidth of 20 kHz and shows slightly larger linewidths at values of the output power between 200 mW and 240 mW. Among several devices that can reach a linewidth of 20 kHz we observed the lowest power at which this linewidth is achieved to be 200 mW for the device *C2-30-2-10-1* (R_f = 10%). The linewidth reduction observed when moving from R_f = 5% to R_f = 10% goes

in hand with the fact that the smallest linewidth-power product of only 1.66 MHz·mW is observed for device *C2-30-2-10-1* (R_f = 10%). However, for devices with R ≥ 10% the linewidth does not monotonically decrease with output power. As can be seen in Fig.3.31 the linewidth starts to oscillate between 20 kHz and 30 kHz with output power at a power level of 150 mW. The device with a large front facet reflectivity of R_f = 30% (*C2-30-2-30-1*) shows a qualitatively different behaviour. The linewidth strongly varies between a few 10 kHz (e.g. 20 kHz) and a couple of 100 kHz (e.g. 600 kHz) as the output power is increased. Fig. 3.33 shows spectra behavior of the devices *C2-30-2-10-1* and *C2-30-2-30-1*. They present unstable single and multi mode operation. Despite that strong variation of the linewidth with output power certain power settings exist at which the linewidth of the device with R_f = 30% is even smaller than the linewidth of the device with R_f = 10%, see Fig. 3.32. Increasing the front facet reflecivity beyond 10% can hence further reduce the linewidth, however linewidth reduction is not stable. This unstable behaviour is attributed to the evolution of an unstable resonator when the optical feedback becomes too strong, as already discussed in section 3.3.1. The unstable behaviour is a consequence of the spatial and spectral hole burning, of carrier heating.

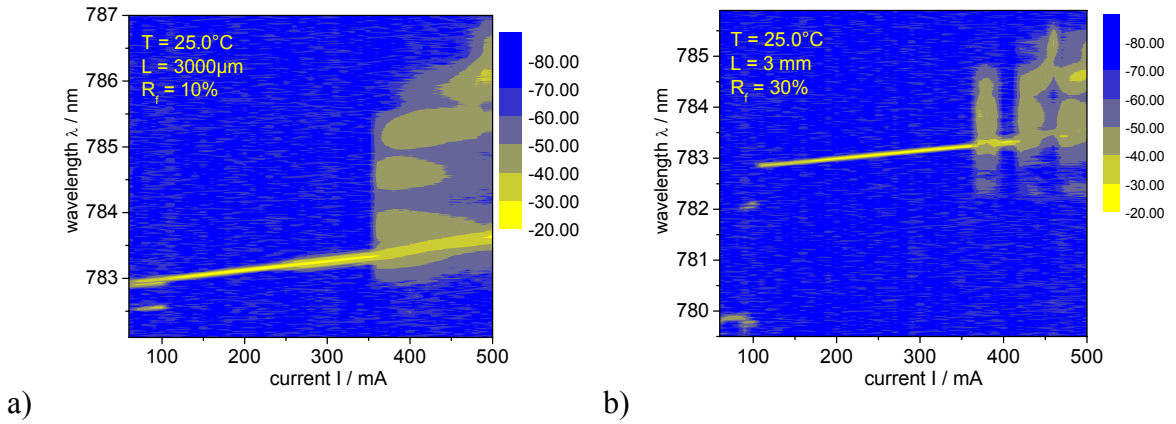

Figure 3. 33. *Spectra behavior of the devices: a) C2-30-2-10-1 (R_f = 10%) and b) C2-30-2-30-1 (R_f = 30%).*

We now would like to summarize the findings of this section. Increasing the front facet reflectivity provides a possibility to reduce the spectral linewidth of DFB diode lasers. A minimum linewidth of 20 kHz was achieved with coatings that provided a front facet reflectivity equal to or exceeding 5%, while the rear facet was coated to provide a reflecitivy of 95%. Maximum power of 270 mW in combination with narrow linewidth was observed for a C-mount device with 5% front facet reflectivity. Although devices with 10% front facet reflectivity and devices with 30% showed the potential to reach the same linewidth at significantly lower output power. Except the *C2-30-2-10-1* device, see Fig. 3.33, all devices with 10% front facet reflectivity switched to

multimode operation at a power level of approximatly 100 mW. Switching to mulit-mode emission occurred at even lower power level for the devices with a front facet reflectivity of 30%. Therefore, we conclude that the DFB diode lasers with 5% front facet and high rear facet reflectivity (95%) correspond to the optimum coating design when high optical output power and narrow spectral linewidth have to be realized simultaneously.

3.9. Recommendations for an optimal design of high power, narrow linewidth DFB lasers

In this chapter, we so far have presented a systematic experimental investigation on how the DFB diode laser linewidth depends on the fundamental laser parameters, namely on the cavity length (L), the coupling coefficient (κ) and the front facet reflectivity (R_f). In this section, we draw the conclusion from this analysis and give recommendations on how to optimally design 780 nm DFB diode lasers that feature high output power (few hundred mW) and small short term linewidth (few 10 kHz at time scales of 10-100 µs).

To yield high-power narrow linewidth DFB lasers all of three parameters (L, κ and R_f) have to be optimized. The optimization of these parameters, in principal, leads to the same result. It should be emphasized, that optimization of one parameter affects the optimum value of the two remaining parameters. Therefore, to reach a high output power together with a narrow linewidth, all three parameters should be optimized together. However, in practice the following procedure appears appropriate for optimizing the laser performance: first select the cavity length (preference for long cavities), then select the coupling coefficient (preference for large coupling coefficient), finally optimize the front facet coating (preference for “large” front facet reflectivity). However, the influence of the various parameters on the linewidth differs. We would finally like to note that the variation in the performance of lasers, that are nominally identical, can be large enough to mask the positive effects of the optimization of one or more of the optimization parameters. Hence, there is no optimum set of parameters but the optimal parameters vary between production runs. To eliminate this variation, reproducibility of the process technology would have to be improved further. We now address the optimization of each parameter in detail to find an optimal laser design.

- We first consider the role of the cavity length. The results presented in section 3.6 clearly show that: in comparison to otherwise identical lasers, DFB lasers with a longer cavity provide a smaller linewidth-power product. Thus, extension of cavity length is considered the most efficient optimization step to yield narrow spectral linewidth, high power DFB lasers. Extension of the cavity length does

not require any additional technology steps, which can be considered an advantage of this optimization step. However, extension of the device length comes at the cost of certain drawbacks, e.g. it causes a degradation of the slope efficiency and it enhances spatial hole burning, which tends to cause multimode emission of long devices at relatively low output power. It is further accompanied by a higher risk of damaging the device during the packaging process. For the 780 nm DFB lasers investigated within the frame work of this thesis none of the devices with a length of 6 mm could be operated successfully. The slope efficiency of these devices was smaller than the slope efficiency of the 3 mm devices by a factor of 3 and thus high power operation was not feasible. Due to spatial hole burning, almost all devices with 6 mm cavity length were emitting multi longitudinal mode even at very low power (typically 30 mW). From the results of this thesis work we conclude that a cavity length of 3 mm for 780 nm DFB diode lasers yields the optimum in terms of spectral stability, electro-optical properties, and output power. Theoretical pedicitons are in agreement with the experimental findings.

- Second, we discuss the influence of the coupling coefficient onto the the linewidth. The experimental data and the discussion of section 3.7 show that doubling of the coupling coefficient has less impact onto the linewidth than doubling of the cavity length. Increasing the coupling coefficient reduces the linewidth but enhances spatial hole burning and reduces the slope efficiency. It is hence advisable to narrow the linewidth by increasing the cavity length while keeping the coupling strength κL constant. This way, gratings featuring a large coupling coefficient can be avoided, which is an advantage in terms of process technology since, in practice, the coupling coefficient strongly depends on growing and processing. This thesis work does not include the analysis of DFB lasers with a coupling coefficient κ that exceeds $2\,\mathrm{cm}^{-1}$. However, the optimization of the cavity length and front facet reflectivity are sufficient to reduce the linewidth to the value provided by a simulation for $\kappa = 5\,\mathrm{cm}^{-1}$. Therefore, there is no motivation to fabricate DFB laser with a coupling coefficient exceeding $2\,\mathrm{cm}^{-1}$.
- Third, we comment on the influence of front facet reflectivity onto the linewidth. The results presented in section 3.8 help to reduce the spectral linewidth selecting an optimal front facet reflectivity. The experimental results show an efficient reduction of the linewidth when the front facet reflectivity is set to 5%. The linewidth reduction achieved this way is comparable to reduction that is achieved when the cavity length is increased from 1.5 mm to 3.0 mm. Therefore, for the applications that request only little or modest output power but at the same time narrow spectral emission, reflection coating the front facet to an appropriate

reflectivity is an appropriate step towards the implementation of narrow linewidth DFB lasers. When both, high power and narrow linewidth are required, first the cavity length and after that the front facet coating should be optimized. Optimization of the coupling coefficient should only be considered secondarly. Currently, for the 780 nm DFB RW diode lasers, coatings of 5% and 95% for the front and rear facet, respectively, provide the optimal result.

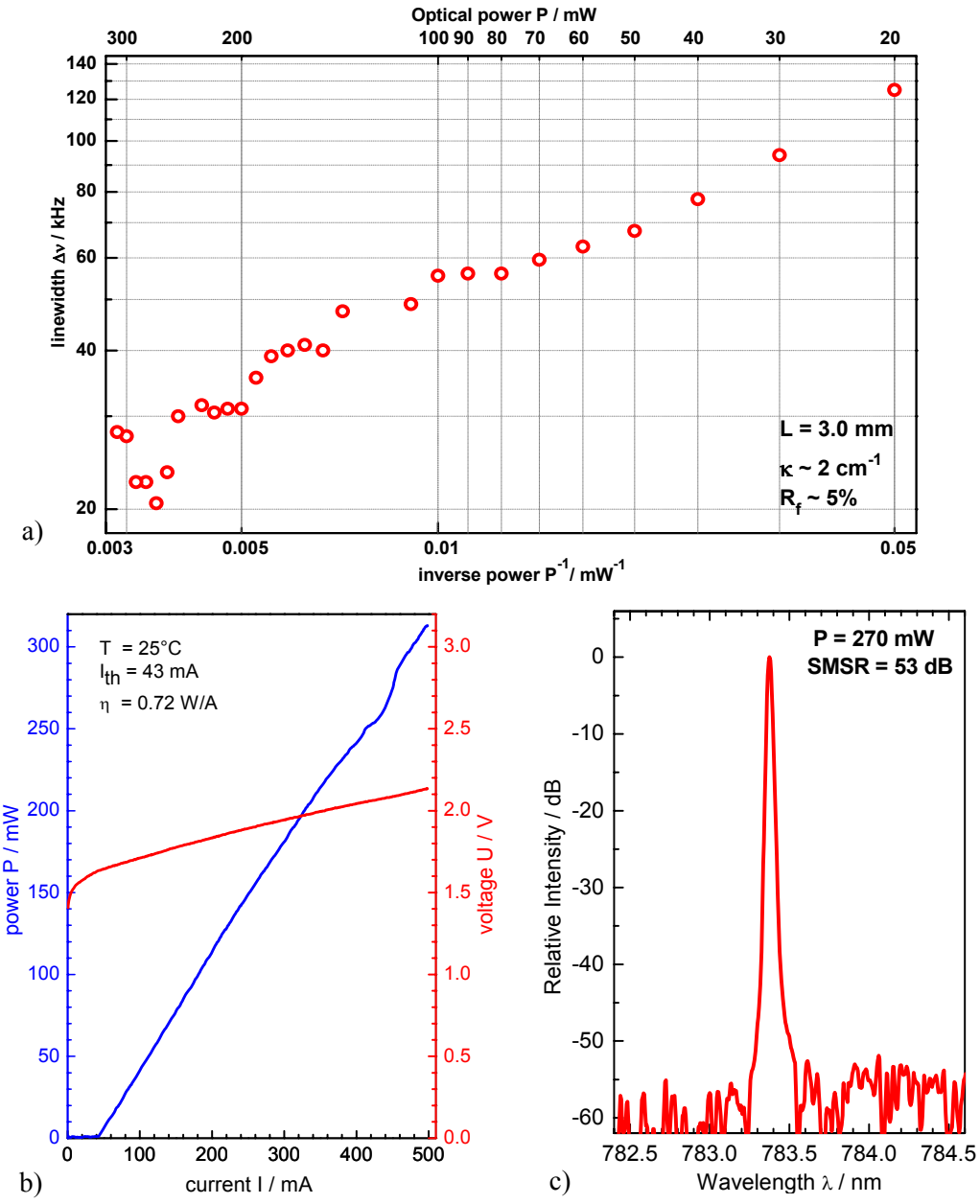

Figure 3.34. *Characterization of the 780 nm DFB laser C2-30-2-05-1 with L = 3 mm, k = 2 cm^{-1}, R_f = 5%. The laser with the narrowest linewidth of 20 kHz at the highest output power of 270 mW*

a) Linewidth vs. output power; b) PUI characteristics; c) Spectrum at 270 mW output power.

Among all lasers analyzed within the frame work of this thesis work the laser with the best spectral performance, i.e. largest single mode output power and narrowest

linewidth was the device *C2-30-2-05-1*, that features a cavity length of L = 3 mm, a coupling coefficient of $\kappa = 2$ cm^{-1}, and a front facet reflectivity of R_f = 5%. This laser provided a short term linewidth of $\Delta\nu$ = 20 kHz at optical output power of P = 270 mW. The corresponding PUI-characteristics, the emission spectrum, as well as linewidth versus output power are shown in Fig 3.34.

Please note that several device provided a minimum linewidth of $\Delta\nu \approx 20$ kHz. These devices are listed in Table 3.15 together with their performance.

Table 3.15. *The summary of lasers that provide the narrowest spectral emission at maximum output power (L= 3 mm, $\kappa = 2\,cm^{-1}$)*

	C2-30-2-30-1 R_f = 30%	*C2-30-2-10-1* R_f = 10%	*T2-30-2-00-1* $R_f < 0.01\%$	*T2-30-2-00-2* $R_f < 0.01\%$	*C2-30-2-05-1* R_f = 5%
$\Delta\nu$ *(kHz)*	20	21	22	20	20
P *(mW)*	120	240	270	270	270

As already discussed in detail in section 3.5.4, the devices packaged in TO3 provide slightly higher output power and narrower spectral linewidth than nominally identical devices that are packed on C-mount. This was attributed to the fact that lasers packeaged in TO3 are better isolated from thermal interference by the environment It is therefore expected, that lasers with a front facet reflectivity of 5% packaged in TO3 outperform the best lasers analyzed sofar and summarized in Table 3.15. However, there is no solution yet to avoid optical feedback from the package window.

Finally, a problem already addressed in section 3.6 and related to cleaving of the laser bars should be kept in mind. Cleaving laser bars leaves the grating phase at the facets uncontrolled. The grating phase, however, significantly affects the laser linewidth. This should be taken into account when DFB diode lasers are designed for applications that require a certain upper limit for the short term linewidth. A safety margin should e build-in into to design to ensure that the linewidth requirements can be met independent of the grating phase defined during the cleaving process.

Summary

This thesis provided a systematic investigation of the optical, electro-optical properties of high power DFB diode laser emitting near 780 nm with a special focus on narrow linewidth emission. The DFB diode lasers were based on an integrated grating index coupling and were designed and fabricated for the spectroscopic applications, that require high optical output power of a few 100 mW and narrow spectral emission (few 100 kHz short term linewidth) at the same time. First, standard characterisation of the DFB diode lasers was carried out to assess the general performance of the devices and to define suitable operating regimes for spectral linewidth characterization. Second, to characterize spectral emission linewidth of diode lasers at the MHz and sub-MHz level a heterodyne linewidth characterization setup was developed. This setup, together with a second-generation heterodyne and self-deleyed heterodyne setup developed by colleagues at FBH, was used to characterize the short term linewidth of the DFB diode lasers.

The investigation of the spectral linewidth of DFB diode lasers focused on the analysis of the linewidth-power dependence. Within a simpe theoretical framework the linewidth monotonically decreases when the optical power increases. However, we found that practical devices do not quite follow this simple model. At or above a certain power level, that is individual to a given DFB diode laser, linewidth rebroadening and a linewidth floor were observed. These effects were shown to be mainly caused by spatial hole burning, with some minor contributions from weak side mode partition noise and nonlinear gain effects. The main results of the experimental analysis is summarized as follows:

- The characterizations of 780 nm DFB diode lasers have been shown a single mode operation excess 300 mW with SMSR large than 50 dB. Almost all of our lasers can be tuned to emit exactly at the absorption wavelength of rubidium atom while keeping high output power regime. For rubidium spectroscopy applications, the best performance belongs to the solitary DFB laser with linewidth of 40 kHz and 190 mW output power. In comparison to other laser configurations with the same performance, this laser shows an advantage about compact aspect.

- The dependence of the linewidth on the cavity length was investigated. The experimental results show a substantial reduction of the linewidth with increasing cavity length. For short cavities the reduction factor was determined to be at least as large as 4 when the cavity length was doubled. However, linewidth reduction by extension of cavity length is limit by the evolution of spatial hole burning at high optical output power. The results suggest that a cavity length of 3 mm optimally combines both, high power operation and narrow linewidth emission.
- The dependence of the linewidth on the coupling coefficient was investigated. To this end DFB diode laser with different coupling coefficient were processed ($\kappa = 1$ cm^{-1} and $\kappa = 2$ cm^{-1}). The experimental results show that increasing the coupling coefficient by a factor of two leads to a linewidth reduction that is significantly less pronounced than doubling of the cavity length, which yields the same coupling strength κL.
- The dependence of the linewidth on the front facet reflectivity was investigated. The experimental results suggest that a front facet reflecitivty of 5% (at a rear facet reflectivity of 95%) provide the best performance in terms of stable single-mode operation at high output power and narrow spectral emission.
- The dependence of the linewidth on diode laser packaging was analyzed. The experimental results suggest that devices in TO3 and SOT packages demonstrate a better spectral performance at high output power than devices packaged on C-mount.

The results of this thesis work point out a strategy for the development and realization of high-power, narrow linewidth DFB diode laser. The laser type with the best performance, both in terms of single-mode operation at high output power and narrow linewidth emission, was a laser type with a cavity length of L = 3 mm, a coupling coefficient of $\kappa = 2$ cm^{-1}, and front facet reflectivity of R_f = 5%. These devices provided a spectral short-term linewidth of $\Delta\nu = 20$ kHz at an optical output power of $P = 270$ mW that never been reached before in our the best of knowledge .

The conclusion drawn from the investigation on 780 nm DFB diode lasers can be transferred to the design of high power, narrow linewidth GaAlAs-based DFB diode lasers emitting at other wavelength.

The analysis presented in thesis work further pointed out the following issues that need to be addressed by future work to fully understand and/or control the spectral behaviour of high power, narrow linewidth DFB diode lasers:

- Due to a lack of control over the cleaving process the phase of the grating at the rear facet is random. However, the grating phase strongly affects the linewidth of the laser. This has a two-fold effect. Firstly, the yield of lasers with similar,

close-to-optimum grating phase at the rear facet is small. Secondly, a systematic comparison of lasers from different bars is difficult to perform as the potential difference of the grating phases may mask the effect under study. The precise control of the grating phase at the rear facet is hence an important request, that has to be addressed by process technology. Progress in process technology has to be complemented by theoretical work that provides a better understanding on how the spectral performance of (weakly coupled) DFB lasers depends on the phase of the grating at the facets. The validity of the theoretical predictions and the progress of process technology have to be proven by further experiments.

- Further experimental investigations have to be carried out in order to analyze in more detail the influence of the packaging type on the laser performance, specifically on the short term spectral linewidth. The main task here will be to compare sealed versus open mounts.

References

[1]. S. Kraft, A. Deninger, C. Trueck, J. Fortagh, F. Lison, and C. Zimmermann, "Rubidium spectroscopy at 778–780 nm with a distributed feedback laser diode", Laser Phys. Lett. **02**(02), pp. 71, 2004.

[2]. A. Klehr, H. Wenzel, O. Brox, F. Bugge, G. Erbert, T-P. Nguyen and G. Tränkle, "High power DFB lasers for D1 and D2 rubidium absorption spectroscopy and atomic clocks", Proc. of SPIE, **7230**, pp. 72301I (2009).

[3]. http://www.toptica.com/page/Raman_spectroscopy_DFB-diode_laser_dfBeam.php

[4]. http://www.eagleyard.com/en/products/dfb-dbr-laser/

[5]. M. Maiwald, G. Erbert, A. Klehr, H-D. Kronfeldt, H. Schmidt, B. Sumpf, and G. Traenkle, "Rapid shifted excitation Raman difference spectroscopy with a distributed feedback diode laser emitting at 785 nm", Appl. Phys. B, **85**, pp. 509, 2006.

[6]. M. H. Anderson, J. R. Ensher, M. R. Matthews, C. E. Wieman, E. A. Cornell, "Observation of Bose-Einstein Condensation in a Dilute Atomic Vapor", Science **269**, pp. 198, 1995.

[7]. O. Carraz, F. Lienhart, R. Charrière, M. Cadoret, N. Zahzam, Y. Bidel, and A. Bresson, "Compact and robust laser system for onboard atom interferometry", Appl. Phys. B, **97**(2), pp. 405, 2009.

[8]. M-W. Pan, R. E. Benner, and L. M. Smith, "Continuous Lasers for Raman spectroscopy", J. Chalmers, P. Griffiths (ed.) Handbook of Vibration Spectroscopy, John Wiley & Sons Ltd., 2002.

[9]. F. Lienhart, S. Boussen, O. Carraz, N. Zahzam, Y. Bidel, and A. Bresson, "Compact and robust laser system for rubidium laser cooling based on the frequency doubling of a fiber bench at 1560 nm", Appl. Phys. B, **89**, pp. 177, 2007.

[10]. L. Hildebrandt, J. Sacher, R. Knispel, and F. Schael, "Robust external cavity diode laser (ECDL) and their application in water vapor and saturated-absorption rubidium spectroscopy", LACEA Conference, Santa Fe, NM, 2000.

[11]. S. E. Park, T. Y. Kwon, and H. S. Lee, "A compact extended-cavity diode laser with a Littman configuration", Instrumentation and Measurement IEEE ransactions on, **52**(2), pp.280–283, 2003.

[12]. A. J. Olson, E. J. Carlson, and S. K. Mayer, "Two-photon spectroscopy of rubidium using a grating-feedback diode laser" , Am. J. Phys., **74**(3), pp. 218-223, 2006.

[13]. B. L. Volodin, S. V. Dolgy, E. D. Melnik, E. Downs, J. Shaw, V. S. Ban, "Wavelength stabilization and spectrum narrowing of high power multimode laser diodes and arrays by use of volume Bragg gratings", Opt. Lett., **29**(16), pp. 1891 – 1893, 2004.

[14]. G. B. Venus, A. Sevian, V. I. Smirnow, and L. B. Glebov, "High-brightness narrow-line laser source with volume Bragg-grating feedback", Proc. of SPIE, **5711**, pp 166 – 176, 2005.

[15]. W. Lewoczko-Adamzyck, "Bose-Einstein Condensation in Microgravity", PhD Thesis, Humboldt-Universität zu Berlin, 2009.

[16]. http://www.iqo.uni-hannover.de/quantus/

[17]. http://www.physik.hu-berlin.de/qom/research/droptower

[18]. LASUS project

[19]. H. Wenzel, A. Klehr, M. Braun, F. Bugge, G. Erbert, J. Fricke, A. Knauer, P. Ressel, B. Sumpf, M. Weyers and G. Tränkle, "Design and realization of high-power DFB lasers", SPIE Proceedings, **5594** - Physics and Applications of Optoelectronic Devices, pp. 110, 2004.

[20]. M. Maiwald, G. Erbert, A. Klehr, B. Sumpf, H. Wenzel, T. Laurent, J. Wiedmann, H-D. Kronfeldt, and H. Schmidt, "Reliable operation of 785 nm DFB diode lasers for rapid Raman spectroscopy", Proc. of SPIE, **6456**, pp. 64560W-1, 2007

[21]. Bahaa. E. A. Saleh and M. C. Teich, "Fundamentals of Photonics", John Wiley & Sons, Inc., 1991.

[22]. F. Bachman, P. Loosen, R. Poprawe (ed.), "High-Power Diode Lasers. Technology and Applications (Topics in Applied Physics)", Springer Verlag Berlin Heidenberg 2007.

[23]. M. Weyers, A. Bhattacharya, F. Bugge, and A. Knauer, "Epitaxy of High-Power Diode Laser Structures", R. Diehl (ed.), "High-Power Diode Lasers. Fundamentals, Technology, Applications", Topics Appl. Phys. **78**, pp. 83-200, Springer Verlag Berlin Heidenberg 2000.

[24]. L. A. Coldren, S. W. Corzine, "Diode Lasers and Photonic Integrated Circuits", John Wiley & Sons, Inc., 1995.

[25]. P. Unger, "Introduction to Power Diode Lasers", R. Diehl (ed.), "High-Power Diode Lasers. Fundamentals, Technology, Applications", Topics Appl. Phys. 78, pp. 1-54, Springer Verlag Berlin Heidenberg 2000.

[26]. E. Kapol, "Semiconductor Lasers II: Materials and Structures", Academic Press, 1999.

[27]. G. P. Agrawal, "Semiconductor lasers", Kluwer Academic Publishers, 1993.

[28]. G. Erbert, A. Baerwolff, J. Sebastian, and J. Tomm, "High-Power Broad-Area Diode Lasers and Laser Bars", R. Diehl (ed.), "High-Power Diode Lasers. Fundamentals, Technology, Applications", Topics Appl. Phys. **78**, pp. 173-223, Springer Verlag Berlin Heidenberg 2000.

[29]. G. P. Agrawal, "Fiber-Optic Communications Systems", John Wiley & Sons, Inc., 2002.

[30]. F. Traeger, "Springer Handbook of Lasers and Optics", Springer 2007.

[31]. R.F. Kazarinov, C.H. Henry, "Second-Order Distributed Feedback Lasers with Mode Selection Provided by First-Order Radiation Losses", IEEE Journ. Quant. Electr. **QE-21**(2), pp. 144-150, 1985.

[32]. A.M. Shams-Zadeh-Amiri, J. Hong, X. Li, W. Huang, "Second- and Higher-Order Resonant Gratings with Gain or Loss. Part I: Green's Function Analysis", IEEE Journ. Quant. Electr. **QE-36**(12), pp. 1421-1430, 2000.

[33]. K. Paschke, A. Bogatov, A.E. Drakin, R. Güther, A.A. Stratonnikov, H. Wenzel, G. Erbert, G. Tränkle, "Modeling and Measurements of the Radiation Characteristics of High-Power α-DFB-Lasers", IEEE Journ. Sel. Topics in Quantum Electronics **9**(3), pp. 835-843, 2003.

[34]. K. Paschke, A. Bogatov, F. Bugge, A.E. Drakin, J. Fricke, R. Güther, A.A. Stratonnikov, H. Wenzel, G. Erbert, G. Tränkle, "Properties of Ion-Implanted High-Power Angled-Grating Distributed-Feedback Lasers", IEEE Journ. Sel. Topics in Quantum Electronics **9**(5), pp. 1172-1178, 2003.

[35]. K. O. Hill, G. Meltz, "Fiber Bragg Grating Technology Fundamentals and Overview", IEEE J. Lightwave Technol., **15**(8), pp. 1263-1276, 1997.

[36]. H. Ghafouri-Shiraz, "Distributed Feedback Laser Diodes and Optical Tunable Filters", John Wiley and Sons, Inc., 2003.

[37]. K. David, J. Buus, and R. Baets, "Basic analysis of AR-coated, partly gain-coupled DFB lasers: the standing wave effect", IEEE J. Quantum Electron., **28**(2), pp. 427-433, 1992.

[38]. Y. Luo, Y. Nakano, K. Tada, T. Inoue, H. Homsomatsu, and H. Iwaoka, "Fabrication and characteristics of gain-coupled distributed feedback semiconductor lasers with a corrugated active layer", IEEE. J. Quantum Electron., **QE-27**(6), pp. 1724-1732, 1991.

[39]. Y. Nakano, Y. Luo, and K. Tada, "Facet reflection independent, single longitudinal mode oscillation in a GaAlAs/GaAs distributed feedback laser equipped with a gain-coupling mechanism", Appl. Phys. Lett., **55**(16), pp. 1606-1608, 1989.

[40]. K. David, G. Morthier, P. Vankvikelberge, and R. Baets, “Yield analysis of non-AR-coated DFB lasers with combined index and gain coupling”, Electron. Lett., **26**(4), pp. 238-239, 1990.

[41]. G. Morthier, P. Vankvikelberge, K. David, and R. Baets, “Improved performance of AR-coated DFB lasers by the introduction of gain coupling”, IEEE Photon. Technol. Lett., **2**(3), pp. 170-172, 1990.

[42]. H. Kogelnik, C. V. Shank, “Coupled-Wave Theory of Distributed Feedback Lasers”, J. Appl. Phys., **43**(5), May 1972.

[43]. T. Suhara, “Semiconductor Laser Fundamentals” Marcel Dekker, Inc., 2004.

[44]. J. Carroll, J. Whiteaway, and D. Plumb, “Distributed feedback semiconductor lasers”, The Institution of Electrical Engineers and SPIE Optical Engineering Press, 1998.

[45]. J. E. A. Whiteaway, B. Garrett, G. H. B. Thompson, “The static and dynamic characteristics of single and multiple phase-shifted DFB laser structures”, IEEE J. Quantum Electron. **28**, pp. 1277-1293, May 1992.

[46]. M. Okai, M. Suzuki, T. Taniwatari: Strained, “multiquantum-well corrugation-pitch-modulated distributed feedback laser with ultranarrow (3.6 kHz) spectral linewidth, Electron. Lett. **29**, pp. 1696-1697, September 1993.

[47]. A. Talneau, J. Charil, A. Ougazzaden, J. C. Bouley, “High power operation of phase-shifted DFB lasers with amplitude modulated coupling coefficient”, Electron. Lett. **28**, pp. 1395-1396, July 1992.

[48]. Y. Kotaki, M. Matsuda, T. Fujii, H. Ishikawa, “MQWDFB lasers with nonuniform-depth $\lambda/4$ shifted grating”, 17th European Conference on Optical Communications, Paris 1991, pp. 137-140, (IEEE, Piscataway 1991).

[49]. S. Hansmann, H. Hillmer, H. Walter, H. Burkhard, B. Hübner, E. Kuphal, “Variation of coupling coefficients by sampled gratings in complex coupled distributed feedback lasers”, IEEE J. Sel. Top. Quantum Electron. **1**, pp. 341-345, June 1995.

[50]. H. Hillmer, K. Magari, Y. Suzuki, “Chirped gratings for DFB laser diodes using bent waveguides”, IEEE Photon. Technol. Lett. **5**, pp. 10-12, 1993.

[51]. M. Usami, S. Akiba, “Suppression of longitudinal spatial hole-burning effect in $\lambda/4$-shifted DFB lasers by nonuniform current distribution”, IEEE J. Quantum Electron. **25**, pp. 1245-1253, June 1989.

[52]. P. Goldberg, P. W. Milonni, and B. Sundaram, “Theory of the fundamental laser linewidth”, Physical Review A, **44**(3), pp. 1969, 1991.

[53]. P. Goldberg, P. W. Milonni, and B. Sundaram, "Theory of the fundamental laser linewidth II", Physical Review A, **44**(7), pp. 4556, 1991

[54]. A. L. Schawlow and C. H. Townes, "Infrared and Optical Masers", Physical Review, **112**(6), pp. 1940, 1958.

[55]. C. H. Henry, "Theory of the linewidth of semiconductor lasers", IEEE Journ. Quant. Electr. **QE-38**(2), pp. 259, 1982.

[56]. B. A. Saleh, "Fundamental of Photonics", John Wiley & Sons, Inc., 1991.

[57]. K. Petermann, "Laser diode modulation and noise", Kluwer Academic Publishers, 1991.

[58]. Y. Yamamoto (ed.), "Coherence, Amplification, and Quantum Effects in Semiconductor Lasers", John Wiley & Sons, Inc., 1991.

[59]. A. Mooradian, Physics Today, pp. 43-48, May, 1985.

[60]. D. Welford and A. Mooradian, "Output Power and Temperature Dependence of the Linewidth of Single Frequency cw (GaAl)As Diode Lasers", Appl. Phys. Lett. **40**, pp. 865-867, 1982.

[61]. T. L. Koch, U. Koren, and B. I. Miller, "High Performance tunable 1.5 μm InGaAs/InGaAsP Multiple Quantum Well Distributed Bragg Reflector Lasers", Appl. Phys. Lett. **53**, pp. 1036-1038, 1988.

[62]. X. Pan, B. Tromborg, and H. Olesen, "Linewidth Rebroadening in DFB Lasers Due to Weak Side Modes", IEEE Photon. Technol. Lett. **3**(2), pp. 112, 1991.

[63]. F. Girardin, G.-H. Dum, and P. Gallion, "Linewidth Rebroadening Due to Nonlinear Gain and Index Induced by Carrier Heating in Strained Quantum-Well Lasers", IEEE Photon. Technol. Lett. **8**(3), pp. 334, 1996.

[64]. F. Kano, M. Fukuda, and J. Yoshida, "Correlation of Noise Characteristics and Line Shape with Linewidth Rebroadening of MQW DFB Lasers", IEEE Photon. Technol. Lett. **4**(1), pp. 13, 1992.

[65]. H. Yamazaki, M. Yamaguchi and M. Kitamura, "Spectral Linewidth Rebroadening in MQW-DFB LDs Caused by Spontaneous Emission Noise in SCH/Barrier Layers", IEEE Photon. Technol. Lett. **6**(3), pp. 341, 1994.

[66]. G. P. Agrawal, "Intensity Dependence of the Linewidth Enhancement Factor and Its Implications Semiconductor Lasers", IEEE Photon. Technol. Lett. **1**(8), pp. 212, 1989.

[67]. P. Vankwikelberge, G. Morthier, and R. Baets, "CLADISS-A Longitudinal Multimode Model for the Analysis of the Static, Dynamic, and Stochastic

Behavior of Diode Lasers with Distributed Feedback", IEEE Journ. Quant. Electr. **26**(10), pp. 1728, 1990.

[68]. G. P. Agrawal, "Effect of Gain and Index Nonlinearities on Single-Mode Dynamics in Semiconductor Lasers", IEEE Journ. Quant. Electr. **26**(11), pp. 1901, 1990.

[69]. K. Kikuchi, "Effect of l/f-Type FM Noise on Semiconductor-Laser Linewidth Residual in High-Power Limit", IEEE Journ. Quant. Electr. **25**(4), pp. 684, 1989.

[70]. K. Kojima, K. Kyuma, "Analysis of the spectral linewidth of distributed feedback laser diodes", Electron. Lett., **20**(21), pp. 869, 1984.

[71]. K. Kojima, K. Kyuma, and T. Nakayama, "Analysis of the spectral linewidth of distributed feedback laser diodes", IEEE J. Lightwave Technol., **LT-3**(12), No.5, pp. 1048, 1985.

[72]. Y. Dai and J. Yao, "Numerical Study of a DFB Semiconductor Laser and Laser Array With Chirped Structure Based on the Equivalent Chirp Technology", IEEE Journ. Quant. Electr. **44**(10), pp. 938, 2008.

[73]. A. Champagne, J. Camel, R. Maciejko, K. J. Kasunic, D. M. Adams, and B. Tromborg, "Linewidth Broadening in a Distributed Feedback Laser Integrated With a Semiconductor Optical Amplifier", IEEE Journ. Quant. Electr. **38**(11), pp. 1493, 2002.

[74]. H. J. Wünsche, U. Bandelow, and H. Wenzel, "Calculation of Combined Lateral and Longitudinal Spatial Hole Burning in λ/4 Shifted DFB Lasers", IEEE Journ. Quant. Electr. **29**(6), pp. 1751, 1993.

[75]. H. Wenzel, and H. J. Wünsche, "A Equation for the Amplitudes of the Modes in Semiconductor Lasers", IEEE Journ. Quant. Electr. **30**(9), pp. 2073, 1994.

[76]. H. Wenzel, H. J. Wünsche, and U. Bandelow, "Linewidth Rebroadening in Semiconductor Lasers due to Lateral Spatial Holeburning", Electron. Lett., **27**(25), pp. 2301, 1991.

[77]. A. Baliga, D. Trivedi and N. G. Anderson, "Tensile-strain effects in quantum-well and superlattice band structures", Phys. Rev. B **49**, pp.10402, 1994.

[78]. A. Klehr, M. Braun F. Bugge, G. Erbert, J. Fricke, A. Knauer, P. Ressel, H. Wenzel and G. Tränkle, "High-power ridge-waveguide and broad-area lasers with a DFB resonator in the wavelength range 760-790nm", Proceedings SPIE, **5738** - Novel In-Plane Semiconductor Lasers IV, p. 416-424, April 2005.

[79]. O. Brox, J. Wiedmann, F. Scholz, F. Bugge, J. Fricke, A. Klehr, T. Laurent, P. Ressel, H. Wenzel, G. Erbert and G. Tränkle, "Integrated 1060nm MOPA pump

source for high-power green light emitters in display technology", Proc. of SPIE, **6909**, Novel In-Plane Semiconductor Lasers VII, pp. 6091G-1, 2008.

[80]. P. Ressel and G. Erbert, "Verfahren zur Passivierung der Spiegelflächen von Optischen Halbleiterbauelementen," German Patent Application102 21 952.4/13.05.2002.

[81]. J. W. Tomm, and J. Jimenez (eds.), "Quantum-well laser array packaging", McGraw-Hill, 2007.

[82]. D. Derickson, "Fiber Optics Test and Measurement", Prentice-Hall, Inc., 1998.

[83]. T. Okoshi, K. Kikuchi, and A. Nakayama, "Novel method for High Resolution Measurement of Laser Output Spectrum", Electron Lett., **16**, pp. 630-631, 1980.

[84]. G. Genty, "Supercontinuum generation in microstructured fibers and novel optical measurement techniques", PhD Thesis, Helsinki University of Technology, Espoo 2004.

[85]. P. B. Gallion, and G. Debarge, "Quantum phase noise and field correlation in single frequency semiconductor laser systems", IEEE J. Quantum Electron. **20**, pp. 343-349 (1984).

[86]. H. Ludvigsen, and E. Bodtker, "New Method for Self-Homodyne Laser Linewidth Measurements with a Short Delay Fiber", Opt. Commun. **110**, pp. 595-598 (1994).

[87]. H. Ludvigsen, M. Tossavainen, and M. Kaivola, "Laser linewidth measurements using self-homodyne detection with short delay", Opt. Commun. **155**, pp. 180-186 (1998).

[88]. L.D. Turner, K.P. Weber, C.J. Hawthorn, R.E. Scholten, "Frequency noise characterisation of narrow linewidth diode lasers", Optics Comm., **201**, pp.391, 2002.

[89]. D.S. Elliott, R. Roy, S. J. Smith, "Extracavity laser band-shape and bandwidth modification", Phys. Review A, **26**, pp. 12, 1982.

[90]. A.Yu. Nevsky et al, " A narrow-line-width external cavity quantum dot laser for high-resolution spectroscopy in the near-infrared and yellow spectral ranges", Appl. Phys. B, **92**(4), pp. 501-507, 2008.

[91]. M. Ohtsu (ed.), "Frequency Control of Semiconductor Lasers", John Wiley & Sons, Inc., 1996.

[92]. B. Daino, P. Spano, M. Tamburrini, and S. Piazolla, "Phase noise and spectra line shape in semiconductor lasers", IEEE Journ. Quant. Electr. **QE-19**, pp. 266, 1983.

[93]. S. Kunze, S. Wolf , G. Rempe, "Measurement of fast frequency fluctuations Allan variance of a grating-stabilized diode laser", Optics Comm., **128**, pp. 269, 1996.

[94]. O. Ishida, “Delayed-Self-Heterodyne Measurement of Laser Frequency Fluctuations”, IEEE J. Lightwave Technol. **9**(11), 1991.

[95]. M. A. Linne, “Spectroscopic Measurement An Introduction to the Fundamentals”, Elsevier Science Ltd. 2002.

[96]. L. B. Mercer, “1 over f Frequency Noise Effects on Self-Heterodyne Linewidth Measurements”, IEEE J. Lightwave Technol. **9**(4), 1991.

[97]. J. Humlicek, “An efficient method for evaluation of the complex probability function and its derivatives,” J. Quant. Spectrosc. Radiat. Transfer., **21**, pp. 309-313, 1979.

[98]. J. Humlicek, “Optimized computation of the Voigt and complex probability function,” J. Quant. Spectrosc. Radiat. Transfer., **27**, pp. 431-444, 1982.

[99]. www.ilxlightwave.com

[100]. www.newport.com

[101]. www.linos-catalog.com

[102]. G. P. T. Lancaster, W. Sibbett, and K. Dholakia, “An extended-cavity diode laser with a circular output beam”, Rev. Sci. Instrum., **71**(10), pp. 3646, 2000.

[103]. C. J. Hawthorn, K. P. Weber, and R. E. Scholten, “Littrow configuration tunable external cavity diode laser with fixed direction output beam”, Rev. Sci. Instrum., **72**(12), pp. 4477, 2001.

[104]. I. Shvarchuck, K. Dieckmann, M. Zielonkowski, and J.T.M. Walraven, “Broad-area diode-laser system for a rubidium Bose–Einstein condensation experiment”, Appl. Phys. B, **71**, pp. 475, 2000.

[105]. S. Stry, L. Hildebrandt, J. Sacher, C. Buggle, M. Kemmann, and W. von Klitzing, “Compact tunable diode laser with diffraction limited 1 Watt for atom cooling and trapping”, SPIE High-Power Diode Laser Technology and Applications II, **5336**, pp. 17, 2004.

[106]. M. Gilowski , Ch. Schubert, M. Zaiser, W. Herr, T. Wuebbena, T. Wendrich, T. Mueller, E.M. Rasel, and W. Ertmer, “ Narrow bandwidth interference filter-stabilized diode laser systems for the manipulation of neutral atoms”, Opt. Comm., **280**, pp. 443, 2007.

[107]. R. J. Thompson, M. Tu, D. C. Aveline, N. Lundblad, and L. Maleki, “High power single frequency 780nm laser source generated from frequency doubling of a seeded fiber amplifier in a cascade of PPLN crystals”, Opt. Express **11**(14), pp. 1709, 2003.

[108]. J. Feng, Y. Li, X. Tian, J. Liu, and K. Zhang, "Noise suppression, linewidth narrowing of a master oscillator power amplifier at 1.56μm and the second harmonic generation output at 780nm", Opt. Express **16**(16), pp. 11871, 2008.

[109]. J. Sacher, R. Knispel, S. Stry, "High-frequency tuning of high-powered DFB MOPA system with diffraction limited power up to 1.5W", SPIE, **6133**, pp. 276, 2006.

[110]. S. W. Chiow, S. Herrmann, H. Mueller, and S. Chu, "6W, 1 kHz linewidth, tunable continuous-wave near-infrared laser", Opt. Express **17**(7), pp. 5246, 2009.

[111]. S. Takigawa, T. Uno, M. Kume, K. Hamada, N. Yoshikawa, H. Shimizu, and G. Kano, "50 mW Stable Single Longitudinal Mode Operation of a 780 nm GaAlAs DFB Laser", IEEE Journ. Quant. Electr. **25**(6), pp. 1489, 1989.

[112]. T-P. Nguyen, A. Klehr, A. Wicht, G. Erbert, and G. Traenkle, " High-power distributed feedback diode laser at 780 nm with sub-100 kHz linewidth", Conference Digest CLEO/ Nguyen_cb12.2-thu, Europe 2009.

[113]. S. Kraft, A. Deninger, C. Trueck, J. Fortagh, F. Lison, and C. Zimmermann, "Rubidium spectroscopy at 778–780 nm with a distributed feedback laser diode", Laser Phys. Lett. **02**(02), pp. 71, 2004.

[114]. M. Kanskar, J. Cai, C. Galstad, Y. He, S.H. Macomber, E. Stiers, and S.R. Tatavarti-Bharatam, "High Power Conversion Efficiency and WavelengthStabilized, Narrow Bandwidth 975nm Diode Laser Pumps", Laser Source and System Technology for Defense and Security II, Proc. of SPIE, **6216**, pp. 621609, 2006.

[115]. D. Botez, "High-power, Al-free diode lasers", Compound Semiconductor **5**(6), pp. 24-29, 1999.

[116]. R. W. Dixon, F. R. Nash, R. L. Hartman, and R. T. Hepplewhite, "Improved light-output linearity in stripe-geometry double-heterostructure (Al,Ga)As lasers", Appl. Phys. Lett., **29**(6), pp. 372, 1976.

[117]. J. E. Whiteaway, B. Garrett, G. H. B. Thompson, A. J. Collar, C. J. Armistead, and M. J. Fice, "The Static and Dynamic Characteristics of Single and Multiple Phase-Shifted DFB Laser Structures", IEEE Journ. Quant. Electr. **28**(5), pp. 1277, 1992.

[118]. S. Miller, "The Effect of Side Modes on Linewidth and Intensity Fluctuations in Semiconductor Lasers", IEEE Journ. Quant. Electr. **24**(5), pp. 750, 1988.

[119]. U. Kruger and K. Petermann, "Dependence of the Linewidth of a Semiconductor Laser on the Mode Distribution", IEEE Journ. Quant. Electr. **26**(12), pp. 2058, 1990.

[120]. G. Morthier and P. Vankwikelberge, “Handbook of Distributed Feedback Laser Diodes”, Artech House, Inc. 1997.

[121]. R. Schatz, E. Berglind, and L. Gillner, “ Parameter Extraction from DFB Lasers by Means of a Simple Expression for the Spontaneous Emission Spectrum”, IEEE Photon. Technol. Lett., **6**(10), pp. 1182, 1994.

[122]. H. Soda, and H. Imai, “Analysis of the Spectrum Behavior Below the Threshold in DFB Lasers”, IEEE. J. Quantum Electron., **QE-22**(5), pp. 637, 1986.

[123]. T. Earles, L. J. Mawst, and D. Botez, “1.1 W continuous-wave, narrow spectral width (< 1 Å). Emission from broad-stripe, distributed-feedback diode lasers (λ = 0.893 mm)”, Appl. Phys. Lett., **73**(15), pp. 2072, 1998.

[124]. G. B. Morrison, D. T. Cassidy, and D. M. Bruce, “Facet Phases and Sub-Threshold Spectra of DFB Lasers: Spectral Extraction, Features, Explanations, and Verification”, IEEE. J. Quantum Electron., **37**(6), pp. 762, 2001.

[125]. A.P. Bogatov, A.E. Drakin, D.V. Batrak, R. Guether, K. Paschke, H. Wenzel, “Spectral properties of a semiconductor α-DFB laser cavity”, Quantum Electron. **36**(8) 745-750 (2006).

[126]. H. Wenzel, “Green’s Function Based Simulation of the Optical Spectrum of Multisection Lasers”, IEEE J. Select. Topics Quantum Electron., **9**(3), pp. 865, 2003.

[127]. N. Yamada, T. Hirata, M. Maeda, and H. Hosomatsu, “ Basic properties, Linewidth enhancement factor and spectral linewidth of SQW laser diodes emitting in the 780 nm region”, Jpn. J. Appl. Phys. **28**(12), pp. L2219, 1989.

[128]. T. Kunii, Y. Matsui, “Narrow spectral linewidth semiconductor lasers”, Opt. Quant. Electr., **24**, pp. 719, 1992.

[129]. H. Lu, G. P. Li, and T. Makino, “ Spectral linewidth reduction in partly gain-coupled 1.55 μm strained multiple quantum-well distributed feedback laser”, Appl. Phys. Lett., **63(5)**, pp. 589, 1993.

[130]. H. Mawatari, F. Kano, N. Yamamoto, Y. Kondo, Y. Tohmori, and Y. Yoshikuni, “Spectral linewidth and linewidth enhancement factor in 1.5 μm modulation-doped strained Multiple-Quantum-Well lasers”, Jpn. J. Appl. Phys., **33**, pp. 811, 1994.

[131]. M. Okai, “Spectral characteristics of distributed feedback semiconductor lasers and their improvements by corrugation-pitch-modulated structure”, J. Appl. Phys. **75**(1), pp. 1, 1994.

[132]. M. B. Willemsen, A. S. van de Nes, M. P. van Exter, J. P. Woerdman, M. Kicherer, R. King, R. Jaeger, and K. J. Ebeling, " Polarization-resolved linewidth-power product of a vertical-cavity semiconductor laser", J. Appl. Phys., **89**(7), pp. 4183, 2001.

[133]. H.Wenzel, FBH Internal results

[134]. K. Takaki, T. Kise, K. Maruyama, N. Yamanaka, M. Funabashi, and A. Kasukawa, "Reduced Linewidth Re-Broadening by Suppressing Longitudinal Spatial Hole Burning in High-Power 1.55 μm Continuous-Wave Distributed-Feedback (CW-DFB) Laser Diodes", IEEE Journ. Quant. Electr., **39**(9), pp.1060, 2003.

[135]. H. Soda, Y. Kotaki, H. Sudo, H. Ishikawa, and S. Yamakoshi, "Stability in single longitudinal mode operation in GaInAsP/InP phase adjusted DFB-laser," IEEE Journ. Quant. Electr., **QE-23**, pp.804-814, 1987.

[136]. X. Pan, H. Olesen, and B. Tromborg, "Spectral linewidth of DFB lasers including the effects of spectral holeburning and nonuniform current injection," IEEE Photon. Technol. Lett., **2**, pp. 312–315, 1990.

[137]. K. Kikuchi and H. Tomofuji, "Analysis of linewidth of separatedelectrode DFB laser diode," Electron. Lett., **25**, pp. 916-918, 1989.

[138]. P. Vankwikelberge, F. Buytaert, A. Franchois, R. Baets, P. Kuindersma, and C. W. Fredriksz, "Analysis of the carrier-induced FM response of DFB lasers: Theoretical and experimental case studies," IEEE Journ. Quant. Electr., **QE-25**, pp. 2239-2254, 1989.

[139]. X. Pan, H. Olesen, and B. Tromborg, "Modulation characteristics of tunable DFB/DBR lasers with one or two passive tuning sections," IEEE Journ. Quant. Electr., **QE-25**, pp. 1254-1260, 1989.

[140]. Y. Kotaki, S. Ogita, M. Matsuda, Y. Kuwahara, and H. Ishikawa, "Tunable, narrow-linewidth and high-power λ/4-shifted DFB laser," Electron. Lett., **25**, pp. 990-992, July 1989.

[141]. H. Soda, Y. Kotaki, H. Sudo, H. Ishikawa, S. Yamakoshi, and H. Imai, "Stability in single longitudinal mode operation in GaInAsP/InP phase-adjusted DFB lasers," IEEE Journ. Quant. Electr., **QE- 23**, pp. 804-814, 1987.

[142]. F. Girardin, G-H. Duan, P. Gallion, A. Talneau and A. Ougazzaden, "Experimental investigation of the relative importance of carrier heating and spectral-hole-burning on nonlinear gain in bulk and strained multi-quantum-well 1.55 μm lasers", Appl. Phys. Lett. **67**, pp. 771, 1995.

[143]. T. Q. Tran, " Investigation of high-power diode lasers by spectroscopic techniques", Dissertation, Technischen Universität Berlin, 2007.

[144]. S. Doherty, "Effect of Packaging Related Stress on Distributed Feedback Ridge-waveguide Lasers", Master Thesis, Technische Fachhochschule Berlin, 2008.

[145]. M. A. Fritz, G. B. Morrison, and D. T. Cassidy, "The Effect of Die Bonding Distributed Feedback Lasers", IEEE Journ. Quant. Electr., **40**(8), pp. 996, 2004.

[146]. G. B. Morrison, D. T. Cassidy, J. E. Johnson, M. Sipics, H. Wang, and R. Wolf, "Bonding-Induced Strain Effects in InP DFB Components Soldered p-Side-Up on AlN Substrates", IEEE Journ. Quant. Electr., **45**(8), pp. 937, 2009.

[147]. J. Zoz, U. Barabas, "Linewidth enhancement in laser diodes caused by temperature fluctuations", IEEE Proc. Optoelectron., 141(3), pp 191-3, 1994.

[148]. Ogita, Y. Kotaki, K. Kihara, M. Matsuda, H. Ishikawa, and H. Imai, "Dependence of spectral linewidth on cavity length and coupling coefficient in DFB laser", IEEE Electron. Lett., **24**(10), pp. 613, 1988.

[149]. M. Kitamura, H. Yamazaki, T. Sasaki, N. Kida, H. Hasumi, and I. Mito, "250 kHz Spectral Linewidth Operation of 1.5 μm Multiple Quantum Well DFB-LD's", IEEE Photon. Technol. Lett., **2**(5), pp. 310, 1990.

[150]. J. Wang, N. Schunk, K. Petermann, "Linewidth Enhancement For DFB Lasers Due to Longitudinal Field Dependence in the Laser Cavity", IEEE Electron. Lett., **23**(14), pp. 715, 1987.

[151]. K. Kudo, S. Arai, and K. C. Shin, "The optical gain coupling saturation effect on the linewidth property of complex coupled DFB lasers", IEEE Photon. Technol. Lett., **6**(4), pp. 482, 1994.

[152]. K. Y. Liou, N. K. Dutta, C. A. Burrus, "Linewidth-narrowed distributed feedback injection lasers with long cavity length and detuned Bragg wavelength". Appl. Phys. Lett. **50**(8), pp. 489, 1987.

[153]. A.M. Shams-Zadeh-Amiri, J. Hong, X. Li; W-P. Huang, "Second- and Higher Order Resonant Gratings with Gain or Loss - Part I- Green's Function Analysis", IEEE Journ. Quant. Electr., **36**(12), pp. 1421, 2000.

[154]. A.M. Shams-Zadeh-Amiri, J. Hong, X. Li; W-P. Huang, "Second- and Higher Order Resonant Gratings with Gain or Loss - Part II - Designing Complex-Coupled DFB Lasers with Second-Order Gratings", IEEE Journ. Quant. Electr., **36**(12), pp. 1431, 2000.

[155]. Internal result FBH.

[156]. K. Kojima and K. Kyuma, “Analysis of the spectral linewidth of distributed feedback laser diodes using the Green’s function method”, Jpn. J. Appl. Phys. **27**(9), pp. L1721-L1723, 1988.

[157]. G. P. Agrawal, N. K. Dutta, and P. J. Anthony, “Linewidth of distributed feedback semiconductor lasers with partially reflecting Facet”, Appl. Phys. Lett., **48**(7), pp. 457, 1986.

[158]. M. Adams, I. D. Henning, “Linewidth calculations for distributed- feedback lasers”, IEE Proc. J. Optoelectron., **132,** pp. 136-139, 1985.

[159]. S. Ogita, M. Hirano, H. Soda, M. Yano, H. Ishikawa, “Dependence of spectral linewidth of DFB lasers on facet reflectivity”, IEEE Electron. Lett., **23.** pp. 347-349, 1987.

[160]. D. V. Eddolls, C. A. Park, J. Buus, “Dependence of Mode Stability and Linewidth of DFB Lasers on Facet Reflectivity and Coupling Coefficient”, IEEE Electron. Lett., **27**(7), pp. 590, 1991.

[161]. P. Ressel, G. Erbert, U. Zeimer, K. Haeusler, G. Beister, B. Sumpf, A. Klehr, and G. Tränkle, “Novel Passivation Process for the Mirror Facets of Al-Free Active-Region High-Power Semiconductor Diode Lasers”, IEEE Photon. Technol. Lett. **17**(5), pp. 962, 2005.

[162]. K. Kihara, H. Soda, H. Ishikawa, and H. Imai, “Evaluation of the coupling coefficient of a distributed feedback laser with residual facet reflectivity”, J. Appl. Phys., **62**(4), pp. 1526, 1987.

List of publication

[1]. T-P. Nguyen, A. Klehr, O. Brox, G. Erbert and G. Tränkle, "High power 780 nm DFB laser with 500 kHz linewidth" Advances in Optics, Photonics, Spectroscopy and Applications, pp. 267-272, Cantho, Vietnam, 2006.

[2]. T-P. Nguyen, A. Klehr, O. Brox, G. Erbert, and G. Tränkle "200 kHz linewidth of 780 nm high-power distributed feedback diode laser" Conference Digest CLEO/Europe, Paper CB-6-WED, 2007.

[3]. A. Klehr, H. Wenzel, O. Brox, F. Bugge, G. Erbert, T-P. Nguyen, and G. Tränkle "High-power 894 nm monolithic distributed-feedback laser", Optics Express, vol. 15, no. 18, pp. 11364-11369, 2007.

[4]. A. Klehr, H. Wenzel, O. Brox, F. Bugge, G. Erbert, T-P. Nguyen and G. Tränkle, "High power DFB lasers for D1 and D2 caesium absorption spectroscopy and atomic clocks", Proc. of SPIE Vol. 6909, 69091E, 2008.

[5]. A. Klehr, H. Wenzel, O. Brox, F. Bugge, G. Erbert, T-P. Nguyen and G. Tränkle, "High power DFB lasers for D1 and D2 rubidium absorption spectroscopy and atomic clocks", Proc. of SPIE, Vol. 7230, 72301I, 2009.

[6]. T-P. Nguyen, A. Klehr, A. Wicht, G. Erbert, and G. Tränkle " High-power distributed feedback diode laser at 780 nm with sub-100 kHz linewidth", Conference Digest CLEO/Europe, Nguyen_cb12.2-thu, 2009.

Acknowledgement

My PhD works that are described in this thesis had been done at Ferdinand-Braun-Institut (FBH).

First, I am deeply indebted to Prof. Dr. Günther Tränkle, Director of Ferdinand-Braun-Institut Berlin, scientific adviser for my PhD work, who provided me an opportunity to join in FBH. During the time in FBH, I have been motivated by his encouragement and kind help in daily life and the research works.

I wish to convey my gratitude to Dr. Andreas Wicht for his daily guidance, useful supports in experiments and the patience in discussion and correction of my thesis. I would like to send my thank to Dr. Hans Wenzel for his great guidance and special contribution to my thesis by his theoretical simulation.

I am highly appreciate the kind helps from Dr. Andreas Klehr and Dr. Olaf Brox as well as the fruitful discussion with them.

I also thank Dr. Gözt Erbert, Head of Optoelectronics Department for his leadership, kindness and fruitful discussion.

The experiment part of my PhD work has an important contribution of Stefan Spiessberger and Max Schiemangk, I highly appreciate their assistance.

My warm thanks go to my colleagues in Laser Metrology Group (Erdenetsetseg Luvsandamdin, Gregor Mura,; Christoph Pyrlik, Heike Christopher) and in Laser Measurement Group for daily help, collaboration and discussion.

During my working time in Optoelectronics Department, I got very kind help and sharing opinions as well as emotion everyday from Jaqueline Hopp and also lot of good technical supports and helpful discussions from my colleagues in the department, who are very kind with me, so I would like to thank them for everything.

In FBH, I already enjoyed a very nice environment with German colleagues and the colleagues come from many countries, many thanks to them.

Needless to say, I got continuously support from Institute of Engineering Physics (IEP), Hanoi University of Science and Technology. I thank the Director of IEP Prof. Dr. Nguyen Duc Chien, former Director of IEP Prof. Dr.Sc. Do Tran Cat. Many thanks go to my colleagues of Analysis & Measurement Laboratory and other colleagues in IEP and physics community in Vietnam, who indirectly contribute to the success in my PhD works.

The PhD course belongs to the Training Scientific and Technical Cadres in Institutions Overseas with the State Budget (Project 322). I would like to thank the funding from Vietnamese government.

Last but not least, I thank all people in my “big family” for their supports and encouragement continuously. Final thanks, I reserve them to my “small family”: to my beloved, who always see the same way with me; to my baby, who made me smile after working time.

Cảm ơn Việt Nam *and* ***Danke Deutschland !***

Curriculum Vitae

Personal data

Family & Middle name:	**Nguyen Thanh**
Name:	**Phuong**
Date of birth:	June 17th, 1976
Place of birth:	Sonla, Vietnam
Nationality:	Vietnamese
Marital status:	married

Education & Career

1981 – 1989:	Thuanchau Primary & Secondary School, Sonla, Vietnam.
1989 – 1992:	Thuanchau High School, Sonla, Vietnam.
1992 – 1996:	Thainguyen University, Vietnam
1997 – 1999:	Master of Science (Physics) in Institute of Physics, Hanoi, Vietnam. Master Thesis: *Study of Spectroscopy on Vietnamese quartz. Colour center*
1998-2000	Researcher of Laboratory of Applied Spectroscopy and Gemology,, Institute of Materials Science, Hanoi.
Since 2000:	Lecturer at Institute of Engineering Physics, Hanoi University of Technology.
Since 2004:	PhD. student at Optoelectronic Department, Ferdinand-Braun-Institute Berlin.

Berlin, 10.02.2010